ALLFORSK AVH

THE MARITIME TURBULENT WIND FIELD

MEASUREMENTS AND MODELS

PHASE 2 -EXTENSION 1 - TASK 4

EXTENDED ANALYSIS OF THE FRØYA DATA BASE

FINAL REPORT

odd jan andersen
jørgen løvseth

ALLFORSK AVH

UNIVERSITY OF TRONDHEIM
Department of Physics
N-7055 Dragvoll, NORWAY

THE MARITIME TURBULENT WIND FIELD MEASUREMENTS AND MODELS - PHASE 2 - EXTENSION 1

EXTENDED ANALYSIS OF THE FRØYA DATA BASE

Final report for Task 4 of the Statoil Joint Industry Project

Statoil Contract T.7916, Ch.O. No. 3, P2 - Ext.1
Project No. 209 ALLFORSK-AVH

Odd Jan Andersen
Statoil, Technology Division,
Forus, N-4001 Stavanger, Norway

Jørgen Løvseth
ALLFORSK / Department of Physics, University of Trondheim
N-7055 Dragvoll, Norway

Work sponsored by

Amoco Norway Oil Company - Conoco Norway INC. - Exxon Production Research Company - Marin Technology Support Unit - A/S Norske Shell - Norsk Hydro Saga Petroleum A/S

December 1992

TABLE OF CONTENTS

SUMMARY

During this extended analysis of the Frøya data base, air - sea temperature difference is used as a stability indicator, and a detailed comparison to models available in the literature is performed. Only data for the maritime sector of the Sletringen station is discussed in this report.

General procedure

The observed data are time series of mean values over the logging period 600/512 s ≈ 1.16 s. The data are mostly treated for time periods of T = 40 min, giving 2048 measurements per period.

Turbulence intensity and gust factors are defined from modified time series where the synoptic variations are eliminated or reduced by a two step procedure; first the difference between the running 40 min mean and the period mean is subtracted from each element in the time series; second, harmonics with periods T, T/2 and T/3 are digitally filtered out. The resulting time series have a period mean value close to that of the original time series, and contain the turbulence corresponding to harmonic periods of 10 min and shorter.

The Monin-Obukhov length scale coefficient λ' is used to represent atmospheric stability. It is calculated from the air - sea temperature difference, and is defined by

$$\lambda' = \kappa\, g\, \{C_H\, (T_{air} - T_{sea})/T_{air} + \tau'\, C_E\, (q_{air} - q_{sea})\} \tag{1a}$$

$$\tau' = 0.61/(1 + q_{air}), \quad q_{air} = r_H\, q_{sat}(T_{air}), \quad q_{sea} = q_{sat}(T_{sea}), \tag{1b}$$

$$q_{sat}(T) = 0.00375 \exp[\, 19.872\, (\, 1 - 273/T)] \tag{1c}$$

$$\kappa = 0.4, \quad g = 9.81 \text{ m s}^{-2}, \quad C_H = 0.00127, \quad C_E = 0.00128, \quad r_H = 0.75 \tag{1d}$$

where q_{air}, q_{sea} represent the specific humidities in the air and immediately above the sea surface, respectively. They are not measured directly, but related to the temperatures by the above formulae. The air temperature T_{air} is at Sletringen measured at 5 m height. When local temperature data are lacking, substitute data are calculated from the meteorological observations at the Sula lighthouse.

The physical quantities calculated on the basis of the time series are treated as functions of three or four variables, the three being reference wind speed u_r (the period mean at 10 m height), atmospheric stability (λ') and height, z. The mean and the variance of the quantity in question are calculated for a set of cells in the variable space. By a least squares principle, model parameters are then adjusted to reduce the difference between the model and the observed values for the cells in the ensemble of observations. The number of observations in each cell divided by their variance is used as weight factor.

Most of the discussion in the present report is concerned with neutral atmospheric conditions. The majority of the models in the literature are only valid for the neutral case.

From Eq. (10) below, it also follows that the absolute value of the dimensionless Monin-Obukhov stability variable z/L goes to zero at high wind speeds, thus the case of neutral stability will be most relevant for extrapolation to design wind speeds.

Wind speed profiles

Some ten models for the wind speed profiles were examined. The best fits were obtained using the logarithmic law,

$$u(z) = (u_*/\kappa)\, \ln(z/z_0), \quad \kappa = 0.4 \tag{2}$$

where u_* is the friction velocity, κ is von Karman's constant and z_0 is the roughness length. Experimentally, the wind speed ratio

$$u(z)/u_r = 1 + \alpha\, \ln(z/z_r), \quad \alpha = [\ln(z_r/z_0)]^{-1} \tag{3}$$

has been studied, u(z) being the 40 min mean wind speed at height z, and u_r the corresponding reference wind speed at reference height, which for Sletringen is $z_r = 10.5$ m. The observations suggest that the height coefficient α increases approximately linearly with wind speed. Good fits were obtained using the Charnock relation, which relates the roughness length to the friction velocity,

$$z_0 = (a_{Ch}/g)\, u_*^2 \tag{4}$$

where a_{Ch} is Charnock's constant and g the gravitational acceleration. When Eqs. (2) and (4) are combined for $z = z_r$, an implicit relation for z_0 in terms of a_{Ch} results. A least square fit to the data for neutral atmospheric stability gives

$$a_{Ch} = 0.0172 \tag{5}$$

which is within the range of values proposed for Charnock's constant.

The drag coefficient is defined by

$$C_D = (u_*/u_r)^2 \tag{6}$$

From Eqs. (2-3), the logarithmic law may then be expressed as

$$u(z)/u_r = 1 + \alpha\, \ln(z/z_r), \quad \alpha = (C_D)^{1/2} / \kappa \tag{7}$$

Assuming the Charnock relation and the logarithmic law to be valid, the drag coefficient C_D will approximately be a linear function of u_r. The best fit to the neutral data were obtained by assuming a linear C_D - u_r relation, and then fitting the coefficients, the result is

$$C_D = c_1 + c_2 u_r \qquad c_1 = 5.26\ 10^{-4}, \quad c_2 = 7.79\ 10^{-5} \tag{8}$$

In the parameterizations discussed below, where u(z) is used as an input, it made in general very little difference to the fit whether Eqs. (2-5) or (6-8) were used.

For general stability conditions, the standard Monin - Obukhov (M-O) extension of the logarithmic law,

$$u(z) = (u_*/\kappa) \left[\ln (z/z_0) - \psi_m(z/L) \right] \tag{9}$$

combined with the Charnock relation, was found to give a good fit to the data. The M-O variable z/L is defined as

$$z/L = z\, \lambda'\, u_r / u_*^3 \tag{10}$$

The wind speed profile is described by

$$u(z)/u(z_r) = \left[\ln (z/z_0) - \psi_m(z/L) \right] / \left[\ln (z_r/z_0) - \psi_m(z_r/L) \right] \tag{11}$$

where for unstable conditions,

$$\psi_m(z/L) = \ln [(1 + X)^2 (1 + X^2)/8] - 2 \tan^{-1}(X) - \pi/2$$
$$X = [1 - \gamma_m z/L]^{1/4}, \qquad z/L < 0 \tag{12}$$

and for stable conditions,

$$\psi_m(z/L) = - \beta_m z/L, \qquad z/L > 0 \tag{13}$$

In analogy with the neutral case, the Charnock relation and Eq. (9) will implicitly define z_0, which in this case depends both on reference wind speed and stability. A least squares fit to the full set of data for the wind speed profile, where also β_m and γ_m in Eqs. (12-13) were left as free parameters, gives the values

$$a_{Ch} = 0.0178, \quad \beta_m = 3.64, \quad \gamma_m = 17.48 \tag{14}$$

The reader is referred to Sec. 4.2 for the details.

For neutral atmospheric stability, the inertial dissipation method for determining u_* is found to give good agreement with the results following from the Charnock relation and a fit to the profile data. Corrections for aliasing and sampling effects in the spectra are important for the inertial dissipation method. At the Nyquist frequency, $f_{Ny} = 0.43$ Hz in our case, shape corrections, i.e. deviations from the $f^{-5/3}$ behaviour, typically constitute 10%, and an extrapolation procedure was therefore established to find the asymptotic

values. For non neutral atmospheric conditions, the predictions for u_* from the conventional formulation of the inertial method do not agree with the results from the fits of the wind speed profiles discussed above.

Turbulence intensity

The turbulence intensity for a period is defined as the ratio between the standard deviation and the mean value for the wind speed time series

$$I_u(z) = \sigma_u / u(z) \tag{15}$$

For neutral data, a very good fit was obtained by the following ad hoc model

$$I_u(z) = [\ I_0 + I_1\ u_r\ ]\ (z/z_r)^{\ a}$$

$$I_0 = 0.0601, \quad I_1 = 0.0026\ \text{s/m}, \quad a = -0.218 \tag{16}$$

Thus, the turbulence intensity was found to increase linearly with reference wind speed, and decrease rather strongly with height.

For general atmospheric stability, reasonable agreement was found by adding a stability dependent factor to the above formula,

$$I_u(z) = [\ I_0 + I_1\ u_r\ ]\ (z/z_r)^a\ [\ 1 - I_L\ (z/L)\ (u_r/10\text{m/s})^{-b}\ (z/z_r)^{-c}\ ]$$

$$I_L = 1.26 \quad b = 1.52 \quad c = 0.85 \tag{17}$$

Thus, the stability dependence was found to be proportional to the M-O stability variable z/L and to decrease strongly with u_r and z. At design wind speeds, the relation for neutral conditions may be used.

Reference gust factors

The reference gust factor for a time interval t_g is defined as the ratio between the observed maximum mean value over an interval t_g during a period T, and the reference wind speed for the same period.

Good fits for the reference gust factor were obtained by relating it to the the turbulence intensity I_u and the wind speed ratio, the explicit formulation for general atmospheric conditions being

$$G_r(t_g,T,z) = [\ u(z) / u_r\ ]\ \{\ 1 - [\ g_0 + g_1 \ln(t_g/T) + g_2\ (\ln(t_g/T))^2\ ]\ I_u\ \} \tag{18}$$

The ordinary gust factor will be defined if the $u(z)/u_r$ factor is omitted. The above recommended formulae - dependent on the atmospheric stability - should be used for I_u

and $u(z)/u_r$. The coefficients and goodness of fit turns out to be the same for the two formulations of the wind speed profile, thus, either Eqs. (2-5) or (6-8) may be used.

For neutral conditions, the values for the best fit of the "new" parameters in Eq. (18) are

$$g_0 = 0.726, \quad g_1 = 0.655, \quad g_2 = 0.0188 \tag{19}$$

For general atmospheric stability, the corresponding set is

$$g_0 = 0.803, \quad g_1 = 0.732, \quad g_2 = 0.0279 \tag{20}$$

One point turbulence spectra

Some 17 models have been compared to the experimental data. In general, much flatter spectra have been observed in this project than predicted by traditional models of the Kaimal or Harris type. Therefore, the models introduced in the Phase 1 and Phase 2 of this project have been found to give by far the best representation of the data. These models are discussed in Sec. 7.2-M8 and -M13 for neutral data, and in Sec. 7.3-M3 (the Phase 2 model only) for general atmospheric conditions.

For neutral data, the one term model from Phase 1 will for many purposes be practical. It may be written as

$$f\,S(f) = \frac{A(z,u_r)\,\gamma}{[1 + 1.5\,\gamma^n]^{5/3n}} \qquad \gamma = f/f_{max}, \quad f_{max} = u_r / L(z,u_r) \tag{21}$$

where A and L will be functions of u_r and z. In agreement with the main project results, these functions are assumed to be given by power law relations,

$$\begin{aligned} L &= L_0\,(z/z_r)^{Q1}\,(u_r/u_0)^{Q2}, \quad z_r = 10.5\ m, \quad u_0 = 20\ m/s \\ A &= C\,u_r^2\,(z/z_r)^{Q3}\,(u_r/u_0)^{Q4} \end{aligned} \tag{22}$$

A least squares fit to the data gives the following results

$$n = 0.468$$

$$L(z,u_r) = 890\ m\,(z/z_r)^{0.677}\,(u_r/u_0)^{0.251} \tag{23}$$

$$A(z,u_r) = 0.0738\,u_r^2\,(z/z_r)^{-0.216}\,(u_r/u_0)^{0.752}$$

A numerical integration over frequency gives the total variance corresponding to this fit as

$$\sigma^2 = 0.2384\,A(z,u_r) = 0.0176\,u_r^2\,(z/z_r)^{-0.216}\,(u_r/u_0)^{0.752} \tag{24}$$

The two term model from Phase 2 written on the form

$$\frac{f\,S(f)}{u_r^{\,a}} = \frac{C_1\,(z/z_r)^{-b}\,f}{[f_{x1} + 1.5\,f]^{5/3}} + \frac{C_2\,f}{[f_{x2}^{\,n} + 1.5\,f^n]^{5/3n}} \qquad f_{xk} = 1/T_k \tag{25}$$

has been adopted to spectra for both neutral and general stability. For neutral data the parameterization is

$$T_1 = Q_1\,z / u(z) \qquad T_2 = Q_2 / u(z) \tag{26}$$

The values of the parameters are determined by a least squares fit to the data,

$$C_1 = 2.52\ 10^{-5},\quad C_2 = 4.79\ 10^{-5},\quad a = 3.32,\quad b = 1.60,$$
$$n = 0.413,\quad Q_1 = 18.5,\quad Q_2 = 3610\ \text{m} \tag{27}$$

This second parameterization for neutral data gives a somewhat better overall fit. Extrapolations to design wind speeds are given for three spectral regions in Sec. 7.4. The two models for the wind speed profiles discussed above did not show significant differences.

For general stability, Eq. (25) is parameterized to include dependence on the stability variable λ' in the following way

$$T_1 = Q_1\,z / u(z) \qquad T_2 = Q_2\,\exp(-Q_3\,\rho)/\,u(z)$$
$$n = n_0 + n_1\,\exp(Q_4\,\rho) \qquad \rho = \lambda'\,(u_r/10)^{-c} \tag{28}$$

A least squares determination of the parameters yields

$$C_1 = 2.67\ 10^{-5},\quad C_2 = 5.49\ 10^{-4},\quad a = 3.28,\quad b = 1.68,\quad c = 2.68$$
$$n_0 = 0.1893,\quad n_1 = 0.0325,$$
$$Q_1 = 24.3,\quad Q_2 = 17\,380,\quad Q_3 = 40\,240,\quad Q_4 = 26\,960 \tag{29}$$

Aliasing and sampling effects were found to be important for the values of the model parameters, and have been taken into account.

The norm, or frequency integral of the spectral function S(f), is by definition equal to the total variance. A good fit to the observed spectrum will lead to an S(f) having important contributions to the norm below the frequency region studied here. Thus this

norm is not equal to the variance calculated directly from of the observations, which was used as a basis to obtain the turbulence intensity discussed above.

Coherence spectra

Again, the model introduced in Phase 2 was shown to give a considerably better fit to the data for vertical coherence than the alternatives. Only the Sletringen data were treated anew, since the stability variable λ' based on the air - sea temperature difference is not directly applicable to the Skipheia data.

Vertical coherence for neutral stability is described by a modified Davenport model,

$$\begin{aligned} &\mathrm{Coh} = \exp[- a_z \, \Delta z \, f / u(z_g)], \quad \Delta z = | \, z_1 - z_2 \, |, \quad z_g = [z_1 \, z_2]^{1/2} \\ &a_z = [\, a_{z0} + a_{z1} \exp(- b \, f)] \, \Delta z^q / z_{gr}^{\,p}, \quad z_{gr} = [z_1 \, z_2]^{1/2} / 10 \end{aligned} \tag{30}$$

A least squares fit to the data gives

$$a_{z0} = 18.3, \quad a_{z1} = 6.9, \quad b = 103.7, \quad p = 0.44, \quad q = 0.29, \quad \Delta_{rms} = 0.0246 \tag{31}$$

The Phase 2 results for lateral coherence were found to imply a considerably shorter coherence length than predicted by the ESDU and Bowen models. The Phase 2 results are however not incompatible with results due to Kristensen et al. (1981). Experimental results for smaller distances than presently available at Skipheia would clarify the situation.

1. INTRODUCTION

During the main part of the present project, a complete, analytical description of the structure of marine winds in the atmospheric boundary layer was established based on extensive analysis of data. The analytical description was formulated within the present project and was to a small degree only related to earlier published results. The description is valid within the range of wind speeds 10 - 25 m/s for which data were available. However, the adequacy of the description for design conditions with wind speeds of the order of 40 m/s has been questioned. In order to resolve that extrapolation question it becomes urgent to compare the data with available models established by other research groups. In particular, emphasis should be given to descriptions which have a theoretical and sound physical basis and includes "universal" relationships. Clearly, if the present data compare reasonably well with this type of descriptions, then the description for marine winds becomes part of a context with a good experimental and theoretical basis. Extrapolations within that framework are then well justified.

The present report supplements work done within the framework of the project "The maritime turbulent wind field. Measurements and models", and addresses extensively the above type of problems. The report is the final report for Task 4 of the project extension "Phase-2 - Extension-1"

The discussion in this report follows closely the schemes described in the Scope of Work for the present project extension (hereafter referred to as SoW). The relevant literature behind the various models used in this part of the project, is reviewed by O.J. Andersen (Andersen 1991,a, hereafter referred to as OJA-R). The data collection system and the preparatory treatment of the data are described in the final report for the main part of this project (Andersen et al., 1991). In this report, only a very brief description of the operations performed is given. For background and more detailed descriptions, reference is made to the above mentioned sources. Conclusions and comments originating from the present extension of the data analysis, will of course be given.

2. DATA PREPARATION

For the various quantities defined from the experimental data, mean values are defined over a period

$$T_m = 40 \text{ min} \tag{1}$$

The raw data will in general be time series consisting of mean values corresponding to one logging period,

$$T_0 = T_m/2048 \simeq 1.16 \text{ s} \tag{2}$$

The analysis is based on a modified time series obtained from the measured time series through the following steps:

1. From each instantaneous recording the moving 40 min. average is subtracted. The mean value for the 40 min. period in question is added to each element.
2. The new time series is Fourier transformed by the FFT procedure, the coefficients of the first, second and third harmonic are set equal to zero, and then the inverse transform is taken.

The first of these steps will remove trends from the data, the second removes periodic variations corresponding to periods longer than 10 min. Note that the second step will preserve the mean for the period.

The exact heights of the wind speed sensors at Sletringen which are used in this analysis, are 10.5, 20.5, 42.0 and 46.0 m. The first two sensors will henceforth be referred to as being at 10 and 20 m height, respectively, but the exact height values are used in the analysis. The mean wind speed of the 10 m sensor is called the reference wind speed.

The wind direction is measured at 44 m height. Only data having a period mean wind direction within the "maritime sector" running from 160° (S-SE) through south, west and north to 40° (NE), is included in the analysis.

In the present analysis, the Monin - Obukhov length scale parameter λ' is used to represent atmospheric stability. It is defined by

$$\lambda' = \kappa\, g\, \{C_H\, (T_{air} - T_{sea})/T_{air} + \tau'\, C_E\, (q_{air} - q_{sea})\} \tag{3a}$$

$$\tau' = 0.61/(1 + q_{air}), \quad q_{air} = r_H\, q_{sat}(T_{air}), \quad q_{sea} = q_{sat}(T_{sea}), \tag{3b}$$

$$q_{sat}(T) = 0.00375 \exp[\, 19.872\, (\, 1 - 273/T)] \tag{3c}$$

$$\kappa = 0.4, \quad g = 9.81 \text{ m s}^{-2}, \quad C_H = 0.00127, \quad C_E = 0.00128, \quad r_H = 0.75 \tag{3d}$$

The relative humidity r_H has been assigned the typical value 0.75 since humidity has not been measured. Thus, the specific humidity are a function of the air temperature T_{air} only. T_{air} is taken as the mean temperature measured at Sletringen at 5 m height, and T_{sea} as the corresponding sea temperature.

When data for air/sea temperature and wind direction are not available from Sletringen, corrected and interpolated data from the meteorological station at Sula lighthouse are used. These data were established by O.J. Andersen, who also has derived a regression formula giving the connection between T_{air}, T_{sea} and the difference T_{air} - T_{sea} measured at Sletringen and Sula, respectively (Andersen 1991b).

The spectral wind speed data are essentially prepared as discussed in Andersen et al. (1991).

As a result of this data preparation step, a summary tape was produced which in chronological order contains the relevant quantities needed for the subsequent analysis for all periods when the necessary raw data are available.

3. GENERAL DESCRIPTION OF THE PROCEDURE FOR FITTING MODELS TO THE DATA

The fitting program reads data from the data summary tape, period by period. If all needed quantities are available and OK, and if all specified conditions for the particular analysis are satisfied, the period data are processed and included in the fit. Examples of conditions to be fulfilled are that the wind direction for the period is in the maritime sector and that the air - sea temperature difference is within the specified range (cmp. Sec. 4.1 below).

The data were grouped into 16 classes of reference wind speed from 10 to 26 m/s, each of width 1 m/s (occasional data with wind speed in excess of 26 m/s were included in the 26 m/s class). If required, the data were further classified according to the value of λ' (Eq. 3). In units of 10^{-5} ms^{-2}, the values of λ' are found in the range -21 to 6, mostly a class width of 4 is used giving 7 stability classes.

The distribution of the data according to this classification scheme is shown in Table 3.1A-C, for the full data set, and for the selected sets of partially quasi stationary (PQS) periods and quasi stationary (QS) periods, respectively. See Andersen et al (1991) and Aasen (1990) for a discussion of the selection of these periods.

In addition to the two dimensional classification of the data according to period values of u_r and λ', a classification with respect to height is required (4 heights). The gust data will contain gust values for 4 gust periods, and the one point spectral data contain data for 26 spectral ranges (particularities for the spectral data are discussed in the respective sections below).

The data are thus classified in a three or four dimensional scheme according to the type of analysis. For each cell c_i in this multi dimensional space, a mean value M_i and a standard deviation σ_i is estimated by an ensemble averaging for the N_i periods belonging to the cell:

$$M_i = < Q >_i \tag{1}$$

$$\sigma_i^2 = N_i <[Q - M_i]^2>_i /(N_i-1) \tag{2}$$

where Q is the value of the quantity in question calculated from the data, and the brackets $< >_i$ indicate that only events belonging to the particular cell No. i should be included in the averaging. The correction factor $N_i/(N_i-1)$ to the variance is included because the mean value M_i is also estimated from the sampled values.

Table 3.1A The total set of data (1717 periods) classified according to reference wind speed u_r (m/s) and stability variable λ'. The mean values for the periods in a line or in a coloumn is shown in the heading.

	M-O length coefficient λ' (10^{-5} m s^{-2})						
u_r	-1.9	-1.6	-1.2	-0.8	-0.4	0.0	0.3
10.5	0	17	16	66	114	46	3
11.5	1	22	18	79	87	70	6
12.5	2	21	24	65	81	56	9
13.5	3	19	22	50	67	64	3
14.5	1	13	12	28	61	69	4
15.5	0	2	5	11	41	85	8
16.5	0	1	4	5	20	39	6
17.5	0	1	1	17	27	39	2
18.5	0	0	3	9	13	34	4
19.5	0	0	0	4	19	25	3
20.4	0	0	0	3	13	15	7
21.6	0	0	0	0	2	5	2
22.6	0	0	0	0	1	8	1
23.3	0	0	0	0	1	5	0
24.6	0	0	0	0	0	4	0
25.8	0	0	0	0	0	3	0

Table 3.1B As Table 3.1A, but for the PQS set of data (522 periods).

	M-O length coefficient λ' (10^{-5} m s^{-2})						
u_r	-1.9	-1.6	-1.2	-0.8	-0.4	0.0	0.3
14.6	0	3	7	3	31	41	3
15.5	0	2	5	6	31	71	6
16.5	0	1	3	2	20	33	7
17.5	0	0	0	10	26	35	2
18.5	0	0	3	7	13	33	4
19.5	0	0	0	3	21	25	3
20.4	0	0	0	1	12	13	7
21.6	0	0	0	0	1	4	2
22.6	0	0	0	0	1	8	1
23.3	0	0	0	0	0	5	0
24.6	0	0	0	0	0	4	0
25.8	0	0	0	0	0	3	0

Table 3.1C As Table 3.1A, but for the QS set of data (370 periods).

	M-O length coefficient λ' (10^{-5} m s^{-2})						
u_r	-1.9	-1.6	-1.2	-0.8	-0.4	0.0	0.3
14.6	0	3	3	2	22	30	1
15.5	0	2	3	2	22	62	3
16.5	0	1	2	1	14	24	4
17.5	0	0	0	7	19	23	2
18.5	0	0	3	6	8	17	2
19.5	0	0	0	2	15	17	2
20.4	0	0	0	1	6	8	7
21.5	0	0	0	0	0	3	2
22.6	0	0	0	0	0	7	1
23.3	0	0	0	0	0	4	0
24.6	0	0	0	0	0	4	0
25.8	0	0	0	0	0	3	0

The model value of the quantity Q for the cell No. i is denoted F_i. It is calculated for the mean value of u_r and λ' in the cell. The goodness of fit for the particular model is then indicated by the quantity

$$Z = \Sigma\ W_i\ [M_i - F_i]^2 \tag{3a}$$

$$W_i = N_i\ /\ <\sigma_i^2>_{\lambda'} = (\sigma_{Mi})^{-2} \tag{3b}$$

In calculating the weights W_i, σ_i^2 is averaged over the λ'-classes, as indicated, in order to reduce the statistical fluctuations (the dependence on λ' is normally not very strong). The quantity σ_i, as defined by Eq. (2), represents an estimate for the standard deviation of the individual values Q within the variable cell i. W_i will then represent an estimate of the inverse square of the standard deviation of the cell mean value M_i of the quantity being analysed. Thus the sum defined in Eq. (3a) is expected to have elements with an average value of the order of 1 and a total value of the order of # cells.

In the analysis discussed in the remaining sections of this report, parameters in the models are normally fitted by minimalizing the sum Z defined by Eq.(3). The minimum can be taken as an estimate of the χ^2 value of the fit,

$$\chi^2 = \text{Minimum}\ (\ Z\ ) \tag{4}$$

For a perfect model, the value of χ^2 is expected to be close to the number of degrees of freedom, N_f, if N_f is large. In our case,

$$N_f = N_c - 1 - N_p \tag{5}$$

where N_c is # cells, and N_p is # parameters being fitted.

This least squares minimalization is performed by a specially constructed routine, that handles both linear and non linear parameter dependence very efficiently.

A χ^2 - test may also be performed on a completely established theory with no adjustable parameters. Then $\chi^2 = Z$ (from Eq. 3a), and $N_f = N_c - 1$.

4. SUBTASK 4.1: WIND SPEED PROFILES

4.1 Near neutral profiles

In the SoW, near neutral is defined as conditions when the air - sea temperature difference satisfy

$$\Delta T = T_{air} - T_{sea}, \quad -3.0 < \Delta T < 0.0 \text{ K} \tag{1}$$

Data for periods satisfying this criterion are analysed in this section. In discussing the logarithmic profile combined with the Charnock relation in subsection 4.1-M4 below, a different selection criterion in terms of the Monin-Obukhov length scale parameter λ' is introduced. The indication is that

$$| \lambda' | < 2\ 10^{-5}\ ms^{-2}$$

gives a somewhat better selection for neutral stability.

4.1-M1: Standard power law profile

The power law profile is defined as

$$u(z) / u(z_r) = [\ z / z_r\ ]^{a} \tag{2}$$

As discussed in Andersen et al. (1991), the power law is not a very good candidate for describing our data. Plots of the observed wind speed ratios (with standard deviations to indicate the spread) for the "near neutral data", a best fit of Eq. (2) to the data, and Eq. (2) for the exponent values a = 0.09, 0.10, 0.11 and 0.12 are shown in Fig. 4.1-M1. The best fit corresponds to a = 0.0867.

The striking feature of the data is an increasing value of the wind speed ratio with reference wind speed, a property not accounted for by the power law with a constant exponent. A more subtle feature is that the power law predicts too rapid growth of the wind speed ratio vs. the height z, and this makes the logarithmic law a potentially better candidate for modifications.

In the literature, cmp. OJA-R Table 2.1.1, a range of values for the exponent a from 0.09 to 0.19 is suggested. In Table 4.1.1, Z values (as defined by Eq. 3.3a) are shown for representative values of a in the same range. As is seen, Z is increasing rapidly, as the exponent value is increased from the lsq. fit value. All Z values are much too large for a statistically acceptable description, which is also readily apparent from the plot. The value a = 0.12 gives a larger wind speed ratio than any of the observed mean values for heights above 40 m.

Table 4.1.1 Z and # degrees of freedom for various values of the exponent a when the power law, Eq. (2) is compared to the "near neutral" data. a = 0.087 represent a lsq. fit.

a	0.0877	0.09	0.10	0.11	0.12	0.15	0.19
χ^2 or Z	1 990	2 072	4 303	9 664	18 274	64 828	180 192
N_{free}	46	47	47	47	47	47	47

The selected set of "near neutral data" is probably "contaminated" by some data for unstable conditions, as will be discussed in Sec. 4.2. However, all our analysis in this project suggest that there is an increase of the wind speed ratio with wind speed for neutral data. Therefore, if one wants to use the simple power law, Eq. (2), the exponent should be chosen according to the wind speed regime and use in question.

4.1-M2: USGS power law profile

The USGS (1978) recommendation for Mexico-gulf conditions can be written

$$u(z) / u(z_r) = [(z - z_c) / (z_r - z_c)]^a \qquad (3)$$

$$z_c = 2.2 \text{ m} \quad a = 0.1128$$

This model compared to the "near neutral" data is shown in Fig. 4.1-M2 as the dashed line. The full drawn line is a lsq. fit to the data. Parameter values and χ^2 values are shown in Table 4.1.2.

Table 4.1.2 χ^2 and # degrees of freedom for the USGS version of the power law. Values corresponding to the original parameters and for a least squares fit to the "near neutral" data are shown.

Parameter set	a	z_c/m	χ^2	N_{free}
USGS	0.1128	2.20	28 220	47
Least squ. fit	0.0613	5.14	1 519	45

The least squares fit is somewhat better than for the standard power law, as the z-dependence of the wind speed ratio is better described with this model with an extra parameter. But the fit is still far from acceptable statistically, as the model does not allow for a wind speed dependence of the ratio.

The USGS parameter set seems to be relevant for wind speeds approaching 30 m/s, or design winds.

4.1-M3: Ishizaki power law profile

For typhoon design conditions, Ishizaki (1983) has proposed the following law

$$u(z) / u(15m) = [\, z / 15m]^n \qquad n = 1 / \ln u(15m) \tag{4}$$

The reference height was originally assumed to be 15 m. Assuming this model to be valid down to 10 m, and using the law to calculate the value of the exponent expressed as a function of the our standard reference wind speed $u_r = u(z_r)$, $z_r = 10.5$ m, we get

$$u(z) / u(z_r) = [\, z / z_r]^a$$

$$a = 2 / \{ \ln u_r + [\, (\ln u_r)^2 + 4 \ln(15m/z_r)]^{1/2} \} \tag{5}$$

As is apparent from both the above equations, a power law exponent is predicted which decreases with wind speed, quite contrary to what is prescribed by our data. The values of the exponent for a set of wind speeds are shown in Table 4.1.3. A comparison to e.g. Fig. 4.1-M1 shows that the predicted values of the exponent are much to high.

The Ishizaki version of the power law thus appears to have little relevance when compared to our data.

Table 4.1.3 Ishizaki power law profile - predicted exponent and wind speed ratio at 46 m height (z_r = 10.5 m).

u_r (m/s)	15.0	20.0	25.0	30.0
a	0.353	0.322	0.301	0.285
$u(46m)/u_r$	1.68	1.61	1.56	1.52

4.1-M4: Standard logarithmic law profile

The logarithmic profile is defined as

$$u(z) = (u_*/\kappa) \ln (z/z_0) \tag{6}$$

where u_* is the friction velocity, z_0 is the roughness length, and κ is the Von Karman constant, here assumed to be $\kappa = 0.4$. As discussed in Andersen et al. (1991), it is practical to rewrite this law as

$$u(z) / u(z_r) = [\ 1 + \alpha \ln(z/z_r)] \quad \alpha = [\ \ln (z_r/z_0)]^{-1} \tag{7}$$

before fitting it to the data. A plot of the "near neutral data", a least squares fit of Eq. (7) to the data, and Eq. (7) for the coefficient values of $\alpha = 0.09$, 0.10, 0.11 and 0.12 are shown in Fig. 4.1-M4. The best fit corresponds to $\alpha = 0.0927$ and $z_0 = 0.22$ mm. The corresponding values of z_0 and χ^2 are given in Table 4.1.4. The value $z_0 = 0.15$ mm suggested by Standing et al. (1990) as representative for offshore conditions corresponds, to $\alpha = 0.0896 \simeq 0.09$. As may be seen, our fitted value is quite close to the Standing et al. value.

Table 4.1.4 χ^2 or Z and # degrees of freedom for various values of the coefficient α when the logarithmic law, Eq. (7) is compared to the "near neutral" data. α = 0.0927 represents a lsq. fit.

α	0.0896	0.0927	0.10	0.11	0.12	0.13	0.15
z_0 (mm)	0.150	0.217	0.477	1.18	2.52	4.79	13.4
Z or χ^2	1 938	1 821	2 459	5 413	10 773	18 537	41 281
N_{free}	47	46	47	47	47	47	47

Even the logarithmic model predicts a somewhat faster rise of the wind speed ratio with z than exhibited by the "near neutral data". Because of this, the USGS power law model gives a better fit to the data than the present logarithmic model. However, this should be considered fortuitous. Crudely speaking, our data represent only two independent height ratios, 20/10 and 40+/10. A model using two parameters to fit the z-dependence, will therefore always give an optimal fit to this data set. For large z-values, however, the USGS model predicts a modified power law behaviour

$$u(z) / u(z_r) \simeq z^p / (z_r - z_c)^p \qquad z >> z_c \tag{8}$$

where p is the USGS model exponent. This asymtotic behaviour is not expected.

As with the other models discussed so far, the great problem of the present one is the predicted constancy of the wind speed ratio with increasing wind speed. The comments given at the end of Sec. 4.1-M1 will therefore apply in this case too.

4.1-M5: Logarithmic law with Charnock relation

The Charnock relation assumes that the roughness length z_0 increases with the square of the friction wind velocity u_*,

$$z_0 = (a / g)\, u_*^2 \tag{9}$$

where a is Charnock's constant and g is the gravitational acceleration. Combining Eqs. (6) and (9) for $z = z_r$, we find a transcendental equation that can be used to determine u_* from the reference wind speed u_r,

$$u_r = (u_* / \kappa) \ln\{ z_r / [(a / g)\, u_*^2]\} \tag{10}$$

This establishes u_* as a function of u_r, and thus the drag coefficient C_D, defined by

$$u_*^2 = C_D\, u_r^2 \tag{11}$$

will also be a function of u_r.

Table 4.1.5 χ^2 or Z and degrees of freedom N_f for the least squares fit and for the selected set of values for the Charnock constant a. "Near neutral" data set.

a	0.00768	0.012	0.015	0.020	0.032
χ^2 or Z	899	1 212	1 650	2 572	5 217
N_{free}	46	47	47	47	47

In the literature, cmp. OJA-R Table 2.3.2.2, a range of values for the Charnock constant a from 0.0123 to 0.032 is suggested. In Fig. 4.1-M5.1, plots are shown of the the wind speed ratio for the "near neutral" data and predictions from the logarithmic law

with the Charnock relation, Eqs. (6) and (9-10). Results are shown for a = 0.012, 0.015, 0.020 and 0.032, together with a least squares fit yielding a = 0.00768.

In Table 4.1.5, χ^2 or Z values are shown for the same set of a-values. The lsq. fit is much improved compared to the models discussed above, but it is still far from satisfactory. This could be explained by the selection of the "near neutral" data by Eq. (1), which most certainly will give an overweight of data for unstable conditions. According to the Monin-Obukhov (M-O) theory, deviations from neutral conditions will be scaled by

$$z/L = z\,\lambda'\,u_r/\,u_*^3 \tag{12}$$

where the M-O coefficient λ' may be defined in terms of the present data by Eq. (2.3). Using Eq. (11), one gets

$$z/L = z\,\lambda'\,/\,(\,C_D^{(3/2)}\,u_r^2) \tag{13}$$

indicating that the largest deviations are expected for large z-values and small values of u_r^2. Provided an overweight of unstable data as mentioned, the deviations seen in Fig. 4.1-M5.1 are quite compatible with this picture.

A new data selection was therefore made,

$$-2\ 10^{-5} < \lambda' < 2\ 10^{-5}\ ms^{-2} \tag{14}$$

The corresponding results are shown in Fig. 4.1-M5.2 and Table 4.1.6.

Table 4.1.6 **χ^2 or Z and degrees of freedom N_f for the least squares fit and for the selected set of values for the Charnock constant a. Data set limited by Eq. (14)**

a	0.01721	0.012	0.015	0.020	0.032
χ^2 or Z	158	428	200	212	1 245
N_f	46	47	47	47	47

We see that the fit with the more narrow data selection is much better. The number of periods involved in the last fit is 567, and the mean value of λ' is $<\lambda'> = -0.03\ 10^{-5}\ ms^{-2}$, whereas the "near neutral" set contains 757 periods with a corresponding mean value of λ' of $-3.25\ 10^{-5}\ ms^{-2}$. Whereas the selection by Eq. (14)

ensured a more truly neutral sample, and an estimate of Charnock constant in the main ballpark, the unstable character of the "near neutral" set forced a rather low value of Charnock constant, reflecting the very low value of z_0 pertinent to unstable data when interpreted as neutral.

The Charnock relation implies that the the so called drag coefficient C_D defined by

$$C_D = (u_*/u_r)^2 \tag{15}$$

can be approximately representated as a linear function of u_r,

$$C_D = c_1 + c_2\, u_r \tag{16}$$

A review of the values of the coefficients c_1 and c_2 found in the literature is given by OJA-R, Table 2.3.3.2. From Eq. (15) and the logarithmic law, Eq. (7), it follows that the coefficient α may be expressed as

$$\alpha = (C_D)^{1/2} / \kappa \tag{17}$$

A fit to the neutral data set limited by Eq. (14), using the logarithmic law and the representations given by Eqs. (16-17), gives the result

$$c_1 = 5.26\ 10^{-4},\quad c_2 = 7.79\ 10^{-5},\quad \chi^2 = 123,\quad N_f = 45 \tag{18}$$

A comparison of this fit with the fit based directly on the Charnock relation discussed above, and with the polynomial expansion of α in u_r is shown in Fig. 4.1-M5.3

4.1-M6: NPD (1988) logarithmic law profile

The NPD (1988) version of the logarithmic law,

$$u(z) / u(z_r) = [\ 1 + 0.15 \ln(z/z_r)] \tag{15}$$

is a special version of Eq. (7) with a = 0.15. A comparison to the near neutral data is shown in Fig. 4.1-M6. The corresponding statistical results are included in Table 4.1.4. This prescription gives a very conservative estimate for design purposes.

4.1-M7: Ad hoc logarithmic law profile

From Fig. 4.1-M5.2, where the data were selected according to Eq. (14), it may be seen that both the data and the fit of the logarithmic law with the Charnock relation, suggest that the characteristic coefficient, α, has a close to linear dependence on the reference wind speed. One may then as well take this as a starting point of a model, e.g.

$$u(z) / u(z_r) = [\ 1 + \alpha \ln(z/z_r)]$$

$$\alpha = \alpha_0 + \alpha_1 x + \alpha_2 x^2 \qquad x = u_r/10 - 1 \tag{16}$$

where $u_r = 10$ (m/s) was taken as a reference point for the expansion. Also a second order term was included. One may also arrive at such a relation from the Charnock relation by performing a chain of expansions through the pertinent formulae, Eqs. (7), (9) and (11). Since the experiments are our prime guidance in any case, a free fit of Eq. (16) to the data was performed giving the result

$$\alpha_0 = 0.0903, \quad \alpha_1 = 0.0263, \quad \alpha_2 = -0.00242, \quad \chi^2 = 123, \quad N_f = 44 \tag{17}$$

This fit to the neutral data is as good as that obtained with the linearized Charnock constant, Eqs. (16-18). A plot is shown in Fig. 4.1-M7. Comparing to Fig. 4.1-M5.2, it is seen that the present result implies a slightly stronger linear rise than the with the Charnock relation, but the two fits are very close.

4.2 Extended logarithmic description for general stability

The extension of the logarithmic law Eq. (6) to apply to a wider range of stability conditions is within the M-O theory conventionally written as

$$u(z) = (u_*/\kappa) [\ \ln (z/z_0) - \psi_m(z/L)\ ] \tag{1}$$

where the function ψ_m depends on the atmospheric stability according to

$$\psi_m(z/L) = \ln [(1 + X)^2 (1 + X^2)/8] - 2 \tan^{-1}(X) - \pi/2, \qquad z/L > 0,$$

$$X = [\ 1 - \gamma_m z/L]^{1/4} \tag{2}$$

for unstable conditions, and

$$\psi_m(z/L) = - \beta_m z/L, \qquad z/L < 0 \tag{3}$$

for stable conditions. Using again the Charnock relation, the transcendental relation from which the friction velocity u_* may be determined will now be

$$u_r = (u_* / \kappa) \{ \ln[(g z_r)/(a u_*^2)] - \psi_m(z_r/L)\} \tag{4}$$

Thus, in view of Eq. (4.1.12), the friction velocity is stability dependent and is determined for each γ' class by fitting Eq. (4) to the reference wind speed data.

The wind speed ratio follows from Eq. (1),

$$u(z)/u(z_r) = [\ \ln (z/z_0) - \psi_m(z/L)\ ] / [\ \ln (z_r/z_0) - \psi_m(z_r/L)\ ] \qquad (5)$$

where z_0 through the Charnock relation depends both on wind speed and stability.

As discussed in Chapter 3, and shown in Table 3.1, the data have been divided into 9 stability classes. In Figs. 4.2.1 - 3, the observed values of the wind speed ratio is compared to the model for the three height ratios available. In the plots, mean, weighted results are given for 4 stability ranges. The weight used is simply # events in the respective u_r - λ' classes involved. The stability classes in the plots are defined in Table 4.2.1.

Results are given both for the standard parameter set, and for a least squares fit when the values of a, β_m and γ_m are taken as variables. In Fig. 4.2.4 - 6, the corresponding material is shown for the PQS data set. The plot (and fit) now running from 14 m/s. The results for the QS data are shown in Fig. 4.2.7 - 9. In this case the least squares fit did not converge inside the boundaries specified, but reached the value $\beta_m = 1$ which was specified as the lower limit on this parameter. The resulting values of χ^2 and the parameters are given in Table 4.2.1. The total number of periods, N, in each of the data sets are also indicated.

Table 4.2.1 Stability classes used in the plots related to the classes used in the fits.

Plot notation	Fit class(es)	Range $10^{-4}ms^{-2}$
Stable	8 - 9	0.0 to 0.6
Neutrl	7	-0.3 to 0.0
Unstab	5 - 6	-0.9 to -0.3
S.Unst	1 - 4	-2.1 to -0.9

The trends in the data show some inconsistencies with increasing wind speed, which partly may be due to the way the M-O length L is estimated here. There are also rather few data for wind speeds $u_r > 20$ m/s. But on the whole, the present model seems to give a reasonable description of the data.

Table 4.2.2 χ^2 and # degrees of freedom N_f for the M-O logarithmic law description, Eq. (5). Results for standard parameters and lsq. fits to the full, the PQS and the QS data sets are given.

Data	Paramet.	a	β_m	γ_m	χ^2	N_f
All	Std.	0.0144	4.80	15.20	1002	287
N = 1717	Lsq. fit	0.0178	3.64	17.48	852	284
PQS	Std.	0.0144	4.80	15.20	720	167
N = 522	Lsq. fit	0.0202	1.69	17.47	461	167
QS	Std.	0.0144	4.80	15.20	804	158
N = 376	Lsq. fit	0.0227	1.00	22.14	502	155

4.3 The inertial-dissipation method to determine u*

This is an alternative method to determine u_* and, at least in principle, z/L from the spectral turbulence energy function S(f). The method is supposedly valid in the intermediate high frequency range where both dissipation and production of turbulent energy is assumed to be small. In the discussion below we will, however, question if such a region exists for unstable atmospheric conditions and maritime wind.

Based on the references given in the literature review by Andersen (1991), the spectral function in the intermediate region may be written

$$S(f) = \alpha\, u_*^2\, \beta(z/L)\, [2\,\pi\,\kappa\, z/u(z)]^{-2/3}\, f^{-5/3} \qquad (1)$$

where the recommended value of the constant α is 0.5. The stability dependent factor (denoted $\phi_\varepsilon^{2/3}$ in Andersen (1991)) is given by

$$\beta(z/L) = 1 + \lambda\, |z/L|^{2/3} \qquad (2a)$$

$$\lambda = \begin{cases} \lambda_- = 0.5 & z/L < 0 \text{ (unstable conditions)} \\ \lambda_+ = 2.5 & z/L > 0 \text{ (stable conditions)} \end{cases} \qquad (2b)$$

Thus β has a minimum $\beta = 1$ for neutral stability.

The spectral turbulence data and the spectral function S(f) are discussed in the main report and in Chapter 7 of the present report. The characteristic feature in the inertial subrange is the $f^{-5/3}$ dependence of S(f). Judging from the experimental data for neutral stability displayed in e.g. Fig. 7.2-M3, the $f^{-5/3}$-dependence is seen to be approximately valid only for the very highest frequencies. This part of the spectrum has not been focussed in the present project, and we will first discuss some corrections due to aliasing and the method of observation.

We will first discuss the high frequency corrections, and then combine the results with the Kaimal spectral model, which has the correct asymptotic behaviour, to determine u_*, as defined by Eq. (1).

4.3.1 Spectral corrections near the Nyquist frequency

The aliasing effect is due to the fact that when a digital Fourier transform (DFT) is made, energy from frequencies above those involved in the transform will contribute near the top of the frequency range. Thus the DFT coefficients in this region will contain contribution from the region above the Nyquist frequency. With a model for S(f), however, both this effect and the effect of averaging in the measurment process can be accounted for. By comparing a corrected DFT spectrum to the experimental results, parameters in the model can be adjusted by a least squares fit. The model will then define the inertial subrange behaviour, if necessary, by extrapolation.

In the present project, the elements in the observed time series, x_1, x_2, .. are defined by an integral over the time dependent quantity X(t) in question,

$$x_k = (1/\Delta) \int_{t_-}^{t_+} X(t)\, dt \qquad k = 1, 2, .. N \qquad t_+ = k\,\Delta; \qquad t_- = (k - 1)\,\Delta \tag{3}$$

where Δ is the time interval between the loggings, related to the period T by

$$T = N\,\Delta, \qquad T = 40 \text{ min.} \qquad N = 2048 \tag{4}$$

N is the number of loggings in each period. We assume that X(t) is periodic and defined by an infinite Fourier series,

$$X(t) = \sum_{j=1}^{\infty} \{ A_j \cos(\omega_j t) + B_j \sin(\omega_j t)\} \qquad \omega_j = 2\,\pi\, j\,/\,T \tag{5}$$

If continuous observations of X(t) were available over a sufficient set of periods, the ensemble mean square of the coefficients in this expansion would be related to S(f) by

$$S(f_j) = (T/2) < A_j^2 + B_j^2 > \qquad f_j = j\,/\,T \tag{6}$$

By DFT, the observed time series x_k may also be used to define a continuous time function,

$$x(t) = \sum_{j=1}^{M} \{ a_j \cos(\omega_j t) + b_j \sin(\omega_j t)\} \qquad \omega_j = 2\,\pi\, j / T \qquad M = N/2 - 1 \tag{7}$$

This function will satisfy

$$x(t_k) = x_k \qquad t_k = (k + \tfrac{1}{2})\,\Delta \tag{8}$$

provided the coefficients a_j and b_j are defined by

$$a_j = (2/N) \sum_{k=1}^{N} x_k \cos(\omega_j t_k) \qquad\qquad b_j = (2/N) \sum_{k=1}^{N} x_k \sin(\omega_j t_k) \tag{9}$$

In a simplified approach, the coefficients defined this way are identified with A_j and B_j appearing in Eq. (6) and used to estimate S(f). However, if Eqs.(3-5) are used to define x_k in terms of the coefficients A_j, B_j, and Eq. (9) subsequently is used to estimate a_j, b_j, the following result is obtained,

$$\langle a_j^2 + b_j^2 \rangle = [\sin\gamma_j / \gamma_j]^2 \{[A_j^2 + B_j^2] + [A_{N-j}^2 + B_{N-j}^2]_j^2 /(\pi - \gamma_j)^2 \}$$
$$\gamma_j = j\,\pi/N \tag{10}$$

The $\sin\gamma_j/\gamma_j$ term is due to the averaging implied in Eq. (3), whereas the A_{N-j}, B_{N-j} terms constitute the so called aliasing effect (in principle, also higher order at $\gamma_j + 2\pi$ etc. will enter, but their contribution is negligible). Using Eq. (6), (10) may be rewritten as

$$\langle a_j^2 + b_j^2 \rangle = \frac{2\,[\sin\gamma_j]^2}{T\,\gamma_j^2} \left\{ S(f_j) + \frac{f_j^2}{(f_L - f_j)^2} S(f_L - f_j) \right\} \qquad f_L = 1 / \Delta \tag{11}$$

where f_L is the logging frequency (twice the Nyquist frequency f_{Ny}). Thus, near the upper end of the spectrum, S(f) is not directly observable. If a model for S(f) is used, the mean values of the successive sums of squares of the coefficients a and b can be calculated from Eq. (11). This prediction can be compared to the corresponding quantity evaluated from the experimental time series by Eq. (9). By a least squares fit, parameters in the model can then be adjusted in the ordinary way.

In the intermediate region where Eq. (1) is valid, (11) may be written as

$$\langle a_j^2 + b_j^2 \rangle = \frac{2\,[\sin\gamma_j]^2\, S(f_j)}{T\,\gamma_j^2} \left\{ 1 + \frac{f_j^{11/3}}{(f_L - f_j)^{11/3}} \right\} \qquad f_L = 1 / \Delta \tag{12}$$

At the Nyquist frequency, both Eqs. (11) and (12) simplify to

$$<a_j^2 + b_j^2> = \frac{16}{T\,\pi^2}\ S(f_{Ny}) \qquad j \simeq N/2 \qquad (\text{and } j \leq N/2) \tag{13}$$

An uncorrected estimate by Eq. (6) in a narrow frequency band close to f_{Ny} would therefore give a value a factor $\pi^2/8 = 1.23$ too large.

Only b_j can be evaluated by DFT for $j = N/2$. However, in a practical situation, this is not very important if N is large. To reduce the the observational variance, an average over j values close to N/2 is usually done to evaluate the lhs. of the above equation.

The spectral function in the inertial subrange has a frequency dependence $f^{-5/3}$ as defined by (1), and will be denoted $S_{IS}(f)$, to separate it from the spectral functions valid in the range 0.001 - 0.43 Hz generally discussed in the present project. If S_{IS} is known, it follows from Eq. (1) that u_* is given as

$$u_*^2 = S_{IS}(f)\,[2\,\pi\,\kappa\,z/u(z)]^{2/3}\,f^{5/3} / [\alpha\,\beta(z/L)] \tag{14}$$

Our approach will be to assume that S_{IS} can be found as the high frequency limit from S(f) which is determined by a fit to our spectral data in the range 0.1 - 0.43 Hz,

$$S_{IS}(f) = \lim_{f \to \infty} S(f) \tag{15}$$

4.3.2 Neutral thermal stability

Various spectral models are discussed in Chapter 7 of this report. Limiting the choice to those having the explicite u_* dependence and high frequency limit defined by Eq. (1), the best fitting one is the Kaimal model

$$\frac{f\,S(f)}{u_*^2} = \frac{105\,C\,x}{(B + 33\,x)^{5/3}} \qquad x = f\,z/u(z) \tag{16}$$

In the original formulation, B = C = 1. A least squares fit to the complete set of neutral data, discussed in Sec. 7.2-M3, yields B = 0.444 and C = 0.680 when the Charnock relation with a = 0.0172 (Table 4.1.6) is used to calculate u_*. Fitting to the neutral data for f > 0.1 Hz, with the alias and averaging corrections implied by Eq. (10) taken into account, gives the following result,

$$C = 0.897, \qquad B = 0.740, \qquad \chi^2 = 3464, \qquad N_f = 381 \tag{17}$$

From a statistical point of view the fit is not very good, and is shown in Fig. 3.4.1. The main problem is the z-dependence, however, more than the f-dependence.

Judging from the plot, this model describes the data reasonably well in the high frequency limit for $u_r > 20$ m/s and $z > 20$ m. Expanding the model for high frequencies one gets

$$f\,S(f) \simeq 105\,C\,u_*^2\,x/(33\,x)^{5/3}\,[\,1 - (5/3)\,(B/33x)\,\cdots\,]$$
$$f\,S(f) \simeq 0.277\,u_*^2\,x^{-2/3} = f\,S_{IS}(f) \qquad (18)$$

Thus $S(f) \simeq S_{IS}(f)$ provided

$$x = f\,z/u(z) >> (5/3)B/33 = 0.037 \qquad (19)$$

The asymptotic region is closest for high z and low u values. Comparing Eqs. 1 and 18,

$$\alpha = 0.277\,(2\,\pi\,\kappa)^{2/3} = 0.51 \qquad (20)$$

which probably is well within the error limit of the quoted value of $\alpha = 0.5$. Thus the profile fit determination of u_* based on the logarithmic law and the Charnock relation with the parameter a = 0.0172 (Sec. 4.1-M5), gives a very good agreement with the inertial dissipation method.

Using the linear fit to the drag coefficient to determine u_*, as defined in Eqs. (4.1.15-18), gives a slightly worse fit to the data for $f > 0.1$ Hz, and $\alpha = 0.52$.

Concluding, the method used above allow us to correct for aliasing effects and to extrapolate cleanly to the asymptotic region where the S(f) is proportional to $f^{-5/3}$. In the neutral case, the value of u_* defined by the inertial dissipation method agrees very well with the results obtained in Section 4.1-M5 based on the logarithmic law and the Charnock relation.

4.3.3 General thermal stability

In the main report (p. 64) it was observed that the maritime turbulence spectra showed a "cross over" feature. For frequencies below 0.01 Hz, the turbulence is highest for unstable conditions, for frequencies above this value, and for the frequency range in question here, the turbulence is generally higher for stable conditions. This was interpreted as a cleaning effect, the large scale turbulence taking place for unstable conditions sweeps away the small scale turbulence generated from the ground. This mechanism will reduce the turbulence, and thus violate the underlying condition for Eq. (1). At Skipheia, this feature was only observed for the maritime sector.

With corrections for aliasing and averaging, the spectral data for $f > 0.1$ Hz were compared to the following spectral function,

$$\frac{f\,S(f)}{u_*^2} = \frac{105\ C\ x\ \beta(z/L)}{[\ B\ \exp(\ -\ \gamma\ z/L) + 33\ x]^{5/3}} \qquad x = f\ z/u(z) \tag{21}$$

where $\beta(z/L)$ is defined by Eq. (2a), and u_* and L were determined from the profile fit using the Charnock relation with a = 0.0172 and the generalized logarithmic law as described in Sec. 4.2. The above equation will reduce to Eq. (16) for neutral data. The B-term in the denominator was given an ad hoc multiplier which in a general way will satisfy the known dependence of the spectral maximum on z/L.

A least squares fit gave the results

$$C = 0.844,\ B = 0.683,\ \gamma = 1.31,\ \lambda_+ = 1.18,$$
$$\lambda_- = -\ 0.122,\ \chi^2 = 21503,\ N_f = 2298 \tag{22}$$

The resulting fit is compared to the averaged Sletringen data for 42 and 46 m in Fig. 4.3.2, and to data for 20 and 10 m in Figs. 4.3.3-4.

Calculating the value of α appearing in Eq. (1) from the above results in the same way as in Sec. 4.3.3, one gets

$$\alpha = 0.48 \tag{23}$$

This is in reasonable agreement with the conventional value. The fit is not very good, however. From the general dependence of the wind speed profiles on stability, we know that for a given value of u_r, u_* will increase with increasing instability. Experimentally, however, S(f) decreases at high frequencies with increasing instability, at least from 20 m and up, as discussed in the beginning of the present section. This explains the negative value of λ- from the fit, in contradiction to Eq. (2a).

4.3.4 Conclusion

It has been shown that the inertial dissipation method will work well as an independent way to determine u_* for neutral stability data. Good agreement is obtained with the results for u_* found in fitting the wind speed profile to the logarithmic law and the Charnock relation.

To use the method, data for S(f), u(z) and the air - sea temperature difference must in general be present. S(f) must be determind in the inertial frequency region or as a limit from a lower frequency region, as defined by Eq. (18 - 19) for neutral data. The relative value of the first order correction term to the inertial subrange value S_{IS} was found to be 0.037 u(z) / (f z), thus the frequency must typically be of the order of 1 Hz to be in the relevant subrange.

For general stabilty, new values $\lambda_+ = 1.18$ and $\lambda_- = -0.122$ had to be introduced in the definition of $\beta(z/L)$, Eq. (2), in order to obtain agreement with the determination of u_* and L from the wind speed profile data discussed in Sec. 4.2.

With the limitation mentioned, the inertial subrange method to determine u_* seems to work well. Care must be taken, however, to include possible correction terms, dependent on the measurement strategy, to the high frequency end of the DFT spectra.

An indepeendet determination of z/L by the inertial subrange method does not seem to be possible for maritime data.

5. SUBTASK 4.2: TURBULENCE INTENSITY

Turbulence intensity is defined as the ratio between the r.m.s. value of the longitudinal wind speed fluctuations and the mean wind speed, both at height z,

$$I_u(z) = \sigma(z) / u(z) \tag{1}$$

The values of $I_u(z)$ presented here are calculated from the filtered time series, as described in Sec. 2.

5.1 Near-neutral conditions

It was observed in Sec. 4. that the two types of near-neutral data set investigated lead to slightly different results. The first of these data set was defined according to a limit on the air - sea temperature difference, Eq. (4.1.1), and was found to be biased towards unstable conditions with $<\lambda'> = -3.25\ 10^{-5}$ m/s^2. The "truly" neutral data, selected according to a condition on λ', had a corresponding mean value of $0.03\ 10^{-5}$ m/s^2. Turbulence intensity do in general depend less on stability than the wind speed profile. The data set used for a particular comparison will be stated.

5.1-M1: The modified Vickery (1983) model

Vickery (1983) proposed the simple model

$$I_u(z) = 0.10\ (z/80\text{m})^{-0.2}\ [u(80\text{m})/(50\text{m/s})]^{0.5} \tag{2}$$

i.e. a model using wind speed at 80 m as a reference. Since this is outside the height range of the present study, we will base the fit on the corresponding model using $z_r = 10$ m as reference height and $u_{r0} = 10$ m/s as a normalizing wind speed (this choice should make translation to other wind speeds as convenient as possible). What we have called the modified Vickery model will then be

$$I_u(z) = I(z_r,u_{r0})\ (z/z_r)^{-a}\ [u(z_r)/u_{r0}]^b\ , \quad u_{r0} = 10\ \text{m/s} \tag{3}$$

where $I(z_r,u_{r0})$, a and b are parameters to be fitted from the data. A least squares fit to this model is compared to the "near" neutral data in Fig. 5.1-M1, and is seen to give a reasonable fit with the following characterizing values:

$$I(z_r,u_{r0}) = 0.089,\quad a = 0.226,\quad b = 0.350,\quad \chi^2 = 172,\quad N_f = 60 \tag{4}$$

The qualitative properties of turbulence intensity are an increase with wind speed, and a decrease with height. Both these properties are exhibited by this model.

5.1-M2: The modified Standing (1990) model

The Standing model is also based on observations at 80 m height as a reference,

$$I_u(z) = I_u(80m)\ u(80m)/u(z) \tag{5}$$

and is supposed to be valid for the height range 40 - 80 m. As in the case of the Vickery model, we want to rewrite this model using $z_r = 10$ m as reference height,

$$I_u(z) = I_u(z_r)\ u(z_r) / u(z) \tag{6}$$

where $I_u(z_r)$ is taken as a parameter multiplying the inverse wind speed ratio. The wind speed ratio was in Sec. 4.1-M5 found to follow closely the logarithmic law with Charnock's relation. Using this, and allowing for a power-law dependency on the wind speed ratio, the revised model reads

$$I_u(z) = I_u(z_r)\ [\ln(z_r/z_0) / \ln(z/z_0)]^a \qquad z_0 = (a_{Ch}/g)\ u_*^2 \tag{7}$$

A comparison of this model to the experimental "truly" neutral data is shown in Fig. 5.1-M2, using the corresponding best fit value for the Charnock constant, $a_{Ch} = 0.0172$ (Table 4.1.6) and calculating u_* from the logarithmic profile subject to the Charnock relation (Sec.4.1-M5). The resulting values for the model parameters and statistical quantities were

$$I(z_r) = 0.103, \quad a = 2.42, \quad \chi^2 = 2953, \quad N_f = 61 \tag{8}$$

The modified model was able to follow the z-dependence of the data, but this resulted in a high value of the exponent a. The model is not able to fit both the observed z- and u_r-dependence of the turbulence intensity, and is therefore incompatible with our data.

Depending on the wind speed range chosen, the absolute value of the turbulence intensity at 80 m, $I_u(80m) = 0.07$ - 0.075, as recommended by Standing (1990), is compatible with an extrapolation of our data with height, using e.g. the modified Vickery model, Eqs. (3-4).

5.1-M3: The Ishizaki (1983) typhoon model

For the maximum turbulence intensity in typhoons, Ishizaki (1983) found

$$I_u(z) = 0.6 / \ln u(z) \qquad = \begin{cases} 0.20 & u(z) = 20 \text{ m/s} \\ 0.17 & u(z) = 30 \text{ m/s} \end{cases} \tag{9}$$

The concept of "maximum turbulence intensity" is not defined.

An examination of the distribution of turbulence intensity values was not included in this extension of the project. However, in the main part of the project, the cumulative

distributions of turbulence intensity were examined. For example, the value $I_{u1\%}$, which was exceeded by 1 % of the observations, was found to be stability dependent, and to decrease with wind speed for neutral and unstable atmospheric stability in the wind speed region 10 - 22 m/s where sufficient data were available. The observed decrease with wind speed for these two stability classes is in qualitative agreement with Ishizaki's relation. For stable conditions, the (extrapolated) $I_{u1\%}$ value seemed to increase with wind speed, and that may very well be the case for an overall value for wind speeds of 30 m/s and beyond.

As a conclusion, Ishizaki's relation is found to be too unspecific to be of much practical value.

5.1-M4: The Naito (1983) data

Naito (1983) found that

$$I_u(z) = \begin{cases} 0.089 & u < 12 \text{ m/s} \\ 0.11 & u > 12 \text{ m/s} \end{cases} \quad \text{for } z = 6.4 \text{ m} \tag{10}$$

Certainly, our data do not indicate a step function at u = 12 m/s. Using the modified Vickery model, Eqs. (3-4), to extrapolate down to 6.3 m, and taking u_r = 10 and 15 m/s as typical values for the indicated ranges, we find

$$I_u(z) = \begin{cases} 0.0995 & u_r = 10 \text{ m/s} \\ 0.114 & u_r = 15 \text{ m/s} \end{cases} \quad \text{for } z = 6.4 \text{ m} \tag{11}$$

which is in reasonable agreement with the Naito results.

5.1-M5: ESDU model

The ESDU (1982) model is stated to be valid for strong winds and neutral conditions, and may be written

$$I_u(z) = \frac{u_*}{u} \frac{a\,\eta\,[\,b + c \ln (z/z_0)]^{\,p}}{1 + d \ln [\,u_*/(f_c\, z_0)]} \tag{12}$$

$$\eta = 1 - z / h$$

$$p = \eta^{16}$$

$$h = u_* / (6\, f_c), \quad f_c = 1.31\ 10^{-4}\ s^{-1}$$

where a, b, c and d are parameters and f_c is the Coriolis frequency with the Sletringen value indicated. The ratio u_*/u will here be evaluated using the logarithmic law with the Charnock relation as discussed in Sec. 4.1-M5. A comparison of the model with the "truly" neutral data is shown in Fig. 5.1-M5, using the best fit value a_{Ch} = 0.0172 for the

Charnock constant (Table 4.1.6). The full line represents a fit to the data, the dashed line represents the original parameters given by ESDU, except that the normalizing parameter a is fitted causing the value to be reduced by 16%. This fitting is done since the filtering procedure applied to out data will reduce the turbulence intensity somewhat. The original value was a = 7.5. The parameter values are given in Table 5.1.1. Note that the free fit leads to a completely different structure of the model, the denominator being reduced to 1, and the c parameter changing sign.

Table 5.1.1 Parameter values for the ESDU model, Eq. (12), original set (a value renormalized) and least squares fit, both with χ^2 value and degrees of freedom, N_f.

Para. set	a	b	c	d	χ^2	N_f
ESDU*)	6.32	0.538	0.09	0.156	600	62
Lsq. fit	2.00	1.85	-0.060	$2\ 10^{-14}$	201	59

5.1-M6: Ad hoc model I

Looking at Fig. 5.1-M1 with the "near" neutral data, or Fig. 5.1-M2 with the "truly" neutral data, it is apparent that the u_r dependence may be fitted very well by a straight line at all heights. A fit to the model

$$I_u(z) = [\ I_0 + I_1\ u_r\ ]\ (z/z_r)^{\ a} \qquad (13)$$

gives the following parameter values and fit characteristics

$$I_0 = 0.0601, \quad I_1 = 0.0026\ \text{s/m}, \quad a = -0.218, \quad \chi^2 = 168, \quad N_f = 60 \qquad (14)$$

Replacing u_r by u_r^n in Eq. (13), a least squares fit yields the value n = 1.02 for the exponent, with no significant improvement of the fit. Thus the data suggest a truly linear rise of the turbulence intensity with wind speed, and a power law type decrease with height, as indicated by Eqs. (13 - 14). The resulting fit is shown in Fig. 5.1-M6.

5.1-M7: Ad hoc model II - "a la C_D"

Although the model Eq. (13) subject to Eq. (14) predicts a linear increase with reference wind speed u_r, the data do not exclude a curvature in the I_u - u_r relationship, as

e.g. indicated by the modified Vickery model Eq. (1) and seen at high wind speeds in Fig. 5.1.

A model which is consistent with the Charnock relation, and which corresponds to a curvature in the I_u - u_r relationship can be formulated as follows:

$$I_u(z) = \frac{\sigma_u}{u(z)} = \frac{\sigma_u}{u_*}\frac{u_*}{u(z)} = \frac{\sigma_u}{u_*}\frac{u_r}{u(z)}\frac{u_*}{u_r} \qquad (15)$$

Whereas many boundary layer studies indicate the first factor in the rightmost product to be a constant with values in the range 2.1 - 2.6 (O.J. Andersen, Task 1 report, Sec. 5), the second factor decreases essentially with height. The third factor equals the square root of the drag coefficient. As discussed in the Task 1 report, the drag coefficient may in reasonable agreement with the Charnock relation be written as a linear function of u_r,

$$C_D = A + B\, u_r \qquad (16)$$

Thus, a relation on the form

$$I_u = I_0\, (z/z_r)^{-a}\, [\, 1 + b\, (u_r/10 - 1)]^{1/2} \qquad (17)$$

$$I_0 = I_u \quad (\, z=z_r\,, \quad u_r = 10 \text{ m/s}\,)$$

is indicated by this discussion. Although the variation of $u_r/u(z)$ with z was well described in Sec. 4.1, a power law description was chosen here, in agreement with the model given by Eqs. (13-14). This of course is an indication that σ_u/u_* is not a constant.

A fit to the "truly" neutral data of the model Eq. (17) gives the following parameter values and fit characteristics:

$$I_0 = 0.0848, \quad a = 0.220, \quad b = 0.758, \quad \chi = 177, \quad N_f = 60 \qquad (18)$$

The resulting fit is shown in Fig. 5.1-M7.

5.1.8 Comparison and extrapolation of the neutral models

In Fig. 5.1.8, a comparison is shown between the Vickery, the "ad hoc" (M6) and the "à la C_D" (M7) models, all extrapolated to u_r = 40 m/s. The "truly" neutral data are also shown. As one may notice, there is really not much difference between the models in the range covered by the data. There is an indication that the slope of the data versus u_r increases with z, more than predicted by the models. For this reason, the ad hoc model should probably be used for a conservative extrapolation to high wind speeds for heights of 40 m and more.

The model values at 30 and 40 m/s are shown in Table 5.1.2, together with the statistical characteristics of the best fits to the "truly" neutral data.

Table 5.1.2 Turbulence intensity at three heights predicted by the three best fitting models at reference wind speeds of 30 and 40 m/s.

Model	χ^2	N_f	u_r = 30 m/s			u_r = 40 m/s		
			z=10m	z=20m	z=46m	z=10m	z=20m	z=46m
Vickery	186	60	0.1336	0.1153	0.0965	0.1508	0.1301	0.1089
Ad hoc	168	60	0.1381	0.1194	0.1001	0.1641	0.1418	0.1189
A la C_D	177	60	0.1346	0.1161	0.0972	0.1535	0.1325	0.1109

5.2 General atmospheric stability

The ESDU model, Eq. (12), is not intended for use at general atmospheric stability, although the quantities involved can of course be given a stability dependent definition

5.2-M1: Panofsky model

Panofsky (1977) suggests a relation supposedly valid for unstable atmospheric conditions,

$$\sigma_u / u_* = 12 - 0.5\ (z/L)\ , \quad L < 0 \tag{1}$$

where L is the Monin-Obukhov length. Using the M-O theory for the wind speed profile, as described in Sec. 4.2, a corresponding model for the turbulence intensity becomes

$$I_u(z) = \kappa\ a\ [\ 1 - b\ (z/L)\ ]\ /\ [\ \ln\ (z/z_0) - \psi_m(z/L)\ ] \tag{2}$$

A comparison of this model to the data with the normalizing parameter a fitted and b as specified by Panofsky (b = 0.5/12) is shown in Fig. 5.2-M1.1 for 3 stability classes with L < 0 (unstable conditions). The classes are as specified in Table 4.2.1 ("Neutral" is indeed slightly unstable, due to the cell division chosen). A corresponding least squares fit is shown in Fig. 5.2-M1.2. The quantitative characteristics are summarized in Table 5.2.1.

None of the fits are acceptable. Also, the lack of an adequate u_r-dependence, do in the free fit case force a sign-change in the b parameter. In accordance with M-O theory, the ratio $z/L = z\,\lambda'/(C_D^{3/2}\,u_r^2)$ is used as the stability variable both in Eqs. (1) and (2). As u_r increases, this term will reduce I_u corresponding to a smaller degree of dynamic instability. However, in the neutral limit, the Panofsky model Eq. (1) is reduced to $I_u = 12\,C_D^{1/2}\,u_r / u(z)$. As discussed in Sec. 4.1-M5, C_D increases with u_r. But tis is not sufficient to describe the full increase of I_u, since ratio $u_r/u(z)$ decreases. From Fig. 5.2-M1.1, it is apparent that the original value of the b-parameter in the model gives a qualitatively correct dependence on the stability parameter λ'. Due to the inherently incorrect u_r dependence of this model, the u_r-dependence of z/L causes a change of sign in the b-parameter in the least square fit. This gives an improved dependence on u_r which in the fitting outweighs the resuling incorrect stability dependence.

Table 5.2.1 Parameters of the Panofsky model Eq. (2) for original values (normalized) and a least squares fit. χ^2 and degrees of freedom for the fits are also given.

Parameter set	a	b	χ^2	N_f
Panofsky (nor)	2.16	0.042	5 112	270
Least squ. fit	2.18	-0.100	4 907	269

5.2-M2: General ad hoc model

In Sec. 5.1-M6 a good description was found for the neutral data. In the neutral limit, a model for general stability should be compatible with the neutral description. A general model satisfying this criterion is

$$I_u(z) = [\, I_0 + I_1\, u_r \,]\,(z/z_r)^a\,[\, 1 - I_L\,(z/L)\,(u_r/10\text{m/s})^{-b}\,(z/z_r)^{-c}\,] \qquad (3)$$

where an extra term proportional to the traditional M-O variable z/L is included (see 5.1). A test against the data shows that this stability term must be multiplied by a power of $(u_r/10\text{m/s})$ and a power of (z/z_r) to get the correct reference wind speed and height dependence. The scale factors were introduced to normalize the coefficient I_L at $u_r = 10$ m/s and $z = z_r$. A least squares fit to the data is shown in Fig. 5.2-M2, where the complete data set is included. During the fit, the λ' region was divided into 7 classes of width $0.4\ 10^{-4}$ m/s^2 to get the same neutral class as in the "truly" neutral data set. The ranges for the plot is shown in Table 5.2.2.

The fit did not depend very much on whether we took the first 3 parameters from the corresponding fit of the "truly" neutral data, Eqs. (5.1.13-14) or not. Keeping the parameters defined in the neutral fit as before, the values of the extra parameters in Eq. (3) were found to be

$$I_L = 1.26 \quad b = 1.52 \quad c = 0.85 \tag{4}$$

and the corresponding statistical parameters were

$$\chi^2 = 752 \qquad N_f = 296 \tag{5}$$

Statistically, the fit could have been better, but the main properties of the data are reproduced by the model.

Table 5.2.2 Stability classes used in Fig. 5.2-M2.

Plot notation	Fit class(es)	Range $10^{-4}ms^{-2}$
Stable	7	0.0 to 0.4
Neutral	6	-0.2 to 0.2
Unstab	4 - 5	-1.0 to -0.2
S.Unst	1 - 3	-2.2 to -1.0

When this model is extrapolated to u_r = 40 m/s, the predicted values of the turbulence intensity differs by some one per mille across the stability classes. For practical purposes, the values of the "Ad hoc" model given in Table 5.1.2 may therefore be used at high wind speed values even for this generalized model.

6. SUBTASK 4.3: REFERENCE GUST FACTORS

The gust factor of wind speed at height z for a time interval t_g is defined as the ratio between the highest mean value over the interval and the period mean value

$$G(t_g,T,z) = \max\{ \frac{1}{t_g\, u(z)} \int_0^{t_g} u(z,\tau)\, d\tau \} \quad (1)$$

The corresponding reference gust factor for a time interval t_g is defined by comparison to the reference mean wind speed,

$$G_r(t_g,T,z) = \max\{ \frac{1}{t_g\, u_r} \int_0^{t_g} u(z,\tau)\, d\tau \} \quad (2)$$

Experimental data will be presented for the reference gust factor only. The evaluation has been based on the filtered time series defined in Sec. 2.

The models and data to which the experimental data are going to be compared, are however, defined for G rather than G_r. From the above definitions,

$$G_r(t_g,T,z) = G(t_g,T,z)\, [\, u(z) / u_r \,] \quad (3)$$

The wind speed profile was in Sec. 4 quite successfully described using the logarithmic law combined with the Charnock relation for neutral stability, and the M-O extension of this law for general stability. These relations, with the lsq. fit parameters established in Sec. 4, will therefore be used for the wind speed ratio in Eq. (3) to convert a model for G to a model for G_r.

The time intervals (gust lengths) specified for the present investigation are given in Table 6.1.1 together with the actual values used (they have to be a multiple of the sampling period). The exact values of t_g / T used in the models are also given.

Table 6.1 Length of gust intervals t_g specified and used, and exact value of t_g/T used.

t_g specified	1 s	10 s	1 min	10 min
t_g used	1.17 s	10.5 s	59.8 s	10 min
t_g/T used	1/2048	9/2048	51/2048	1/4

6.1 Near neutral conditions

In this section, the models are compared to the "truly" neutral data discussed in Sec. 4.1 and 5.1, their mean value of the M-O stability parameter was $<\lambda'> = 0.03\ 10^{-5}$. The wind speed ratio entering in (3) is supposed to be given by

$$u(z)/u_r = 1 + \alpha \ln(z/z_r), \qquad \alpha = 1 / \ln(z_r/z_0) \tag{4}$$

The Charnock relation with $a_{Ch} = 0.0172$ (Sec. 4.1-M5) is used to calculate z_0.

6.1-M1: The Mackey et al. model

Mackey et al. (1970) have proposed

$$G(t_g,T,z) = 1 - 0.62\ I_u^{1.27} \ln(t_g/T) \tag{5}$$

The aim is to obtain a model specifying a numerical value for G, rather than comparing two quantities computed from the experimental data, here G and I_u. In comparing Eq. (5) to experimental data, therefore, the ad hoc model described in Sec. 5.1-M6 was used to specify I_u. Furthermore, it might be argued that both the absolute and relative dependence on $\ln(t_g/T)$ may be influenced by the filtering process applied to the data in this investigation. An extra constant multiplying I_u, but independent of $\ln(t_g/T)$, was therefore allowed. Using (3), the final expression for G_r to be compared to the experimental data is

$$G_r(t_g,T,z) = [\ u(z) / u_r\ ]\ \{\ 1 - [\ a + b \ln(t_g/T)\ ]\ I_u^{1.27}\ \} \tag{6}$$

where Eq. (4) was used to calculate the wind speed ratio.

The resulting least squares fit is shown in Fig. 6.1-M1. The values of the fitted parameters and the fit characteristics are

$$a = 1.08, \quad b = 0.98, \quad \chi^2 = 1598 \quad N_f = 253 \tag{7}$$

If also the exponent on I_u in (4) is allowed to vary in a least squares fit, a value not significantly different from 1 is obtained. This model then coincides with the one discussed next.

6.1-M2: The modified Mackey/Ishizaki model

Ishizaki (1983) proposed the relation

$$G(t_g,T,z) = 1 - 0.5\ I_u \ln(t_g/T) \tag{8a}$$

$$I_u = 0.6 / \ln u(z) \tag{8b}$$

to describe extreme gusts during typhoons. The distribution of gust factor values was discussed in the main project, but this topic has not been included in this project extension (cmp. Sec 5.1-M3, where the similar situation for turbulence intensity was described).

As mentioned in the last section, fitting the exponent in the Mackey relation (5) results in a model of the same general type as (8a), if I_u is defined by the ad hoc model of Sec. 5.1-M6. From Fig. 6.1-M1 it is apparent that the dependence on the gust interval t_g is not well described by Eq. (6) for small values of t_g. The dependence on $\ln(t_g/T)$ was therefore generalized to second order, giving the model

$$G_r(t_g,T,z) = [\, u(z) / u_r \,] \{ 1 - [\, a + b \ln(t_g/T) + c\, (\ln(t_g/T))^2 \,] I_u \} \qquad (9)$$

where I_u and $u(z)/u_r$ are defined in the previous sections. The resulting least squares fit is shown in Fig 6.1-M2. The fit is very close. The corresponding parameters and fit characteristics are

$$a = 0.726, \quad b = 0.655, \quad c = 0.0188, \quad \chi^2 = 668, \quad N_f = 252 \qquad (10)$$

I_u increases linearly with u, according to the ad hoc model (5.1.13) used to parameterize I_u. Also the wind speed ratio exhibits a close to linear rise (cmp. Fig. 4.1-M5). Consequently, the rise of G_r with u_r predicted by (10) is also very close to linear. This feature is fully supported by the data. The fit parameters do not change significantly if the wind speed ratio is calculated with the logarithmic law constant evaluated from the linear fit of the drag coefficient, Eqs. (4.1.16-18), instead of the Charnock relation.

6.1-M3: The a + b ln(t_g) relation

The gust factor data examined by Smith and Chandler (1987) followed very closely the parameterization

$$G = a - b \ln(t_g) \qquad (11b)$$

$$a = 1.325, \quad b = 0.044 \qquad (11b)$$

where the parameter values (11b) correspond to a period T = 40 min, and neutral stability. The corresponding reference gust factor will then be given as

$$G_r(t_g,z) = [\, u(z) / u_r \,] [\, a - b \ln(t_g) \,] \qquad (12)$$

Eq. (4) was used to calculate the wind speed ratio. Note that the results (11) are based on data at 10 m only and are independent of wind speed u_r. The resulting least squares fit is shown in Fig. 6.1-M3. The values of the fitted parameters and the fit characteristics are

$$a = 1.290, \quad b = 0.043, \quad \chi^2 = 4221 \quad N_f = 253 \qquad (13)$$

The parameters are very close to those of Smith and Chandler. Looking at Fig. 6.1-M3, it is evident that this model does not reproduce the observed increase of G_r with reference wind speed. If only the data for $u_r > 15$ m/s are considered, coefficients are obtained which are even closer to the values (11b). However, since the model of Sec. 6.1-M2 gave a very good fit to our data, and apparently reproduced all the systematic variations, both with u_r, z and t_g, we do not see a need for further experimentation with the present model (12).

6.1.4 Comparison to Table 4.2 of the Task 1 report

In Table 6.1.1A and 6.1.1B, results based on the model described in Sec. 6.1-M2 are presented for the same heights and gust intervals as used in Table 4.2 of the Task 1 report by Andersen (1991). Results up to $u_r = 40$ m/s are presented. Please note that results for wind speeds higher than 30 m/s and for the heights 80 and 150 m represent extrapolations relative to the present data.

In Table 6.1.1A the results were converted to a one hour period, simply by using T = 3600 s in the model (9). The third column gives the wind speed ratio $u(z)/u_r$.

In Table 6.1.1B the results are calculated for a time base of T = 40 min, whereas the data in Table 4.2 in the Task 1 report are based on T = 1 h.

If data for 1 h periods are filtered the same way as in the persent investigation, much of the increase of the gust factor normally expected for a longer base period T would be taken out. But some increase is still expected.

As already discussed, our data suggest a linearly increasing gust factor with wind speed, whereas a common view in the literature is that there is not much variation with wind speed. When comparing to other data, both the preprocessing of the data and the reference wind speed will be important. Both the removal of trend and the digital filtering of harmonics with period longer than 10 min will reduce the gust factor compared to the "normal" situation where none of these measures are applied. Also the length of the basic period will enter. For comparison to "normal" data, where no or very little filtering is done, we would expect that the values of Table 6.1.1A would be most relevant. If data for a period of 1 h were processed by the same methods as used in this project, and all harmonics with a period longer than 10 min were removed, one would not expect too much change compared to the results for 40 the min periods, and in this case the data displayed in Table 6.1.1B would be of relevance. Thus, the true case is expected to fall somewhere in between the two tables.

Bearing the differences in mind when comparing to the data of Table 4.2 in the Task 1 report (T1-4.2), it is somewhat surprising that our estimates for the gustfactor in general are higher than the values given in this table. We have observed a rather strong increase of the reference gust factor with wind speed. Only the Exxon data (Entries C1, C2 and C3 in T1-4.2) are given for a defined wind speed. The data in Table 6.1.1A (T1A) are 2 - 5 % higher, with the greater differences for stronger wind and shorter gusts. The other entries in T1-4.2 must as a default be supposed to be valid for design wind speed. If this is taken

to be u_r = 40 m/s, almost all data in T1-4.2 are lower than the T1A data, the best match being the US Geological Service data (Entry E), which are some 4 % lower at 10 m height, compatible at 40 m and 4 % higher than our (extrapolated) data at 150 m.

A plot of the reference gust factor based on Eqs. (9-10) is shown in Fig. 6.1.4 for the height and wind speed range covered in the tables. Please bear in mind the extrapolation in z and u_r already mentioned.

Table 6.1.1A The reference gust factor versus height, wind speed and length of gust interval. The results are based on the model described by Eqs. (9-10). Conversion to a 1 h time base is done by using T = 3600 in (9). See text for comments.

z	u_r	$u(z)/u_r$	G_r 600s	G_r 60s	G_r 15s	G_r 5s	G_r 3s
10.0	25.0	1.000	1.049	1.207	1.290	1.350	1.376
	30.0	1.000	1.054	1.228	1.320	1.386	1.415
	35.0	1.000	1.059	1.250	1.350	1.422	1.454
	40.0	1.000	1.064	1.271	1.381	1.459	1.493
20.0	25.0	1.084	1.129	1.276	1.354	1.410	1.434
	30.0	1.089	1.139	1.303	1.389	1.450	1.477
	35.0	1.094	1.149	1.329	1.424	1.491	1.520
	40.0	1.099	1.159	1.355	1.458	1.532	1.564
40.0	25.0	1.167	1.209	1.346	1.418	1.469	1.491
	30.0	1.178	1.225	1.377	1.457	1.514	1.539
	35.0	1.188	1.240	1.407	1.496	1.559	1.586
	40.0	1.198	1.254	1.438	1.535	1.604	1.634
80.0	25.0	1.251	1.290	1.416	1.482	1.529	1.550
	30.0	1.267	1.310	1.451	1.524	1.577	1.600
	35.0	1.282	1.330	1.485	1.567	1.626	1.651
	40.0	1.297	1.349	1.520	1.610	1.675	1.702
150.0	25.0	1.327	1.363	1.479	1.540	1.584	1.603
	30.0	1.347	1.387	1.518	1.586	1.635	1.657
	35.0	1.367	1.412	1.556	1.632	1.687	1.710
	40.0	1.386	1.435	1.595	1.679	1.739	1.765

Table 6.1.1B The reference gust factor versus height, wind speed and length of gust interval. The results are based on the model described by Eqs. (9-10). Time base T = 2400 s. See text for comments.

Height z (m)	u_r (m/s)	$u(z)/u_r$	Gust interval (s)				
			600	60	15	5	3
10.0	25.0	1.000	1.018	1.181	1.267	1.328	1.355
	30.0	1.000	1.020	1.200	1.294	1.363	1.392
	35.0	1.000	1.022	1.218	1.322	1.397	1.429
	40.0	1.000	1.024	1.237	1.350	1.431	1.466
20.0	25.0	1.084	1.101	1.252	1.332	1.390	1.415
	30.0	1.089	1.108	1.276	1.365	1.428	1.456
	35.0	1.094	1.115	1.299	1.397	1.467	1.497
	40.0	1.099	1.122	1.323	1.429	1.506	1.539
40.0	25.0	1.167	1.183	1.323	1.398	1.451	1.474
	30.0	1.178	1.195	1.352	1.434	1.493	1.519
	35.0	1.188	1.207	1.380	1.471	1.536	1.564
	40.0	1.198	1.219	1.408	1.507	1.579	1.610
80.0	25.0	1.251	1.266	1.395	1.463	1.512	1.533
	30.0	1.267	1.283	1.427	1.504	1.558	1.582
	35.0	1.282	1.300	1.460	1.544	1.605	1.631
	40.0	1.297	1.316	1.492	1.585	1.652	1.680
150.0	25.0	1.327	1.340	1.460	1.523	1.568	1.588
	30.0	1.347	1.362	1.496	1.567	1.618	1.640
	35.0	1.367	1.384	1.532	1.611	1.667	1.692
	40.0	1.386	1.405	1.568	1.655	1.717	1.744

6.1.5 Comparison to Table 4.3 of the Task 1 report

The measured values of the gust factor from Table 4.3 in the Task 1 report are reproduced in Table 6.1.2, together with values calculated from the model (9-10) for the corresponding conditions. The wind speed ratio in Eq. (9) is of course excluded, since G is involved rather than G_r (cmp. Eq. 3). From the measured value of u(z) the corresponding values of u_r are given based on Eq. (4).

It is apparent from Table 6.1.2 that the measured values in hurricanes reported by Georgiou et al. (1987) are much higher than indicated by the present investigation (Sec. 6.1-M2) for the heights and wind speeds in question. The primary reason for this is likely to be the structural difference between hurricanes and extra tropical cyclones. But at the same time it is an indication that for certain condition, higher gust values may be expected than those given by the model defined in Eqs. (9-10).

Table 6.1.1 Measured gust factors in hurricanes (Georgiou, 1987), first line in each row, compared to model values based on Eqs. (9-10), second line. The values of the corresponding reference wind speed are also given.

Hurricane	Level (m)	u(z) (m/s) u_r	Gust intervals (s)			
			60	15	5	3
Danny	97	25.3 20.1	1.17±0.06 1.10	1.20±0.07 1.15	1.21±0.07 1.18	1.21±0.08 1.20
	60	19.0 16.0	1.27±0.14 1.10	1.34±0.17 1.15	1.38±0.18 1.18	1.39±0.18 1.19
	10	14.0 14.0	1.32±0.13 1.14	1.43±0.18 1.21	1.57±0.18 1.25	1.64±0.15 1.27
Juan	97	24.8 19.8	1.14±0.02 1.10	1.21±0.02 1.14	1.23±0.02 1.18	1.24±0.02 1.19
Camille	30	29.3 25.8	1.22 1.14	1.40 1.21	1.45 1.26	1.46 1.28

6.2 Reference gust factor for general stability conditions

The model (6.1.9) gives a reasonable description of the reference gust factor for general stability also, provided the wind speed ratio and turbulence intensity I_u are calculated by models with corresponding validity. Thus, the wind speed ratio is calculated by the model discussed in Sec. 4.2, using the least squares fit parameters for the full data set given in Table 4.2.2. The turbulence intensity is calculated by the model discussed in Sec. 5.2-M2, Eqs. (5.2.3-4). The resulting fits for the heights 10, 20 and 44 m (mean of data for 42 and 46 m) are shown in Figs. 6.2.1-3 for the stability classes defined in Table 5.2.2. The corresponding parameters and fit characteristics are

$$a = 0.803, \quad b = 0.732, \quad c = 0.0279, \quad \chi^2 = 3562, \quad N_f = 1196 \tag{1}$$

The properties of the observed reference gust factor at wind speeds below 15 m/s for the strongly unstable and stable stability classes are not very well fitted by the model, in particular that is true for the highest levels, cmp. Fig. 6.1.3. The high values for the stable class are particularly interesting. Since this phenomenon is outside the scope of the present investigation, it has not been further examined at this stage.

7. SUBTASK 4.4: ONE-POINT TURBULENCE SPECTRA

7.1 Introductory remarks

We will in this chapter discuss some 17 models for one point turbulence spectra, and their fit to the data. However, the parameters resulting from such a fit are dependent on the way the fitting is done, and we will start by discussing two technical points.

By definition, the frequency integral of the turbulence spectrum is equal to the variance, or the square of the total standard deviation, σ, of the data considered. In Sec. 7.1.1 it is pointed out that the σ defined in this way is not necessarily equal to the σ defined by turbulence intensity, which was discussed in Chapter 5.

Sec. 7.1.2 gives a brief presentation of how model parameters are determined from the data in the present work.

7.1.1 On the definition of variance

The turbulence spectral function S(f) represents the turbulence energy density as a function of the frequency f. When integrated over the full frequency range, the square of the total standard deviation of the wind speed fluctuations is obtained;

$$\sigma^2 = \int_0^\infty S(f)\, df = \int_0^\infty f\, S(f)\, d[\ln(f)] \qquad (1)$$

Experimental data are usually displayed versus log(f) which gives constant resolution in frequency on a relative scale ($\Delta f/f$). Thus, f S(f) is the relevant quantity to plot versus ln(f) or log(f).

In earlier sections, quite good representations of the turbulence intensity,

$$I_u(z) = \sigma_u(z) / u(z)$$

and the wind speed profile

$$u(z) / u_r$$

were obtained. However, in the determination of turbulence intensity in Chapter 5, the energy for frequencies below $f_0 = (10\ \text{min})^{-1}$ was explicitly removed. From the notion of a spectral gap in the spectral range of $(1\text{h})^{-1}$, one should perhaps expect

$$f\, S(f) \to 0 \text{ when } f \to f_0, \quad f_0 = (10\ \text{min})^{-1} = 4 / T_0 \qquad (2)$$

making the contribution to the integrals (1) negligible in the region below f_0. Looking at e.g. Fig. 7.2-M1, this is not seen to be true for our experimental data. Thus, $S(f_0)$ has an

appreciable value, and the variance corresponding to the turbulence intensity must be defined with a finite value δ of the lower limit of integration in the spectral integral,

$$\sigma_u(\delta)^2 = \int_{\delta}^{\infty} S(f)\, df, \quad \delta \simeq (3 \cdot 4)^{1/2}/T_0 = (693s)^{-1} \tag{4}$$

(the exact value of δ is complicated, as we go from summation to integration). To illustrate this point, one may estimate the magnitude of the remainder

$$\Delta\sigma^2 = \sigma^2 - \sigma_u(\delta)^2$$

for an explicit spectral representation. The best one parameter representation for neutral data discussed in Sec. 7.2 below turn out to be the Kaimal spectral representation which may be written

$$\frac{f\,S(f)}{\sigma^2} = \frac{2/3\ A\ x}{[1 + A\ x]^{5/3}} \qquad x = f\,z/\,u(z) \tag{5a}$$

where A is the characteristic constant of the spectrum, being about 75 for our data and σ^2 is defined by Eq. (1). An alternative, but equivalent formulation is

$$\frac{f\,S(f)}{\sigma^2} = \frac{\gamma}{[1 + 1.5\ \gamma]^{5/3}} \qquad \gamma = f\,/f_{max} \qquad f_{max} = 1.5\ u(z)/(z\ A) \tag{5b}$$

where f_{max} is the frequency where f S(f) has its maximum value. The fraction of the variance below δ may then be expressed as

$$\frac{\Delta\sigma^2}{\sigma^2} = 1 - \frac{1}{[1 + 1.5\ \gamma_0]^{2/3}} = \gamma_0 - 5/4\ \gamma_0^{\,2} + 5/3\ \gamma_0^{\,3} - 55/24\ \gamma_0^{\,4} + \ldots \tag{6}$$

where $\gamma_0 = \delta/f_{max}$. As an example, for u = 10 m/s and z = 46 m, one finds $\gamma_0 = 0.35$ and $\Delta\sigma^2/\sigma^2 = 0.25$ for our data. For higher wind speed values and lower heights, the correction is smaller. The Kaimal model is compared to experimental data in Fig. 7.2-M3, and appears to underestimate S(f) in the region $f < \delta$. Because of the direct z and u(z) dependence of the correction, it will influence the analytical parameterization of the variance in an essential way. Therefore, $\sigma_u = I_u\ u(z)$, evaluated as in Chapter 5, cannot be used instead of σ in normalized spectral formulations as Eq. (5). In the lack of an independent determination, σ must be treated as an unknown function. But theories relating σ to u_* may be used, because u_* is related to the mean wind speed profile.

7.1.2 How models are fitted to the experimental data

The experimental data for f S(f) presented here are calculated from the FFT-coefficients of the wind speed time series of successive 40-min periods. Trends are

removed by subtracting a 40-min moving average from the measured data, as discussed in Sec. 2.

Ensemble averages of the data are calculated for each logarithmically spaced frequency interval, each height and for classes of wind speed and stability. The spectral subdivision is the same as described in Andersen et al. (1991), with three spectral intervals per factor two in the frequency scale. The wind speed classes are of width 1 m/s in the range 10 to 26 m/s. The stability classification is discussed below.

In addition to the ensemble average value M_i for each cell, a standard deviation σ_i is also calculated in the standard way from the experimentally observed spread of the cell values. The weight

$$\begin{aligned} W_i &= N_i / \sigma_i^2 \qquad f \geq f_0 \\ W_i &= 0 \qquad\qquad f < f_0 \end{aligned} \tag{7}$$

where N_i is the number of 40 min. periods included in the variable cell, is used in the least squares fitting to estimate the parameters of the spectral model for S(f). An ad hoc smoothing procedure is used to avoid undue statistical fluctuations in W_i in cases where N_i is small. The χ^2-value defined as

$$\chi^2 = \text{Minimum} \ \{ \Sigma \ W_i \ [M_i - S(f_i)]^2 \} \tag{8}$$

is used to indicate the goodness of fit. Experimental data for the 3 frequencies below f_0 are thus assigned zero weight in the fitting, but are included in the plots shown below.

The spectral corrections discussed in Sec. 4.3.1 are applied to the models of S(f) before comparison with the data.

7.2 Near-neutral conditions

As in the preceding sections, the criterion

$$| \lambda' | < 2 \ 10^{-5} \ m/s^2 \tag{1}$$

is used to select neutral data. This leaves us with 567 time series with $u_r > 10$ m/s in the maritime sector. As noted earlier, the mean value of λ' for this selection is $<\lambda'> = 3.42 \ 10^{-7} \ ms^{-2}$.

When u(z) or u_* appear in the models for S(f), they are evaluated using the logarithmic model in combination with the Charnock relation and the best fit parameters as discussed in Sec. 4.1-M5. If the linear u_r-fit of the drag coefficient, defined by Eqs. (4.1.15-18), is used to calculate u_* and u(z), this does not significantly change neither the fit nor the parameters.

7.2-M1: Harris' model

Harris (1971) proposed the following spectral model

$$\frac{f\,S(f)}{u_*^2} = \frac{4\,C\,x}{(2\,B + x^2)^{5/6}} \qquad x = f\,L/u(z), \quad 1200 < L < 1800\ \text{m}, \quad B = C = 1 \qquad (2)$$

where B and C are introduced as multipliers to the original parameters. In conjunction with this formula, NPD has recommended

$$L = 1800\ \text{m}, \qquad u_*^2 = a\,u_r^2 \quad a = 3\ 10^{-3} \qquad (3)$$

Thus, S(f) can be calculated from (2) and (3) if the mean wind profile is known. Our data and a least squares fit of Eqs. (2-3), with B and C left as free parameters, are shown in Fig. 7.2-M1. Note that u_* is now calculated from (3) and not from the logarithmic model with the Charnock relation. The resulting parameter values are

$$B = 2.64, \qquad C = 0.497, \qquad \chi^2 = 89\ 695, \qquad N_f = 1405 \qquad (4)$$

and the fit as such is rather bad. The Harris spectrum is too peaked when compared to our data, as noted in the main report (Andersen et al. 1991), and a constant scaling length L does not allow any z-dependence (except in u(z)).

7.2-M2: Davenport's model

Davenport (1961) has proposed the spectrum

$$\frac{f\,S(f)}{u_*^2} = \frac{4\,C\,x^2}{(B + x^2)^{4/3}} \qquad x = f\,L/u(z), \quad L = 1200\ \text{m}, \quad B = C = 1 \qquad (5)$$

A least squares fit to the data is shown in Fig. 7.2-M2. The scheme of Sec. 4 based on the Charnock relation was used to evaluate u_* and u(z). The following values resulted from the fit

$$B = 0.977, \quad C = 0.629, \quad \chi^2 = 90\ 123, \quad N_f = 1405 \qquad (6)$$

Defining S(f) proportional to u_*^2 rather than u_r^2 (as implied by Eq. 5) will improve the fit when compared to M1, but the extra power of f (in x^2) is definitely not in agreement with our data, as compared to the other models, and destroys the gain.

7.2-M3: Kaimal's model

The rather popular Kaimal (1972) spectrum can be written as

$$\frac{f\,S(f)}{u_*^2} = \frac{105\,C\,x}{(B + 33\,x)^{5/3}} \qquad x = f\,z/u(z), \quad B = C = 1 \tag{7}$$

where the height z is used as the scaling length. Both u_* and u(z) are needed to calculate S(f). A least squares fit to the data is shown in Fig. 7.2-M3. The following values resulted from the fit

$$B = 0.640, \quad C = 0.834, \quad \chi^2 = 18\,825, \quad N_f = 1405 \tag{8}$$

Compared to the two previous models, the fit is much improved. The Kaimal spectrum is less peaked than the other classical models, and this improves the agreement with our data. Further, the high frequency part of the spectrum scales with z rather than a constant length L.

7.2-M4: Deaves & Harris' model

The model of Deaves and Harris (1978) is rather complicated, and are defined by the following set of equations

$$\frac{f\,S(f)}{\sigma_u^2} = \frac{0.115\,C\,x}{(0.041\,B + x^2)^{5/6}} \qquad x = f\,L(z,u)/u(z), \quad B = C = 1 \tag{9a}$$

$$L(z,u) = \frac{0.48\,\sigma_u^3}{\varepsilon(z)\,B(z)^{3/2}} \tag{9b}$$

$$B(z) = \begin{cases} 1 & z \geq z_c \\ [1 - (1 - z/z_c)^2\,]^{1/2} & z \leq z_c \end{cases} \tag{9c}$$

$$z_c = 0.39\,h\,[u_*/(f_c\,z_0)]^{-1/8} \tag{9d}$$

$$\varepsilon(z) = u_*^2\,\frac{du}{dz}\,[1 - z/h]^2 \tag{9e}$$

$$h = A\,u_*/(6f_c) \qquad A = 1 \tag{9f}$$

Here, f_c is the Coriolis parameter. σ_u was calculated using the ESDU formula Eq. (5.1.12), with the original coefficients. From the stated philosophy of using the best fit logarithmic/Charnock model of Sec. 4 to describe u(z), it follows that

$$\frac{du}{dz} = \frac{u_*}{\kappa\,z} \tag{10}$$

The model is compared to our data in Fig. 7.2-M4. The auxiliary parameters A, B and C introduced were determined by a least squares fitting, giving the result

$$A = 0.368, \quad B = 0.443, \quad C = 0.694, \quad \chi^2 = 36\,011, \quad N_f = 1404 \tag{11}$$

When the complexity of the model is taken into account, the fit is not very good. Mostly this is due to the peaked "Harris" shape imposed by the model, whereas the z- and u-dependence are not too bad.

7.2-M5: The ESDU model

The ESDU (1985) model is developed from the model discussed in the last section.

$$\frac{f\,S(f)}{\sigma_u^{\,2}} = \frac{2.987\,\beta\,x\,C}{[1 + (2\,\pi\,x)^2]^{5/6}} + \frac{1.294\,(1-\beta)\,x\,F_1\,C}{[1 + (2\,\pi\,x)^2]^{5/6}} \qquad x = \frac{f\,L(z,u)}{\alpha\,(u(z)} \tag{12a}$$

$$C = 1, \qquad F_1 = 1 + 0.445\,\exp[-0.76\,x^{-0.8}] \tag{12b}$$

$$\beta = 2.357\,\alpha - 0.761 \tag{12c}$$

$$A = \alpha^{2/3}\,(0.3858 - 0.3298\,\alpha) \tag{12d}$$

$$A = 0.115\,[1 + 0.315\,(1 - z/h)^6\,]^{2/3} \tag{12e}$$

$$L(z,u) = \frac{A^{3/2}\,\sigma_u^{\,3}}{\varepsilon(z)\,K(z)^{3/2}} \tag{12f}$$

$$K(z) = \begin{cases} 0.20\,Q_1 & z \geq z_c \\ 0.20\,Q_1\,[1 - (1 - z/z_c)^2\,]^{1/2} & z \leq z_c \end{cases} \qquad Q_1 = 1 \tag{12g}$$

$$z_c\,\ln(z_c/z_0) = 0.65\,h\,Q_2 \qquad Q_2 = 1 \tag{12h}$$

Here, $\varepsilon(z)$ and h are given by Eq. (9e-f), and σ_u are evaluated by Eq. (5.1.12) using the ESDU coefficient. Eqs. (12d-e) represent an implicit relation from which α is determined, and Eq. (12h) defines z_c implicitly. C is a normalization parameter, and Q_1 and Q_2 are two non linear parameters which are introduced by us to allow an adjustment of the original parameters. A least squares fit of this model to the data is shown in Fig. 7.2-M5. The corresponding parameter values are

$$C = 0.683, \quad Q_1 = 3.08, \quad Q_2 = 0.01, \quad \chi^2 = 26\,211, \quad N_f = 1404 \tag{13}$$

The very low value of Q_2 (actually the minimum value specified for the fitting procedure) means that the upper branch always in chosen in Eq. (12g), or

$$K(z) = 0.2\,Q_1 = 0.616$$

The fit to our set of data is not satisfactory, and is indeed inferior to the simple Kaimal model. The main problem is the "Harris" shape function, the additional F_1-function in the second term works i the wrong direction.

7.2-M6: Standing's model

Standing et al. (1990) have proposed a model which may be written

$$\frac{f\,S(f)}{\sigma_u^2} = \frac{0.66\,C\,x}{[x^{0.15\,Q2} + 9/8\,Q_3\,x]^{5/3}} \tag{14a}$$

$$\sigma_u = 0.075\,u(80m), \quad x = f\,L\,Q_1/u(z), \quad L = 1667\ m, \quad Q_1 = Q_2 = Q_3 = 1 \tag{14b}$$

Here C is a linear multiplier, and Q_1, Q_2 and Q_3 are non linear multipliers to the original parameters. The wind profile was calculated from the logarithmic law in combination with the Charnock relation. A comparison of this model to our data is shown in Fig. 7.2-M6. The multipliers were determined by a least squares fit, giving the result

$$C = 1.13, \quad Q_1 = 0.489, \quad Q_2 = 1.00, \quad Q_3 = 2.15, \quad \chi^2 = 66\,303, \quad N_f = 1403 \tag{15}$$

The z-dependence is not very well fitted by this model, but the frequency dependence is reasonably described.

7.2-M7: The Naito-Kaimal model

Naito (1983) used a normalized Kaimal spectrum, and found the best fit to be

$$\frac{f\,S(f)}{\sigma_u^2} = \frac{19\,x}{[1 + 57\,x]^{5/3}} \qquad x = f\,z/\,u(z) \tag{16}$$

Comparing to Eq. (7.1.5), one will observe that this spectrum is not properly normalized. If σ_u^2 is defined in analogy with eq. (7.1.3), then the r.h.s is too small by a factor of two if the lower limit of integration $\delta = 0$, and by more than a factor two if $\delta > 0$. Assuming that the denominator "57" is correct, the following version was fitted to the data

$$\frac{f\,S(f)}{\sigma_u^2} = \frac{(2/3)\,57\,C\,Q_1\,x}{[1 + 57\,Q_1\,x]^{5/3}} \qquad x = f\,z/\,u(z) \tag{17}$$

where Q_1 and C are auxiliary parameters.

Using the ad hoc model of Sec. 5.1-M6 to calculate σ_u and the logarithmic wind profile combined with the Charnock relation to calculate u(z), the following parameters are found

$$C = 1.53, \quad Q_1 = 1.61, \quad \chi^2 = 45\ 565, \quad N_f = 1405 \tag{18}$$

The fit is rather bad in this case, and much inferior to what was found in Sec. 7.2-M3, demonstrating that the use of σ as defined from the turbulence intensity (Sec. 5) does not work very well.

7.2-M8: The Vickery formula and the Phase I model

Based on data from Shiotani (1975), Vickery (1983) found the following general formula for the turbulent length scale L

$$L(z,u_r) = 200\ (z/z_r)^{0.2}\ (u_r/u_0)^{0.5} \qquad u_r = u(z_r), \quad z_r = 80\ \text{m}, \quad u_0 = 20\ \text{m/s} \tag{19}$$

where L is defined as the value of the ratio of u/f when f S(f) has its maximum value, or

$$L = u(z)/f_{max} \tag{20}$$

Defining f_{max} from our spectra is non trivial, and will in general require a spectral shape function to be fitted to the data. Based on results from the main project, the best single term spectral function can be expected to be on the form

$$f\,S(f) = \frac{A(z,u_r)\ \gamma}{[1 + 1.5\ \gamma^n]^{5/3n}} \qquad \gamma = f/f_{max}, \qquad f_{max} = u_r / L(z,u_r) \tag{21}$$

where A and L will be functions of u_r and z. In agreement with the main project results, these functions are assumed to be given by power law relations,

$$\begin{aligned} L &= L_0\ (z/z_r)^{Q1}\ (u_r/u_0)^{Q2}, \quad z_r = 10.5\ \text{m}, \quad u_0 = 20\ \text{m/s} \\ A &= C\ u_r^2\ (z/z_r)^{Q3}\ (u_r/u_0)^{Q4} \end{aligned} \tag{22}$$

A least squares fit to the data gives the following results

$$n = 0.468$$

$$L(z,u_r) = 890\ \text{m}\ (z/z_r)^{0.677}\ (u_r/u_0)^{0.251} \tag{23a}$$

$$A(z,u_r) = 0.0738\ u_r^2\ (z/z_r)^{-0.216}\ (u_r/u_0)^{0.752}$$

A numerical integration over frequency gives the total variance corresponding to this fit as

$$\sigma^2 = 0.238\ A(z,u_r) = 0.0176\ u_r^2\ (z/z_r)^{-0.216}\ (u_r/u_0)^{0.752} \tag{23b}$$

The fit characteristics were

$$\chi^2 = 4\ 194, \quad N_f = 1400 \tag{24}$$

The fit is shown in Fig. 7.2-M8. This fit is quite good. The powers of the (z/z_r) and (u_r/u_o) factors in A and L are coupled, and their respective values will depend on the frequency region being fitted. Extrapolation of our results to z = 80 m and U(80m) = 20 m/s, gives L ≃ 3250 m, 16 times the value found by Vickery.

7.2-M9: On some of the conclusions of Eidsvik

Eidsvik (1982) has concluded that the inertial subrange law ($f^{-2/3}$ - dependence) is valid for frequencies above 10^{-2} Hz. This is not in agreement with our results, as may be seen by consulting any of the graphs. This point was also discussed in Sec. 4.3. The limit will depend on height and wind speed, and quantitative limits are given by Eqs. (4.3.17-19) for a high frequency parameterization by the Kaimal spectral function.

A second conclusion of Eidsvik is that the spectral density at 10^{-2} Hz and 110 m height is adequately represented by

$$S(f=0.01Hz,\ z=110m) = 2\ 10^{-2}\ u_{110}^{8/3} \tag{25}$$

where u_{110} is the local wind speed.

From eg. Fig. 7.2-M8 it is seen that the value of f S(f) is rather constant, and near the maximum value in the 0.01 Hz region. The value of f S(f) at maximum is from Sec. 7.2-M8 approximately given as

$$[f\ S(f)]_{max} = 2.5^{-5/3n}\ A(z,u_r) = 0.00282\ u_r^2\ (z/z_r)^{-0.216}\ (u_r/u_0)^{0.752} \tag{26}$$

Using this result and the wind speed profile data from Sec. 4.1-M5 (assuming a wind speed region around u_r = 25 m/s giving α = 0.124), we get

$$S(f=0.01Hz,\ z=110m) = 0.018\ u_r^{2.75} = 0.009\ u_{110}^{2.75} \tag{27}$$

The difference in the wind speed exponents (2.75 versus 2.67) means that our result is about 60 % of that of Eidsvik's when compared at u_{110} = 30 m/s. Consulting Fig. 7.2-M8, this is seen to be within one standard deviation of the observed values, which tend to be somewhat higher than the model values in the 0.01 Hz region.

7.2-M10: Lacour's model

Lacour (1979) has proposed the model

$$\frac{f\,S(f)}{u_*^2} = \frac{E\,f}{(1 + E^{3/5} f)^{5/3}} = \frac{f}{(E^{-3/5} + f)^{5/3}} \qquad (28)$$

with the prescription that the quantity E should be estimated by equating the integral of the spectral function S(f) to the integral of the observed spectrum. This is in general a rejectable criterion for determining such a parameter, except in the case that S(f) is constant in the region of interest. The total variance following from (28) is $\sigma^2 = 1.5\, u_*^2\, E^{2/5}$, and equating this to the M8 estimate, Eq. (23b), at z = 20 m and u_r = 20 m/s gives E = 52.6. Applying a least squares fit, which normally also will ensure that the integral condition is approximately fulfilled, gives a much smaller value for E. This is explained by the weighting, which makes the high f region critical in the fitting process. The characteristics of the fits are

$$E = 52.6,\ \chi^2 = 4\ 827\ 598,\ N_f = 1407 \quad \text{(integral principle)}$$
$$E = 2.62,\ \chi^2 = 407\ 808,\ N_f = 1406 \quad \text{(least squares)} \qquad (29)$$

A comparison to the data is shown in Fig. 7.2-M10 (remember the logarithmic scale when judging the fits). Also shown are curves corresponding to E = 1000. Note that the formulation (28) does not include any z-dependence for S(f), and that the wind speed dependence is included in the u_*-term only. Expanding (28) in the large f limit gives

$$\frac{f\,S(f)}{u_*^2} \to \frac{f}{(f^{5/3} + (5/3)\,E^{-3/5} f^{-2/3} + \cdots)} \to f^{-2/3}$$

whereas a more conventional model, like e.g. Kaimal's model Eqs. (7-8) has the large f expansion

$$\frac{f\,S(f)}{u_*^2} = \frac{105\,C\,x}{(B + 33\,x)^{5/3}} \to 0.31\,C\,x^{-2/3} = 0.21\,x^{-2/3} \qquad x = f\,z/u(z)$$

In comparison, the E or B parameters in the two models play a similar role, but the Kaimal model has better scaling properties and the C parameter is essential in adjusting the amplitude in the intermediate and large f region.

7.2-M11: The "blunt" spectrum

This is a Kaimal type of spectrum, but with no z- or u-dependence of neither the spectral (f S(F)) maximum point f_{max} nor the high frequency limit.

$$f\,S(f) = \frac{C\,u_*^2\,\gamma}{[1 + 1.5\,\gamma]^{5/3}} \qquad \gamma = f/f_{max} = f\,T_{max} \tag{30}$$

Assuming u_* to be defined by the Charnock relation as discussed in Sec. 4.1-M5, a least squares fit to the data gave the following parameters

$$C = 4.94, \quad T_{max} = 52.8\ s, \quad \chi^2 = 61\,651, \quad N_f = 1405 \tag{31}$$

The fit to the data is shown in Fig. 7.2-M11. As expected, the lack of z- and u-dependence in the spectral parameterization gives a bad fit compared to the original Kaimal model.

7.2-M12: The "pointed" spectrum

Compared to Eq. (21), the spectrum discussed in the last section had a shape constant n = 1, whereas the "pointed" spectrum has a shape constant n = 5/3, and is given by

$$f\,S(f) = \frac{0.6435\,C\,u_*^2\,\gamma}{[1 + 1.5\,\gamma^{5/3}]} \qquad \gamma = f/f_{max} = f\,T_{max} \tag{32}$$

The numerical factors imply a spectral normalization of $\sigma^2 = C\,u_*^2$. The same general comments as given in the previous section are valid in this case too. A least squares fit to the data gave the following parameters

$$C = 4.47, \quad T_{max} = 54.5\ s, \quad \chi^2 = 64\,555, \quad N_f = 1405 \tag{33}$$

The fit to the data is shown in Fig. 7.2-M12. Compared to the last section, a larger value the shape constant leads to a worse fit. This is not unexpected, since the free fit in Sec. 7.2-M8 gave n = 0.468. The assumption of different shape functions also influence the T_{max} and σ^2 value ($\sigma^2 = C\,u_*^2$). It should be mentioned that all these values are also influenced by the weighting and spectral region over which the fits are performed, since, obviously, all our fits are less than perfect.

A better estimate for T_{max} is given by the spectrum discussed in Sec. 7.2-M8, from which it follows that approximately

$$T_{max} = 420\,(z/z_r)^{0.667}\,u_r^{-0.749} \quad \text{(SI-units understood)} \tag{34}$$

demonstrating that T_{max} depends on height and wind speed. From the main project, and other sources, it is also known that T_{max} will depend on stability as well.

7.2-M13 The P2 spectrum

In the main part of this project, a two term model was used to discuss data for general stability. For neutral conditions, the model may be written

$$\frac{f\,S(f)}{u_r^{\,a}} = \frac{C_1\,(z/z_r)^{-b}\,f}{[f_{x1} + 1.5\,f]^{5/3}} + \frac{C_2\,f}{[f_{x2}^{\,n} + 1.5\,f^{\,n}]^{5/3n}} \qquad f_{xk} = 1/T_k \tag{35}$$

$$T_1 = Q_1\,z / u(z) \qquad T_2 = Q_2 / u(z) \tag{36}$$

Here, a, b and n are exponents to be fitted, Q_1 and Q_2 are two other non-linear parameters, and C_1 and C_2 are linear parameters. A least squares fit to the data yields

$$\begin{aligned} &C_1 = 2.52\ 10^{-5},\quad C_2 = 4.79\ 10^{-5},\quad a = 3.32,\quad b = 1.60,\quad n = 0.413 \\ &Q_1 = 18.5,\quad Q_2 = 3610\ \text{m},\quad \chi^2 = 3\ 504,\quad N_f = 1400 \end{aligned} \tag{37}$$

This represents the best fit to the neutral data. A plot is shown in Fig. 7.2-M13. Compared to Fig. 7.2-M8, where the next best fit is presented, the present model gives a slightly better fit in the low frequency range. Note that the first term becomes less important with increasing height.

7.3 General stability

The parameterization of stability and wind speed etc. will be along the same lines as used in Sec. 4.2 discussing turbulence intensity.

7.3-M1: The Højstrup model

Højstrup (1981, 1982) has proposed a model for unstable conditions which may be written

$$\frac{f\,S(f)}{u_*^{\,2}} = \frac{0.5\,C_1\,\eta_i\,(z_i/L)^{2/3}}{[B_1 + 2.2\,\eta_i^{\,5/3}]} + \frac{105\,C_2\,\eta}{[B_2 + 33\,\eta]^{5/3}} \qquad C_1 = C_2 = B_1 = B_2 = 1 \tag{1a}$$

$$\eta = f\,z/u(z) \qquad \eta_i = f\,z_i/u(z) \tag{1b}$$

where C_1, C_2, B_1 and B_2 are auxiliary parameters introduced for a least squares fitting, and z_i is the height of the convection layer. To evaluate this quantity, the Deaves and Harris expression was used.

$$z_i = u_* / (6\, f_c)$$

The Monin-Obukhov length L was calculated by Eq. (4.1.12), and u_* was calculated using the Charnock relation with parameters resulting from the fit of wind profile data for general stability discussed in Sec. 4.2. Fitting to the data, C_1 comes out negative (this also happens if the original values of the non-linear parameters are used, i.e. $B_1 = B_2 = 1$). The first term in the spectral expression is supposed to describe the convective part of the spectrum. In our experience, this is the least pointed part of the spectrum. In this model it has, however, been assigned to the most pointed of the two spectral terms, and in a free fit, this apparently causes the result described.

Thus, according to the conventional interpretation, $C_1 < 0$ is unphysical. Since the fit is not very good in any case, we see no point in discussing this particular model further. However, the two term model used in the main project, which is similar to the Højstrup model, is discussed in Sec. 7.3-M3 below.

7.3-M2: The Moraes and Epstein scheme

Moraes and Epstein (1987) have proposed a variation of the "pointed" spectrum to describe the data for stable conditions

$$f\,S(f) = \frac{0.744\, \gamma\, \sigma^2}{[1 + 1.5\, \gamma^{5/3}]} \qquad \gamma = f / f_{max} \tag{2}$$

$$f_{max} = 0.0453\, Q_1\, (u/z)\, [1 + 2.5\, Q_2\, (z/L)^{3/5}\,]^{3/2} \tag{3}$$

$$\sigma^2 = C\, u_*^2$$

Here, we introduced the auxiliary parameters C, Q_1 and Q_2 to adjust the numerical parameters to our data ($Q_1 = Q_2 = 1$ in the original formulation, the formula given in Andersen (1991) contains a normalization error).

A least squares fit to the data with u_* and L determined as explained in Sec. 7.3-M1, gave the result

$$C = 3.58, \quad Q_1 = 1.008, \quad Q_2 = 0.456, \quad \chi^2 = 63\,811, \quad N_f = 3340 \tag{4}$$

Three classes in λ' in the range 0 to $0.6\ 10^{-4}$ were used in the fitting. In the plots shown in Figs. 7.3-M2a-c, the mean values for the two higher classes are shown. Of a total of 350 periods with $\lambda' > 0$, the lowest class (labelled "Stable" in the plots) contains 293 periods.

The fit is not very good. The χ^2 value obtained in the next section for all periods (general stability), with twice as many degrees of freedom, is one third of the value found here.

7.3-M3: The P2 spectrum for general stability

In the main part of this project, a two term model was used to discuss data for general stability. In the present context, the model may be written

$$\frac{f\,S(f)}{u_r^{\,a}} = \frac{C_1\,(z/z_r)^{-b}\,f}{[f_{x1} + 1.5\,f]^{5/3}} + \frac{C_2\,f}{[f_{x2}^{\,n} + 1.5\,f^{\,n}]^{5/3n}} \qquad f_{xk} = 1\,/T_k \tag{5}$$

$$T_1 = Q_1\,z\,/\,u(z) \qquad T_2 = Q_2\,\exp(-Q_3\,\rho)/\,u(z)$$

$$n = n_0 + n_1\,\exp(Q_4\,\rho) \qquad \rho = \lambda'\,(u_r/10)^{-c} \tag{6}$$

Here, a, b and c are exponents to be fitted; n_0, n_1 and Q_4 determine the shape of the second spectral function, and Q_1, Q_2, and Q_3 determine the position of the maxima of the spectral functions. C_1 and C_2 are linear parameters. A least squares fit to the data yields

$$C_1 = 2.67\;10^{-5},\quad C_2 = 5.49\;10^{-4},\quad a = 3.28,\quad b = 1.68,\quad c = 2.68$$

$$n_0 = 0.1893,\quad n_1 = 0.0325,$$

$$Q_1 = 24.3,\quad Q_2 = 17\,380,\quad Q_3 = 40\,240,\quad Q_4 = 26\,960 \tag{7}$$

$$\chi^2 = 16\,430,\quad N_f = 6\,588$$

The fitted curves are compared to the data in Figs. 7.3-M3a-c. The stability classes used in the fitting and the plots are given in Table 5.2.2. Although there are systematic deviations between the curves and the data in certain regions, the overall fit is quite good.

7.4 Extrapolation to design wind speed and conclusions

In Fig. 7.4.1-3 observed and calculated low frequency spectra for neutral conditions are shown versus reference wind speed for 46, 20 and 10 m height, respectively. The experimental points represent mean values for three frequency intervals, the mean frequency being 0.00194 Hz. The bars indicate the standard deviation of the sample. The curves represent the Phase 2, Phase 1, Kaimal, Standing, ESDU and Deaves-Harris models evaluated at the mean frequency. Only the Phase 1 and Phase 2 models give a credible representation of the data in this frequency interval.

In Figs. 7.4.4-6 a corresponding set of plots are shown for the 0.01 Hz region. Again the experimental points represent mean values for three frequency interval, the mean frequency being 0.0108. Again, only the Phase 1 and Phase 2 models seem to give a reliable representation of the data at all heights. The Phase 1 model seem to have a slightly more trustworthy wind speed dependence.

The same set for the 0.1 Hz region is shown in Figs. 7.4.7-9. The experimental data are mean values for two frequency intervals, the mean frequency being 0.102 Hz. Only the Standing model is clearly "off" in this case. But again, both the Phase 1 and Phase 2 models give a very good representation of the data.

All observations in this project suggest spectra that are less peaked than those discussed in the literature. The spectra discussed in the main report (Andersen et al. 1991), presented in Secs. 7.2-M8, 7.2-M13 and 7.3-M3 above, gave by far the best fit to the data.

Because f S(f) does not go to zero at the lowest frequency considered, $f_0 \simeq (600\ s)^{-1}$, it is not practical to use the directly observed variance calculated from the turbulence intensity, as discussed in Sec. 4.2, to normalize the spectra. Since the absolute value of the spectral turbulence is given by the experimental data, this is not a great problem. The spectra do indeed demonstrate that if one wants to discuss the total variance, one should always be careful to state the corresponding spectral interval.

8. SUBTASK 4.5: COHERENCE SPECTRA

Coherence is a measure of the correlation (independent of phase) between the individual frequency components of two time series over a given time period. The same methods as discussed in the Phase 2 report, Sec. 5.4, will be used to parameterize the observed coherence spectra.

8.1 Evaluation of the parameters of the coherence spectra

Coherence has to be evaluated from ensemble averages of cospectra, quadrature spectra and the one point spectra of the two sets of time series. A faithful estimate requires an average over many frequency values or many realizations. In the low frequency region, only one frequency value occur within each variable cell, with the intervals chosen in this investigation. Thus, unless the ensemble is divided into subensembles, only one estimate of the coherence for a given variable cell will in general be available, and a direct experimental evaluation of the variance of the coherence estimate is not possible. This is in contrast to the one point spectra, where each time series gives an estimate of the spectral density. Since the variable cells used in this investigation are effectively rather small, a good indication of the effective variance of the estimates is obtained by studying the scatter between estimates for neighbouring variable cells.

The parameters of a particular model are estimated by a least squares minimalization of the difference between experimental and model values,

$$LSQ = \text{Minimum}\{ \sum_i W_i [Coh_{i,Exp} - Coh_{i,Mod}]^2 \} \qquad (1)$$

where W_i is the number of time series available for variable cell No. i, and the sum runs over the set of variable cells available. Note that this weight function is independent of frequency. The same set of frequency intervals is used as in the discussion of one point spectra.

A root mean square value of the deviation between experimental and model values of the coherence will be defined as

$$\Delta_{rms} = [LSQ / N]^{1/2}, \qquad N = \sum_i W_i \qquad (2)$$

Because coherence numerically is limited to the interval [0,1], and is a measure of the correlation (independent of phase) between the frequency components in the time series involved, Δ_{rms} may be used as an overall measure of the goodness of fit when comparing different models. However, the individual plots comparing experimental and model values should also be inspected to check that the fit is reasonable within each region of the variable range.

8.2 Fitting models of coherence for vertical separation

The fits are based on the Sletringen data for neutral stability, as defined by Eq. (7.2.1). Also the other conditions discussed in Sec. 7.2 will apply. Thus the friction velocity u_* and the wind speed at a general height will be evaluated using the Charnock relation and the logarithmic model with the best fit parameters as discussed in Sec. 4.

The four heights at Sletringen give six possible combinations for the pairs of heights, z_1, z_2, which are all used in the fitting described below.

8.2-M1: Davenport's model

Davenport (1961) has proposed the model

$$\text{Coh} = \exp[- a_z \, \Delta z \, f / u(z_g)], \quad \Delta z = | z_1 - z_2 | \tag{1}$$

In our applications, the geometrical mean height,

$$z_g = [z_1 \, z_2]^{1/2} \tag{2}$$

has been used for z. Different values of the damping parameter a_z are reported in the literature. Davenport (1977a) found

$$a_z = 10 \tag{3}$$

Standing (1990) has used the same model, with the parameter value

$$a_z = 20 \tag{4}$$

A least squares fit to our data results in

$$a_z = 29.6, \qquad \Delta_{rms} = 0.080 \tag{5}$$

The fit is not particularly good, and is shown in Figs. 8.2-M1a-b. Mean values are shown for both experimental and model values for four wind speed classes.

The models discussed below indicate that the parameter a_z is a function both of the separation Δz and the geometrical mean height z_g. It is also known that a_z depends on stability. In the Phase 2 report, a_z was found to depend both on frequency and stability. The value of a_z obtained for a particular set of data will thus depend on the range of values of the external variables for the set.

8.2-M2: Shiotani's model

Shiotani (1975) proposed a generalization of the Davenport model, with a_z in Eq. (1) on the form

$$a_z = a_{z0} + a_{z1} \Delta z / z_g \tag{6}$$

with parameter values

$$a_{z0} = 2.7, \qquad a_{z1} = 17 \tag{7}$$

Again, "z" in the original formulation was replaced by the geometric mean of the two heights in question. Fitting this model to the data improves the fit considerably when compared to the simple Davenport model, the result being

$$a_{z0} = 13.7, \qquad a_{z2} = 20.1 \qquad \Delta_{rms} = 0.033 \tag{8}$$

The corresponding plots are shown in Figs. 8.2-M2a-b. The Phase 2 model discussed in Sec. 8.2-M4 below gives an even better fit to the data, and with reference to the discussion at the end of Sec. 8.2-M1, it is not possible to say if Shiotani's results, Eq. (7), are in direct disagreement with our data without looking at the two sets of data in more detail.

8.3-M3: The ESDU model

The ESDU (1985) model for coherence is defined by

$$coh = \exp[- 1.15 Q_3 \eta_1^{1.5 Q4}], \quad Q_3 = Q_4 = 1.0 \tag{9a}$$

where η_1 is given in terms of the quantities introduced in Eqs. (7.2.12e-h), and the additional relations

$$L_z = L(z_g,u) \{ 0.5 - 0.34 \exp[- 35 (z_g / h)^{1.7}] \} \tag{9b}$$

$$r_g = \Delta z / L_z \tag{9c}$$

$$b = 0.35 r_g^{0.2} \tag{9d}$$

$$\alpha = 0.747 r_g \tag{9e}$$

$$\beta = 2 \pi f \Delta z / u(z_g) \tag{9f}$$

$$c = 1.6 r_g^{0.13} [\alpha^2 + \beta^2]^{-b/2} \tag{9g}$$

$$\eta_1 = [\, \alpha^2 + c^2 \beta^2]^{1/2} \qquad (9h)$$

Q_3 and Q_4 are multipliers to the original parameters, and are allowed to vary during the fitting. In addition, the multipliers Q_1 and Q_2 were introduced in Eq. (7.2.12g-h). Numerically, multiplier values of one will give the same result as the original formulation. A least squares fit to the data yields

$$Q_1 = 0.97, \quad Q_2 = 0.01, \quad Q_3 = 3.61, \quad Q_4 = 0.88, \quad \Delta_{rms} = 0.034 \qquad (10)$$

These results are compatible with those obtained in fitting the single spectra to the ESDU model, Eq. (7.2.13). A smaller value for Q_1 in this case is compensated for by the rather large value of Q_3, the resulting model values are very roughly dependent on the product Q_1 Q_3.

Plots of the resulting fit are shown in Figs. 8.2-M3a-b. A striking feature of this model is that the coherence does not go to zero at f = 0, as the Davenport model, Eq. (1) indicate. Experimentally, such an effect will be observed if the wind speed profile is different for different time series, and this will in practice always be the case, for a variety of reasons, e.g small differences in the thermal stability, different history with differences in convective layer thickness, etc.

To our data, the very complicated ESDU-model is seen to give a slightly inferior fit than the Shiotani model. The ESDU model seems to exaggerate the possible deviations at small frequencies. However, the deviations at the lowest frequency values are excluded in calculating the Δ_{rms}, because of the uncertainties discussed earlier.

8.3-M4: Phase 2 models

In the Phase 2 work, a modified Davenport model, Eq. (1), was used. The damping coefficient, a_z, was parameterized as a function of z_g, Δz, f and lapse rate. For neutral stability, an equivalent formulation is

$$a_z = [\, a_{z0} + a_{z1} \exp(- b f)] \, \Delta z^q / z_{gr}^{\,p}, \quad z_{gr} = [z_1 z_2]^{1/2} / 10 \qquad (11)$$

A least squares fit to the data gives

$$a_{z0} = 18.3, \quad a_{z1} = 6.9, \quad b = 103.7, \quad p = 0.44, \quad q = 0.29, \quad \Delta_{rms} = 0.0246 \qquad (12)$$

The fit is shown in Figs. 8.2-M4a-b, and is quite good over the variable range covered. Note that $u(z_g)$ is used in the present model in agreement with Eq. (1), whereas u_{ref} was used in the Phase 2 work. This explains the lower value of p found here (p = 0.51 in the Phase 2 work). The agreement is otherwise reasonable.

Two simplifications of the above model have also been investigated. The most drastic is to skip the exponential term in (11), and write

$$a_z = a_{z0}\, \Delta z^q / z_{gr}^{\,p}, \quad z_{gr} = [z_1\, z_2]^{1/2} / 10 \tag{13}$$

The corresponding least square parameters are

$$a_{z0} = 16.7, \quad p = 0.44, \quad q = 0.35, \quad \Delta_{rms} = 0.0280 \tag{14}$$

The fits are shown in Figs. 8.2-M4c-d. To the eye, the fits are nearly as good as for the full model.

As mentioned in discussing the ESDU model, frequency independent sources could decrease the correlation. The main effect is assumed to be variations in the wind speed profile, with a net result proportional to $\ln(z_1/z_2)$. A possible parameterization is

$$\mathrm{Coh} = \exp[\, -\, \{\, [\, a_z\, \Delta z\, f / u(z_g)]^2 + c\, [\, \ln(z_1/z_2)]^2 \,\}^{1/2} \,] \tag{15}$$

where a_z is defined as in Eq. (13). Concerning the algebraic form of Eq. (15), the root of the sum of squares is assumed to give the combined effect. A least squares fit gives

$$a_{z0} = 16.8, \quad p = 0.42, \quad q = 0.33, \quad c = 0.116, \quad \Delta_{rms} = 0.0252 \tag{16}$$

The corresponding plots are shown in Figs. 8.2-M4e-f. The last model deviate strongly for the three lowest non counting f-values, and should probably not be recommended.

8.3 Models of coherence for lateral separation

Experimental data of coherence for lateral separation must be taken from Skipheia, where measurements from three masts are available. Whereas the air-sea temperature difference was used to define neutral conditions in the previous sections, this will not be a natural choice for the Skipheia station. Due to the distance from the sea, lapse rate must be used to classify the data.

During the Phase 2 work, coherence spectra from the Skipheia station were investigated in great detail. In particular, simple Davenport models were examined, and generalized to obtain a best fit model. In the case of neutral stability and lateral separation, the Phase 2 model may be written

$$\mathrm{Coh} = \exp[\, -\, a_y\, \Delta y\, f / u_r\,], \quad a_y = [\, a_{y0} + a_{y1} \exp(\, -\, b_y\, f)]\, (z/z_r)^{-p}$$

$$a_{y0} = 18.4, \quad a_{y1} = 65.5, \quad b_y = 78.9, \quad p = 0.42 \tag{17}$$

where the values for the restricted maritime sector were used (note that the neutral value of the sigmoid function used to parameterize the stability dependence is 0.5). This model is compared to a Davenport model,

$$\text{Coh} = \exp[- a_y \, \Delta y \, f / u(z)], \qquad a_y = 12 \tag{18}$$

where the coefficient value is due to Bowen et al. (1983), and an ESDU (1985) model in Fig. 8.3.1 for reference wind speed values of 20, 30 and 40 m/s, a height of 46 m and a separation $\Delta y = 80$ m. Whereas the Bowen and ESDU models agree quite well, there is a disagreement with the Phase 2 model. Panofsky and Dutton (1984) present results due to Kristensen et al. (1981) showing that with a model as defined by Eq. (18), $a_y \simeq 14$ at $\Delta y/z = 0$ increasing to $a_y \simeq 50$ for $\Delta y/z \geq 3.5$. A mean value of the height z for the Skipheia data is 40 m. At $u_r = 20$ m/s and $\text{Coh} = 0.5$, $a_y = 48$ is representative with a range in Δy from 79 to 205 m. Thus in the general case, a simple Davenport model (Eq. 18) is probably not able to give a precise description of lateral coherence. To see if there is a real disagreement between a set of results based on an incomplete model, a more complete investigation of the data is necessary.

ACKNOWLEDGEMENTS

The authors wish to thank Sverre Haver and John C. Heidemann for numerous discussions and valuable suggestions. We are in particular indebted to Svein Erik Aasen, Tore Heggem and Knut Mollestad who have made the raw data available and participated in the final stages of the production of this report.

REFERENCES

Aasen, S.E., 1989. "The maritime turbulent wind field, Measurements and models", Appendix report No. 1, ALLFORSK-AVH

Andersen, O.J., T. Heggem, J. Løvseth, K. Mollestad and S.E. Aasen, 1989. "Turbulence structure in the maritime wind field", Final report of Phase 1 of this project, University of Trondheim

Andersen, O.J., T. Heggem, J. Løvseth, K. Mollestad and S.E. Aasen, 1991. "The maritime turbulent wind field. Measurements and models", Final report of Phase 2 of this project, ALLFORSK-AVH

Andersen, O.J., 1991a. "The maritime turbulent wind field, a literature review" Statoil report

Andersen, O.J., 1991b. "The Frøya data base for wind, improvement of the data base for stability and wind direction". Final report for Task 2 of this project Phase 2, Extension 1. Statoil report

Bowen, A. et al., 1983. "Vertical coherence and phase delay between wind components in strong winds below 20m." Bound. L. Met., 25.

Chatfield,C., 1984. The analysis of time series, third ed., Chapman and Hall, London.

Davenport, A.G., 1961. "The spectrum of horizontal gustiness near the ground in high winds." Q. J. Roy. Met. Soc., 87.

Davenport, A.G., 1977. "Wind structure and wind climate. "Int. symp. safety of structures.

Deaves and R.I. Harris, 1978. "A mathematical model of the structure of strong winds." CIRIA Rep. 76.

Det Norske Veritas, 1977. "Rules for the design, construction and inspection of offshore structures."

Eidsvik, K.J., 1982. "Estimates of wind fluctuations during stormy conditions over the ocean." Univ. of Trondheim, Norway.

Eidsvik, K.J., 1984. "Large sample estimates of wind fluctuations over the ocean". Univ. of Trondheim, Norway.

Eidsvik, K.J., 1985. Boundary Layer Met. **32,** 103-132.

ESDU, 1982. "Strong winds in the atmospheric boundary layer. Part 1: Mean hourly wind speeds." Engin. Sc. Data Unit, 82026.

ESDU, 1985. See Ramsay et.al., 1988 for references.

Georgiou, P.N., 1987. "An assessment of the wind speed data measured at the Lena tower site during hurricanes Danny and Juan, 1985" Univ. of W. Ontario, BLWTL.

Harris, R.I., 1971. "The nature of wind, the modern design of wind sensitive structure", CIRIA.

Harris, R.I. and Deaves, 1980. "The structure of strong winds". CIRIA Conf. on wind Eng. in the Eighties.

Højstrup, J., 1981. "A simple model for the adjustment of velocity spectra in unstable conditions to an abrupt change in roughness and heat flux." Bound. L. Met., 21.

Højstrup, J., 1982. "Velocity spectra in the unstable boundary layer", J. Atmos. Sci. **39,** 2239-2248

Højstrup, J. et.al., 1984. "Modelling velocity spectra in the lower part of the planetary boundary layer." Bound. L. Met., 29.

Ishizaki, H., 1983. "Wind profiles, turbulence intensities and gust factors for design in typhoon-prone region." J. Wind Eng. Ind. Aerodyn.

Kaimal et al., 1972. "Spectral characteristics of surface layer turbulence." Q.J. Roy. Met.Soc., 98, 563-589.

Kristensen, L., H.A. Panofsky and D. Stuart Smith, 1981. "Lateral coherence if longitudinal wind components in strong winds" Bound. L. Met. 21, 199-205.

Lacour, E.E., 1979. "Application of wind theory to calculation of wind loads on structures located offshore." Exxon Prod. Res. Co

Macky, S. et al., 1970. "Gust factors." Proc., sem. on wind loads on structures. Hawaii, 1970.

Moraes & Epstein, 1987. "The velocity spectra in the stable surface layer." Bound. L. Met., 40.

Naito, G., 1983. "Spatial structure of surface winds over the ocean." J. of Wind Eng. and Ind. Aerodyn., 13.

NPD, 1988. "Retningslinjer for laster og lastvirkninger." Norwegian Petroleum Directory.

Panofsky, H.A. and J.A. Dutton, 1984. Atmospheric turbulence, John Wiley & Sons, New York.

Panofsky, H.A. et al., 1977. "The characteristics of turbulent velocity components in the surface layer under convective conditions." Bound. L. Met., 11, 355-361.

Ramsay et al., 1988. "Flow structure, sea states and models. Preliminary report no.1."; BLWTL; Univ. of W. Ontario.

Shiotani, M. 1975. "Turbulence measurements at the sea coast during high winds."; J. Met. Soc. Japan.

Standing et al., 1990. "Wind loading and dynamic response of a floating platform in waves." BMT Fluid Mechanics.

USGS, 1978. "Requirements for verifying the structural integrity of OCS platforms." United States Geological Survey.

Vickery, B.J., 1983. "A wind tunnel investigation of the mean and dynamic loads on an offshore guyed drilling platform." Univ. of ontario Eng. Sc. Rep., BLWTL-SS 18-1983.

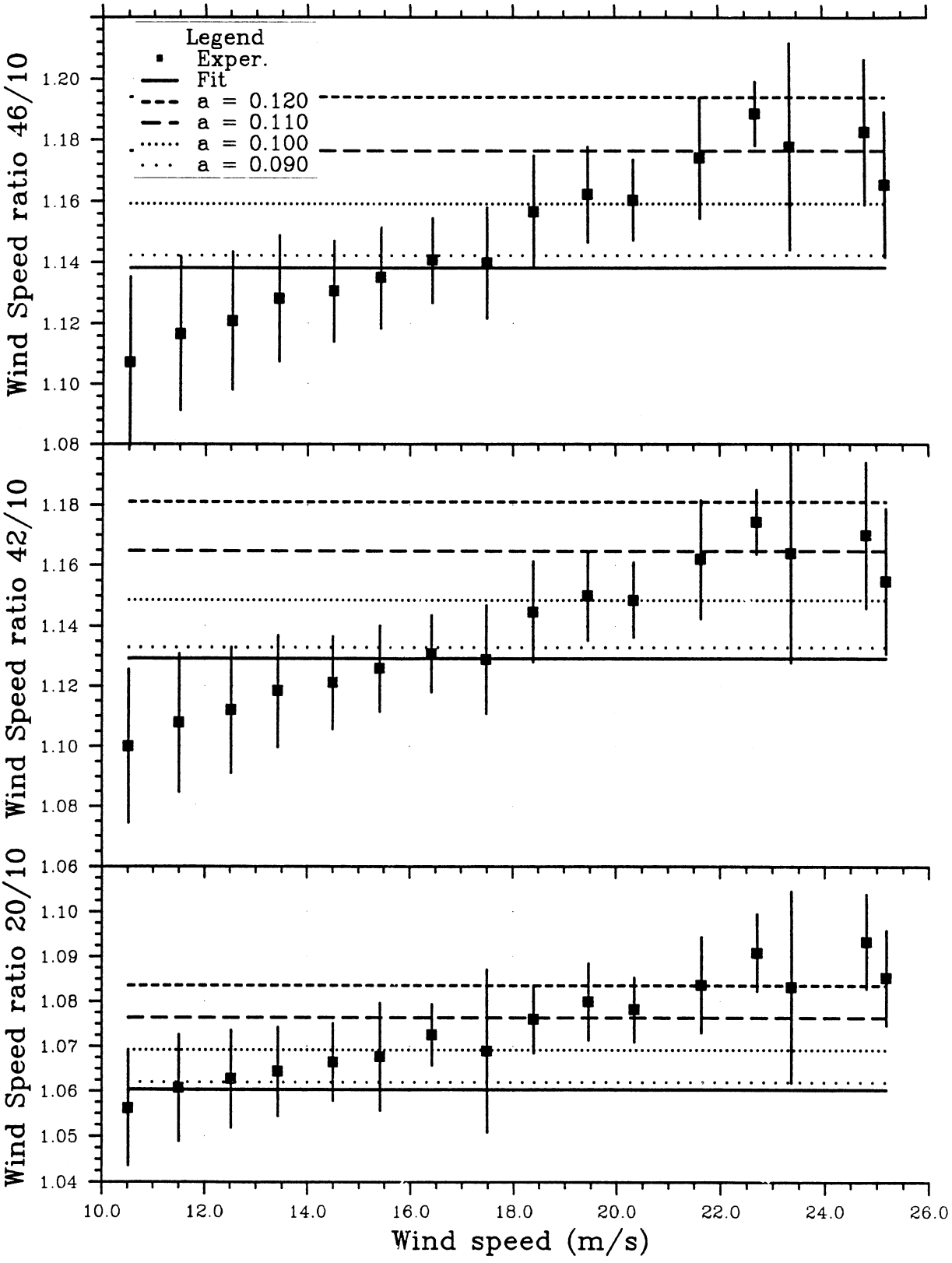

Fig. 4.1-M1 The "near neutral" profile data compared to the power law model Eq. (4.1.2). Curves are shown for a least squares fit, and for exponent values as indicated.

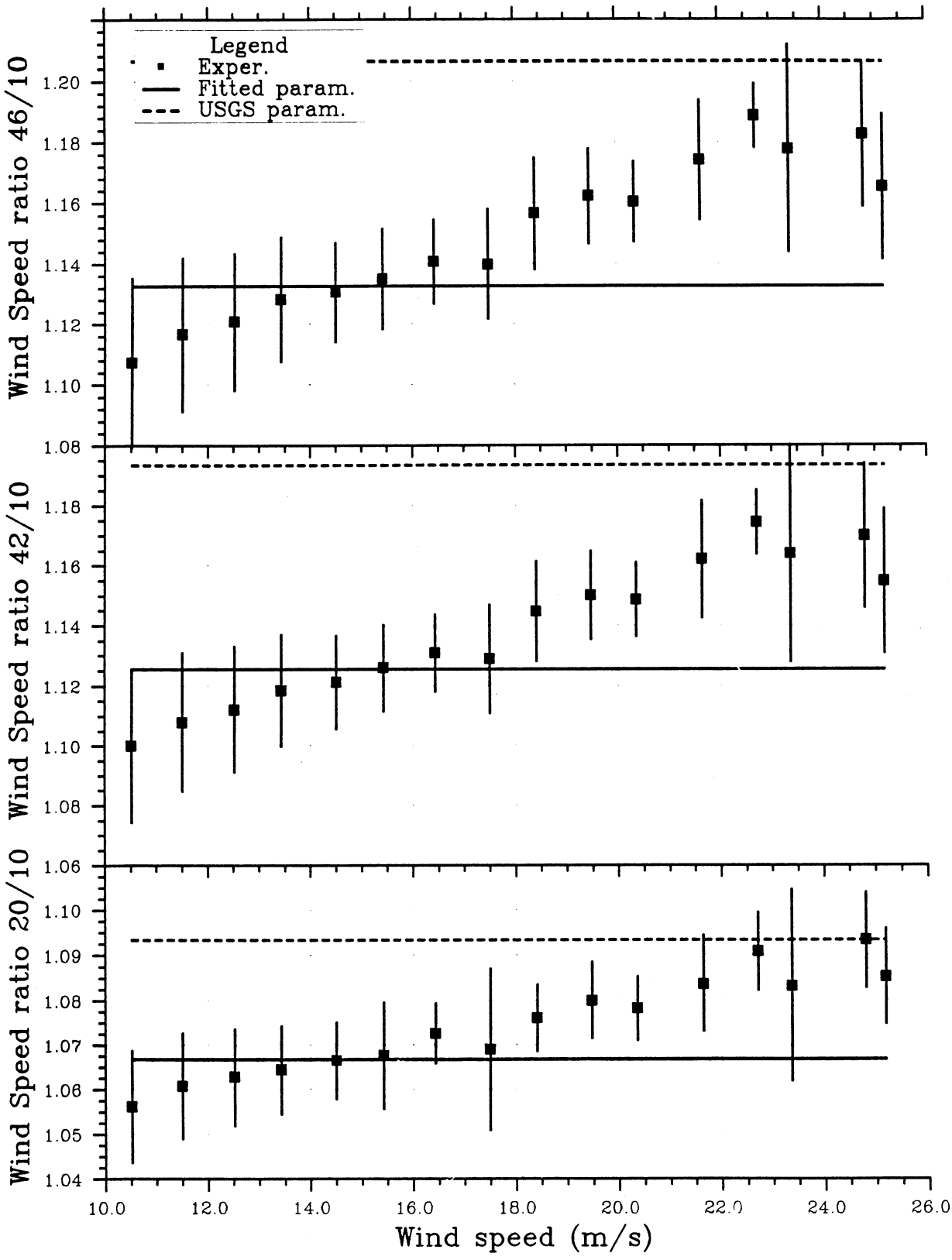

Fig. 4.1-M2 The "near neutral" profile data compared to the USGS power law model Eq. (4.1.3). Curves are shown for a least squares fit, and for the USGS parameter values as indicated.

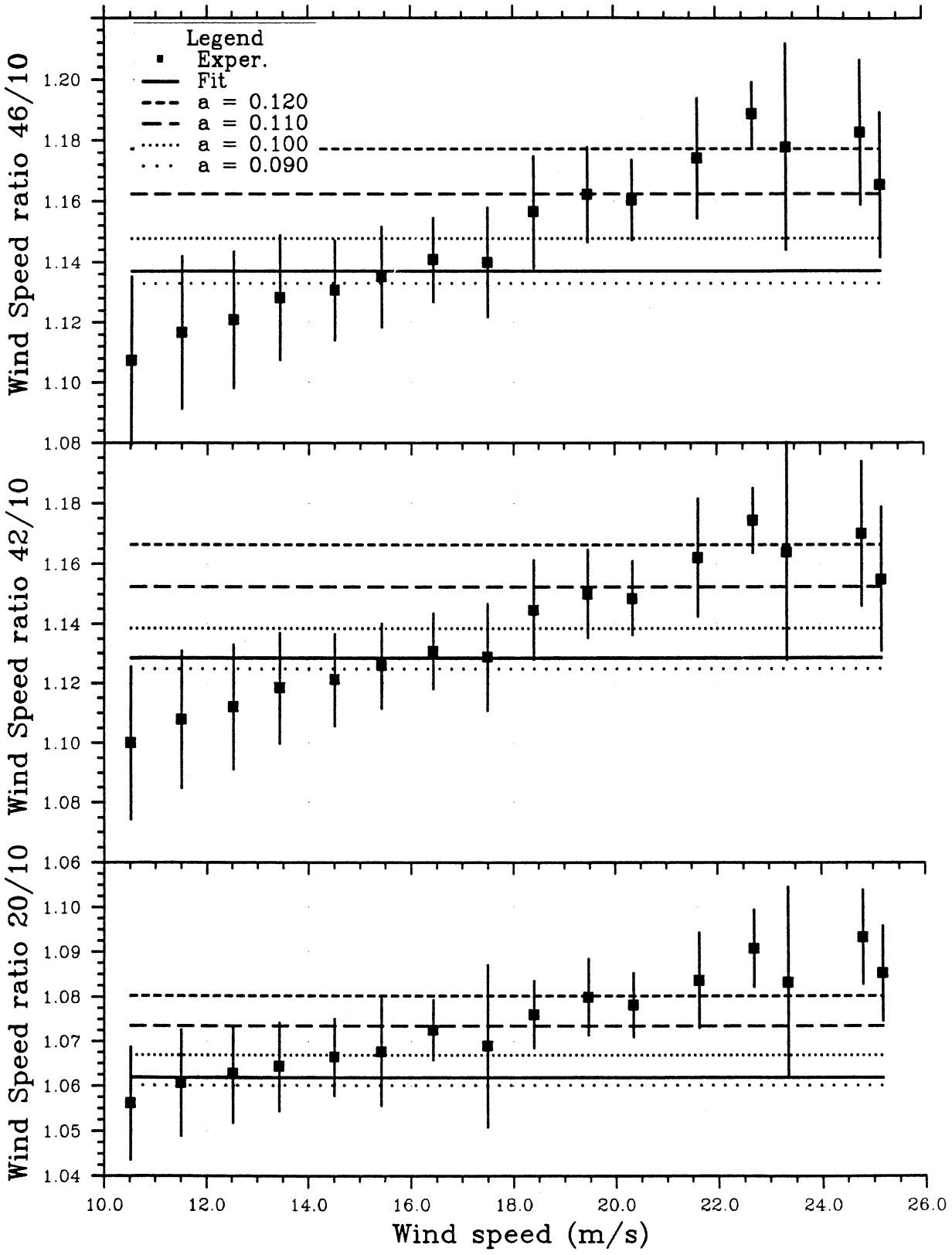

Fig. 4.1-M4 The "near neutral" profile data compared to the logarithmic model Eq. (4.1.7). Curves are shown for a least squares fit, and for coefficient values as indicated.

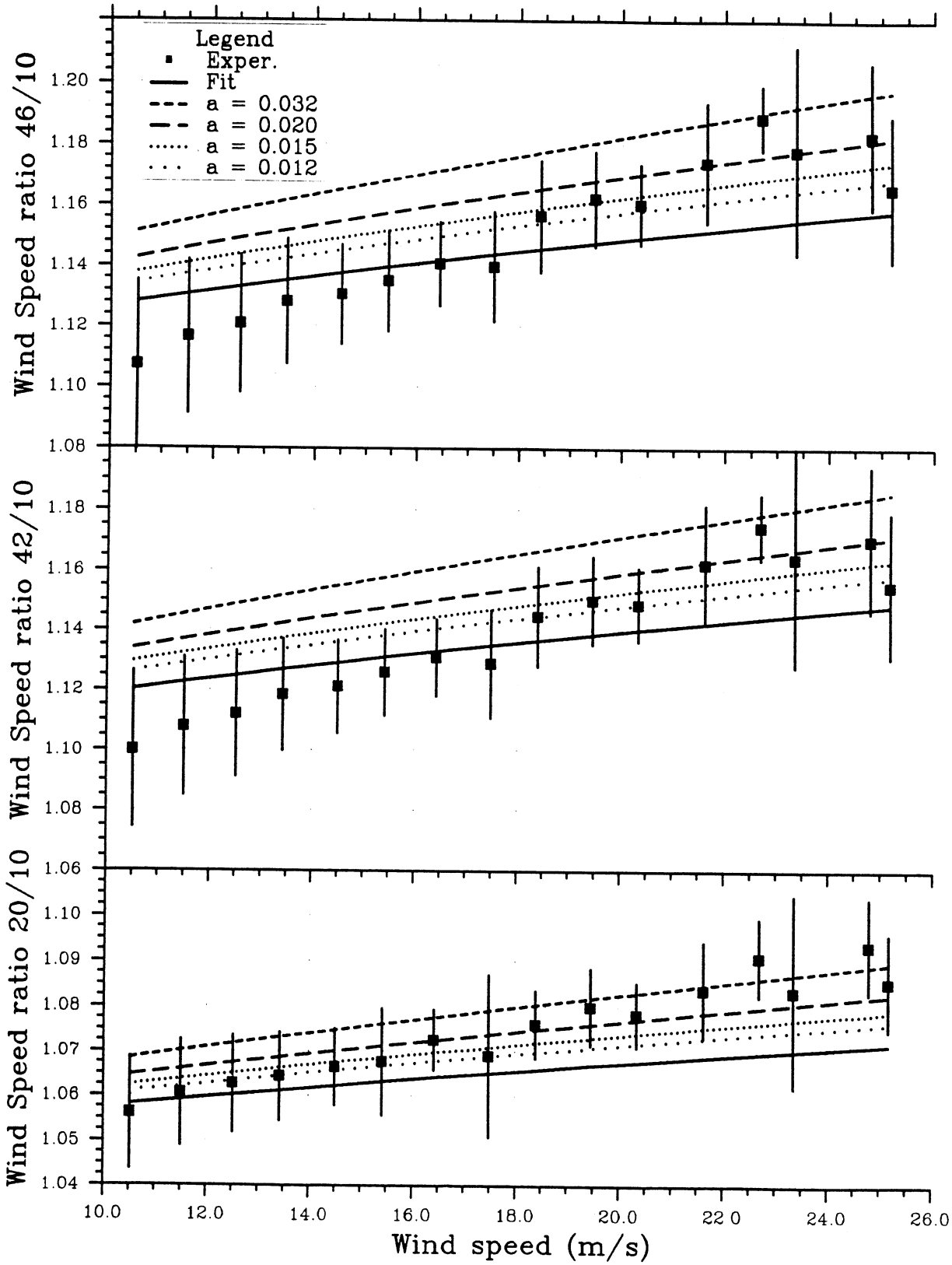

Fig. 4.1-M5.1 The "near neutral" profile data compared to the logarithmic model with z_0 determined by the Charnock relation. Curves are shown for a least squares fit, and for values of the Charnock constant as indicated.

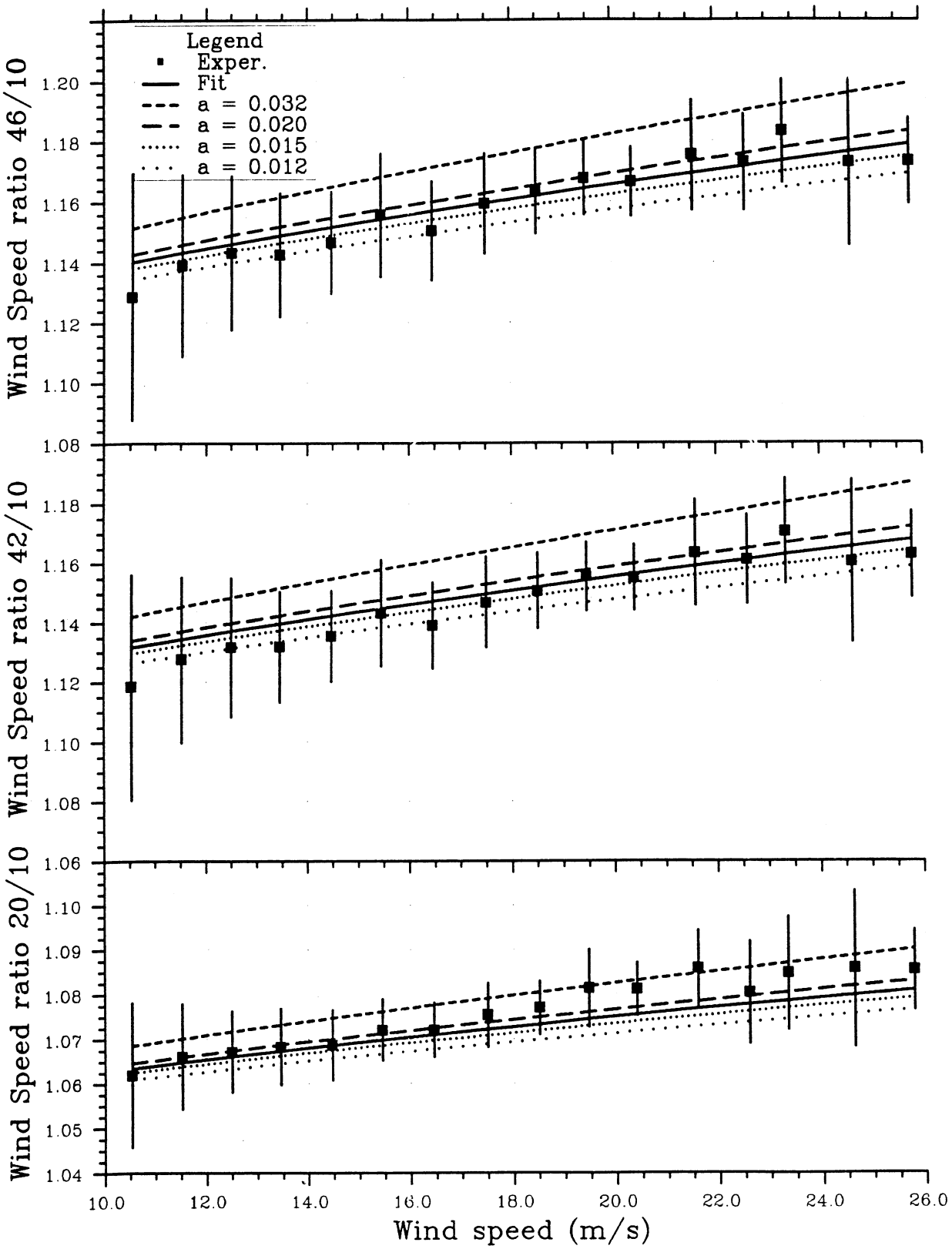

Fig. 4.1-M5.2 As Fig. 4.1-M5.1, but for periods with $-2\ 10^{-5} < \lambda' < 2\ 10^{-5}$ ms^{-2}

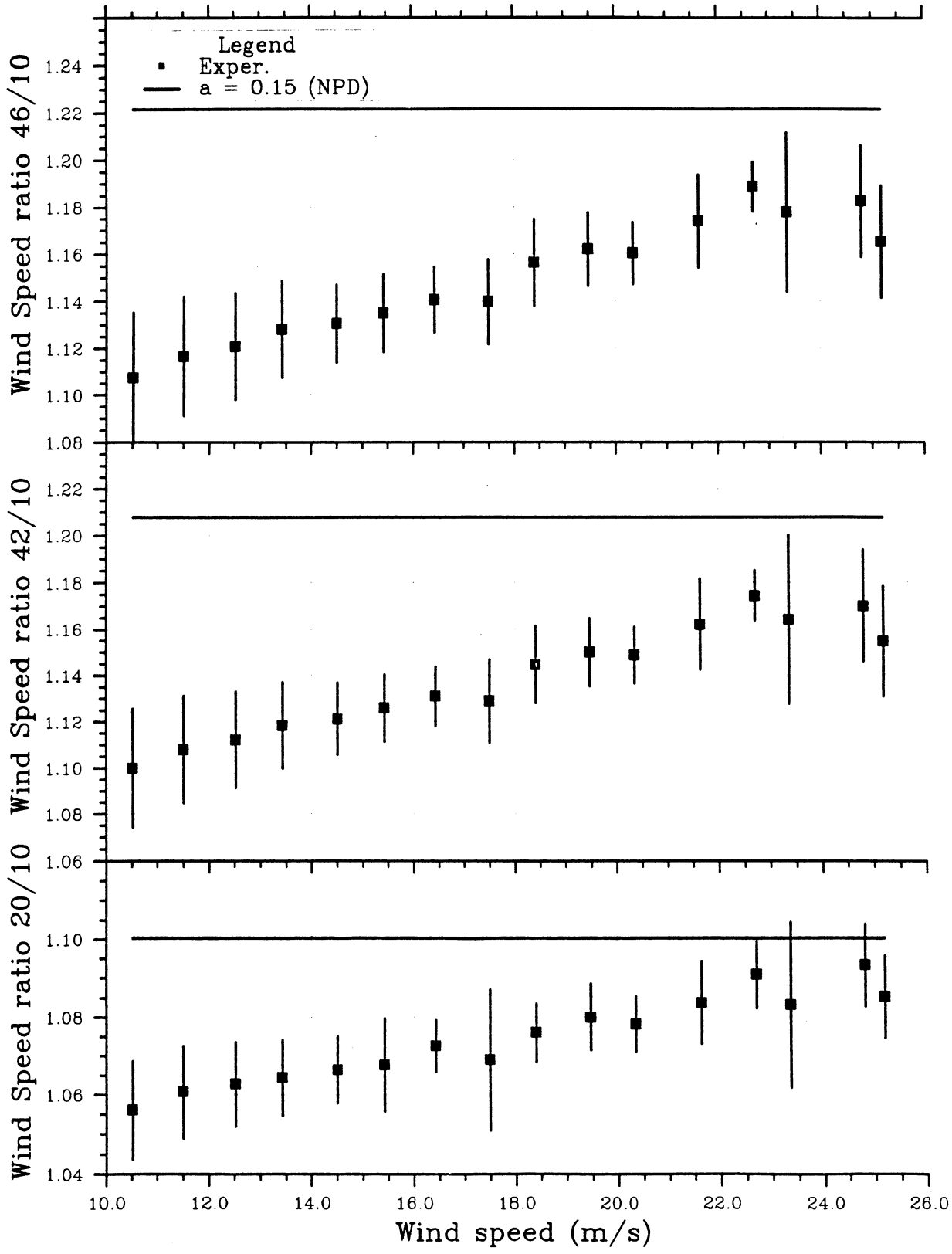

Fig. 4.1-M6 The "near neutral" profile data compared to the logarithmic model Eq. (4.1.7) with the NPD coefficient value.

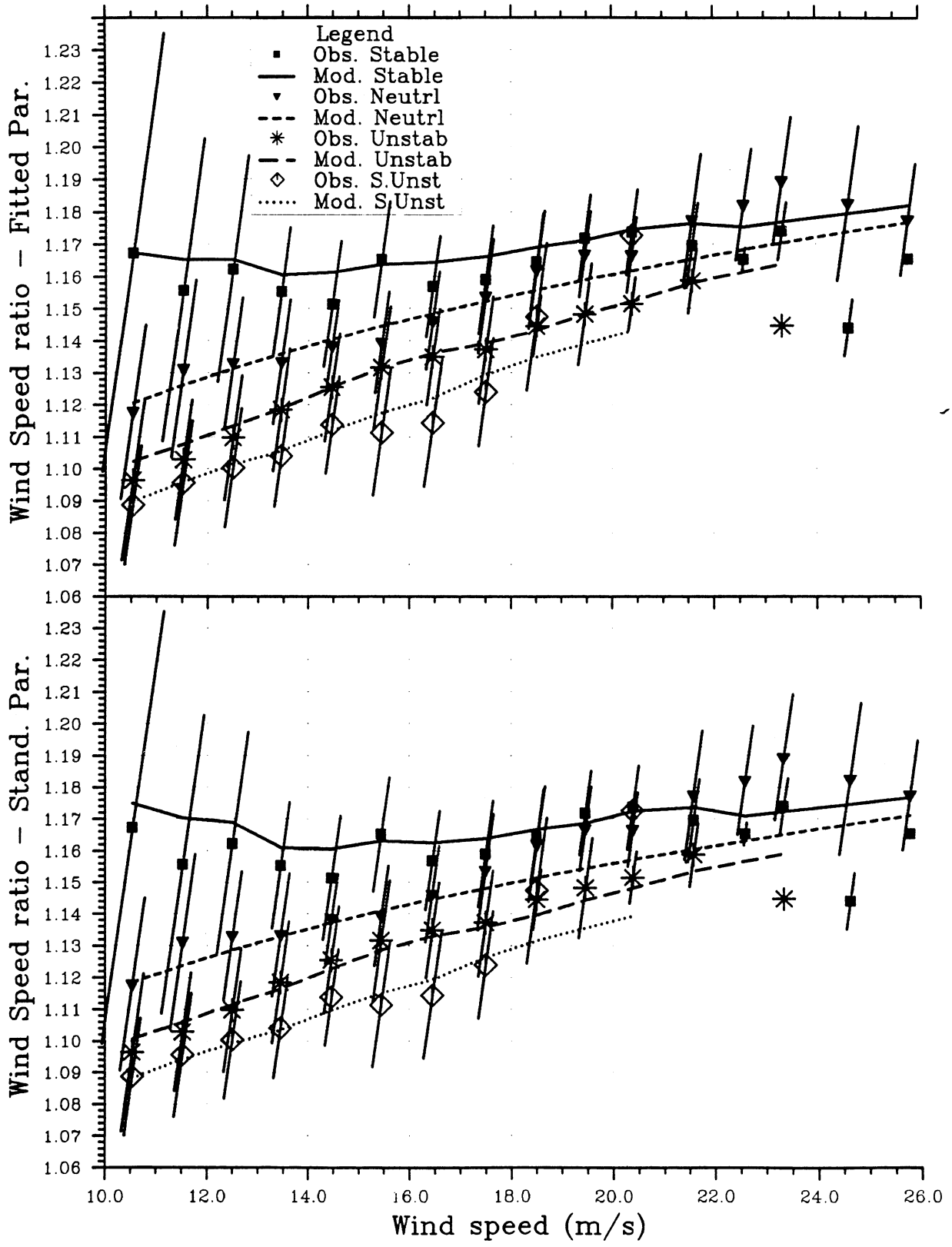

Fig. 4.2.1 The full set of profile data for 46/10 m compared to the extended logarithmic model Eq. (4.2.5) for 4 stability classes as explained in the text. Curves are shown for a least squares fit (upper part) and for the standard parameters.

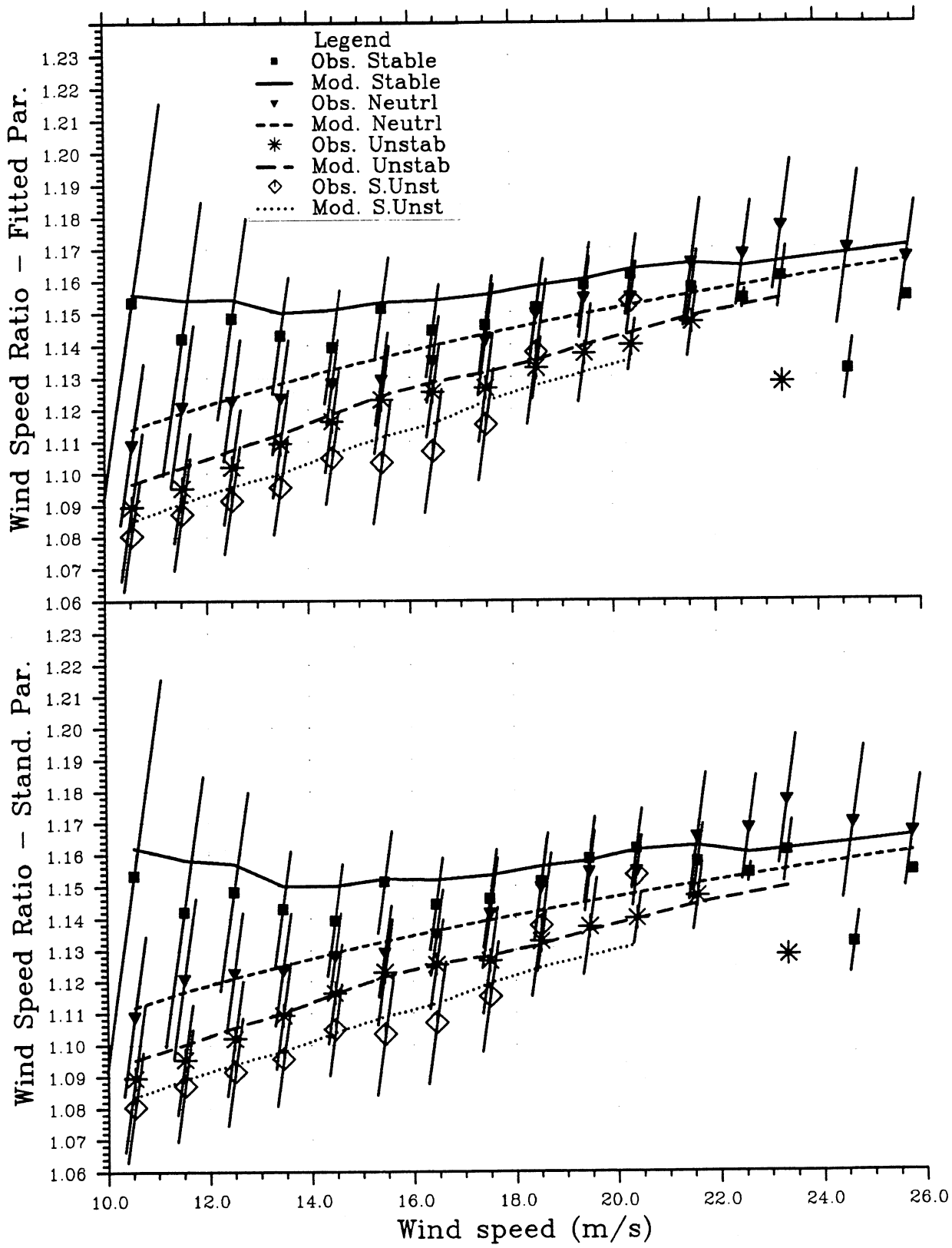

Fig. 4.2.2 As Fig. 4.2.1, but for 42/10 m.

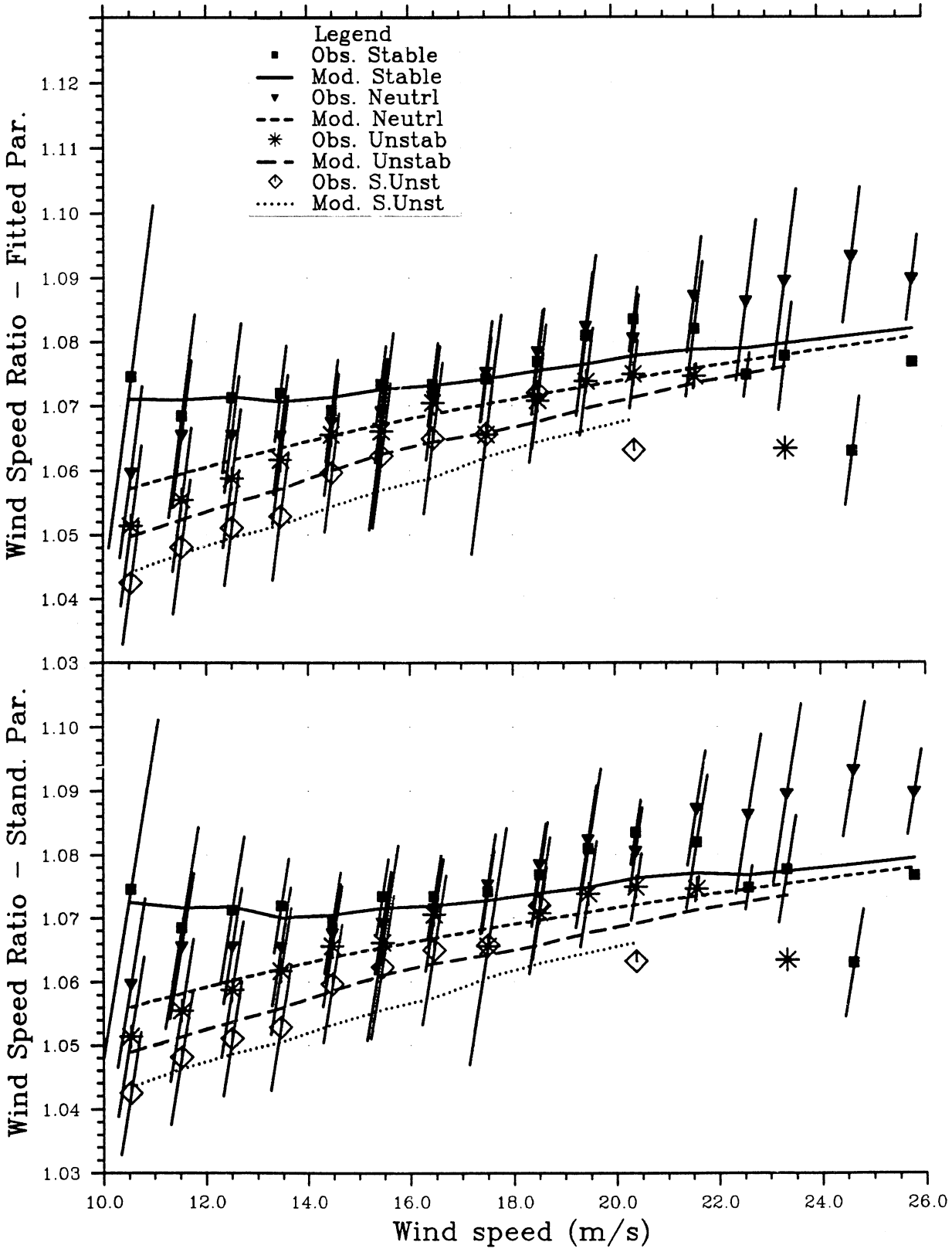

Fig. 4.2.3 As Fig. 4.2.1, but for 20/10 m.

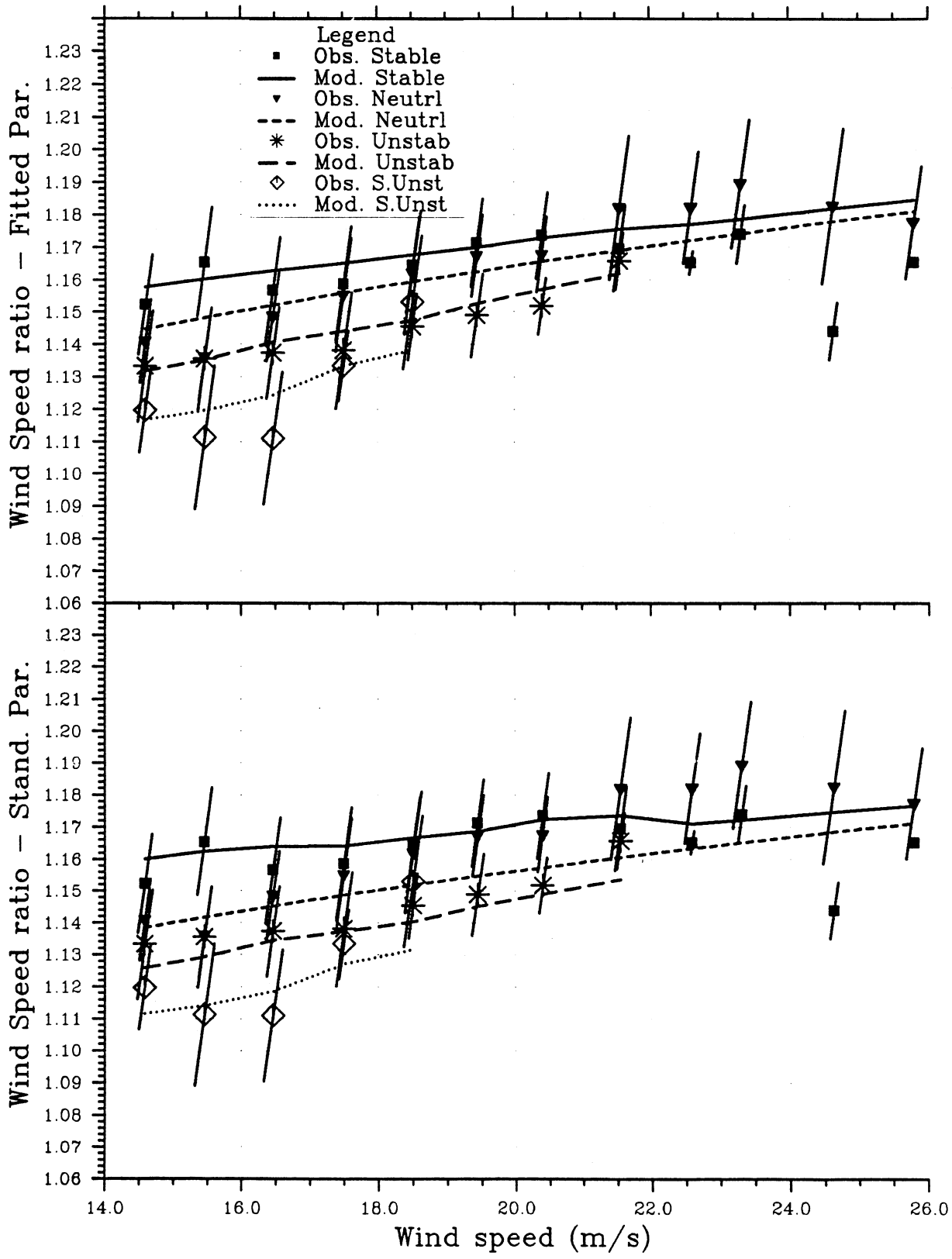

Fig. 4.2.4 As Fig. 4.2.1, but for the PQS data set.

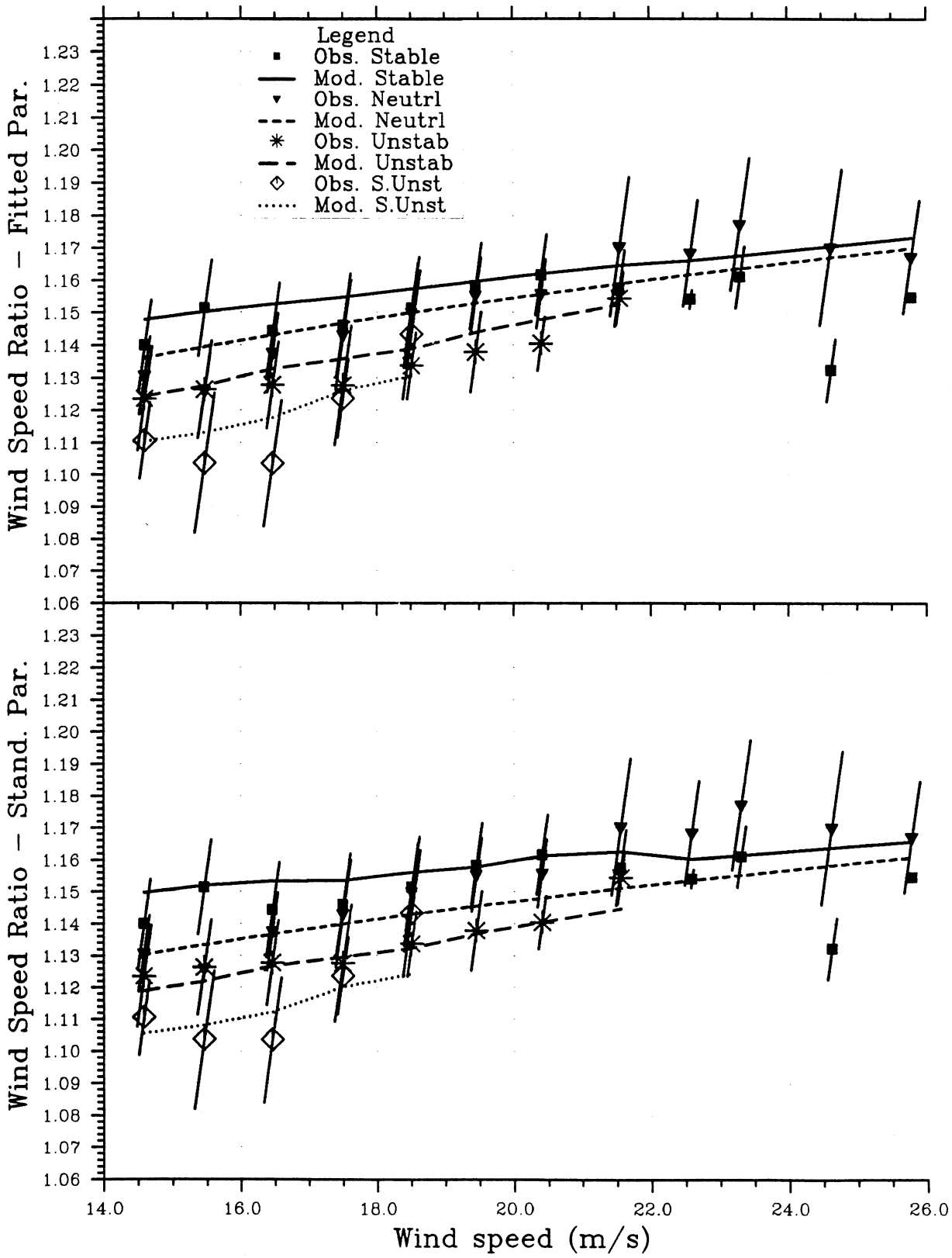

Fig. 4.2.5 As Fig. 4.2.4, but for 42/10 m.

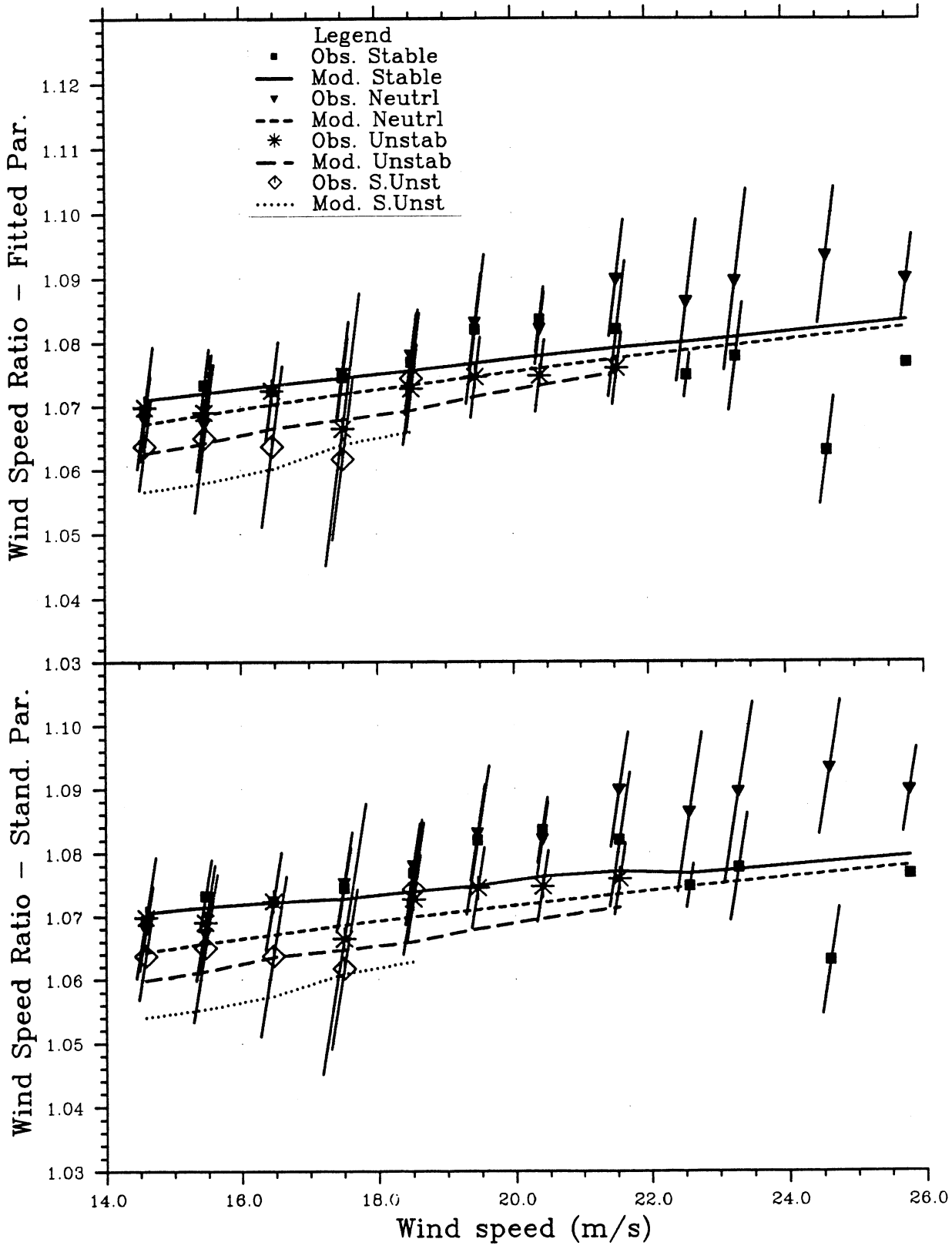

Fig. 4.2.6 As Fig. 4.2.4, but for 20/10 m.

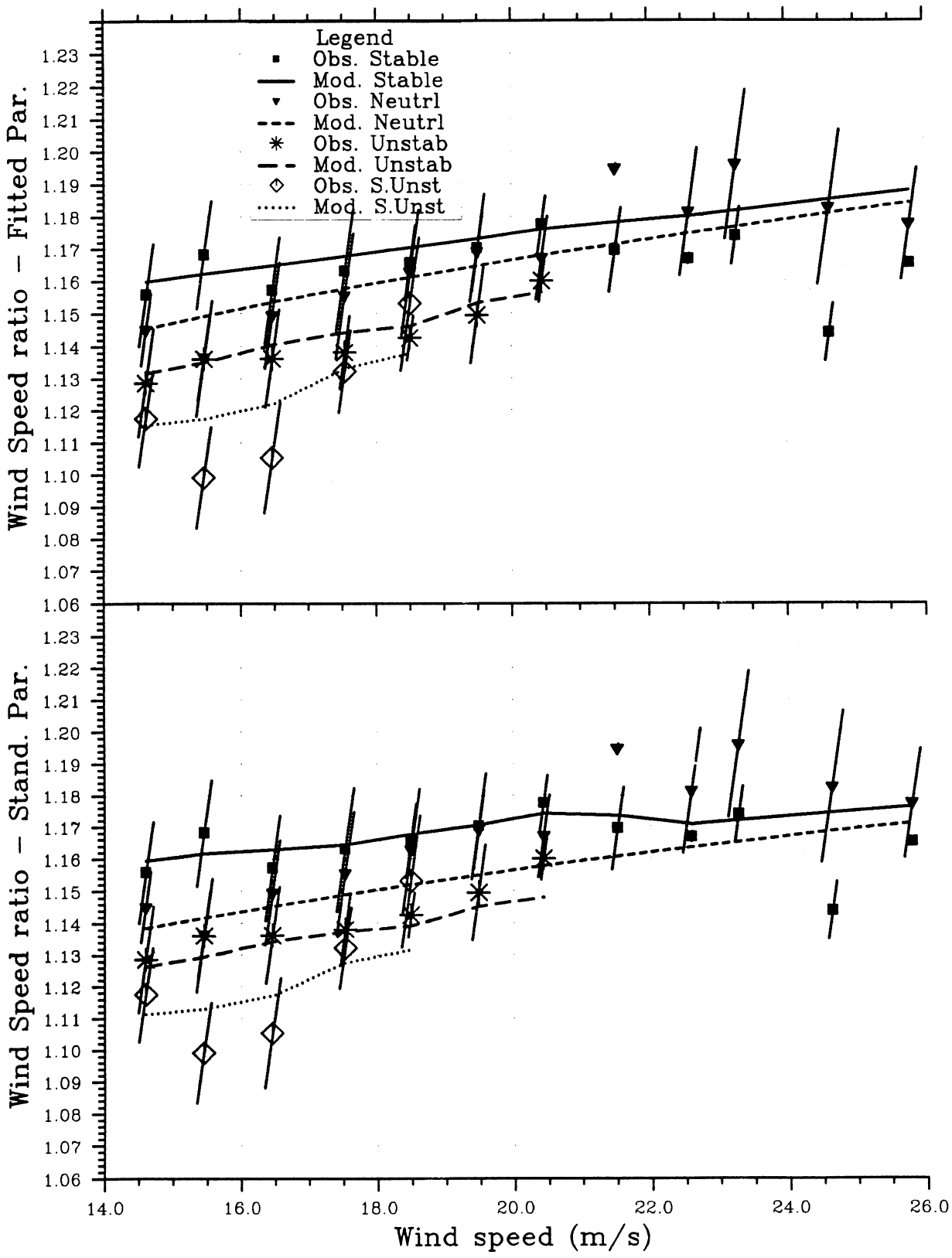

Fig. 4.2.7 As Fig. 4.2.1, but for the QS data set.

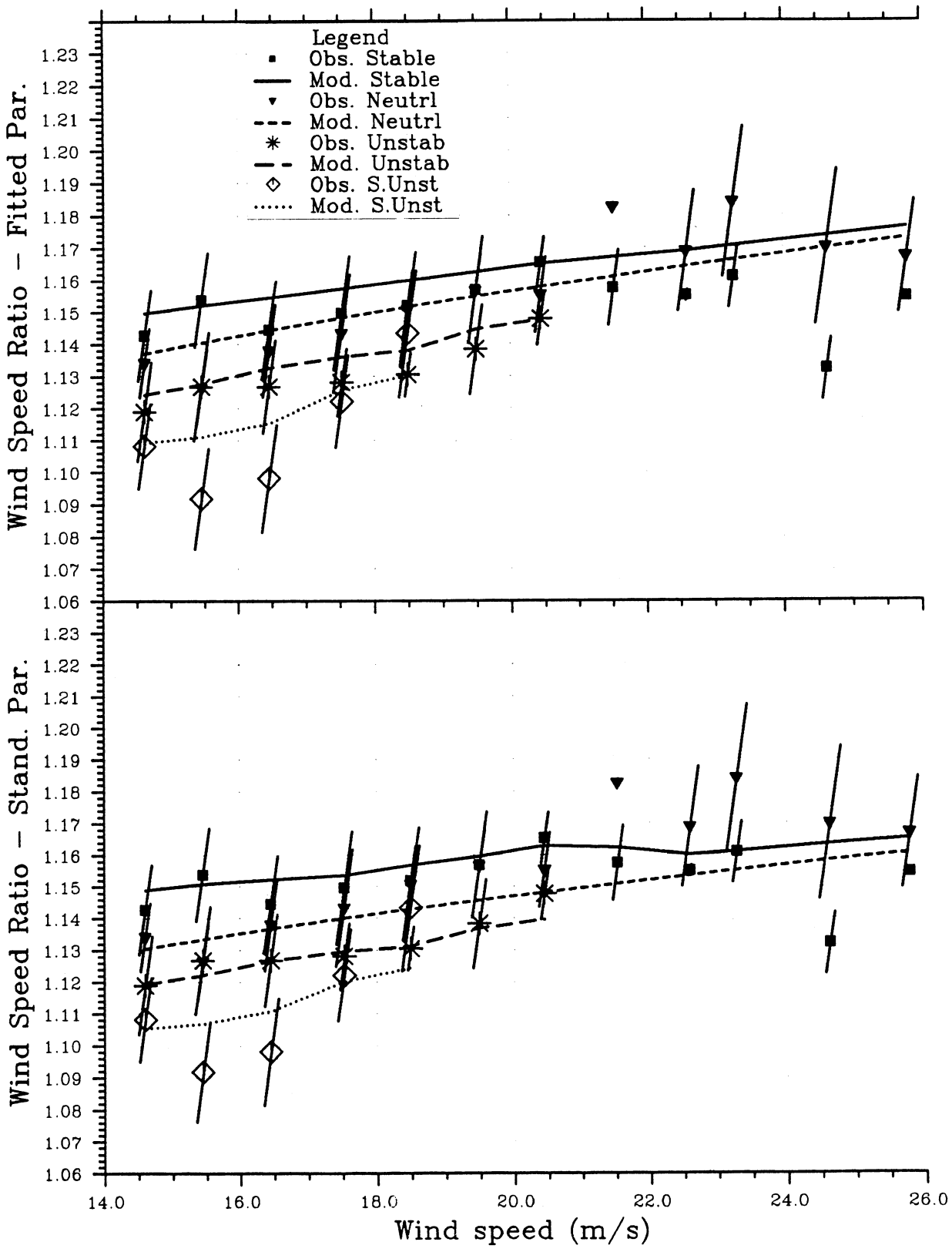

Fig. 4.2.8 As Fig. 4.2.7, but for 42/10 m.

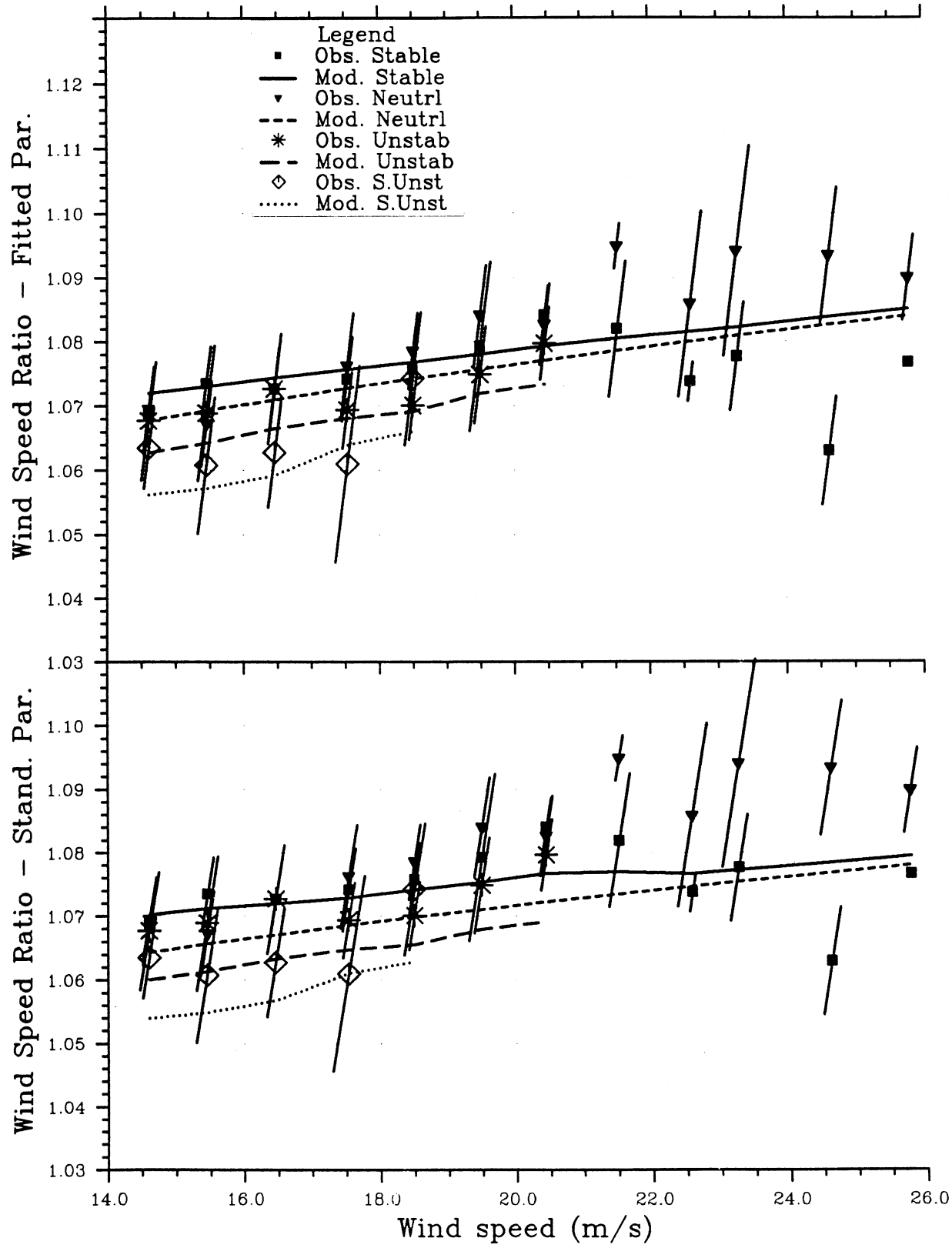

Fig. 4.2.9 As Fig. 4.2.7, but for 20/10 m.

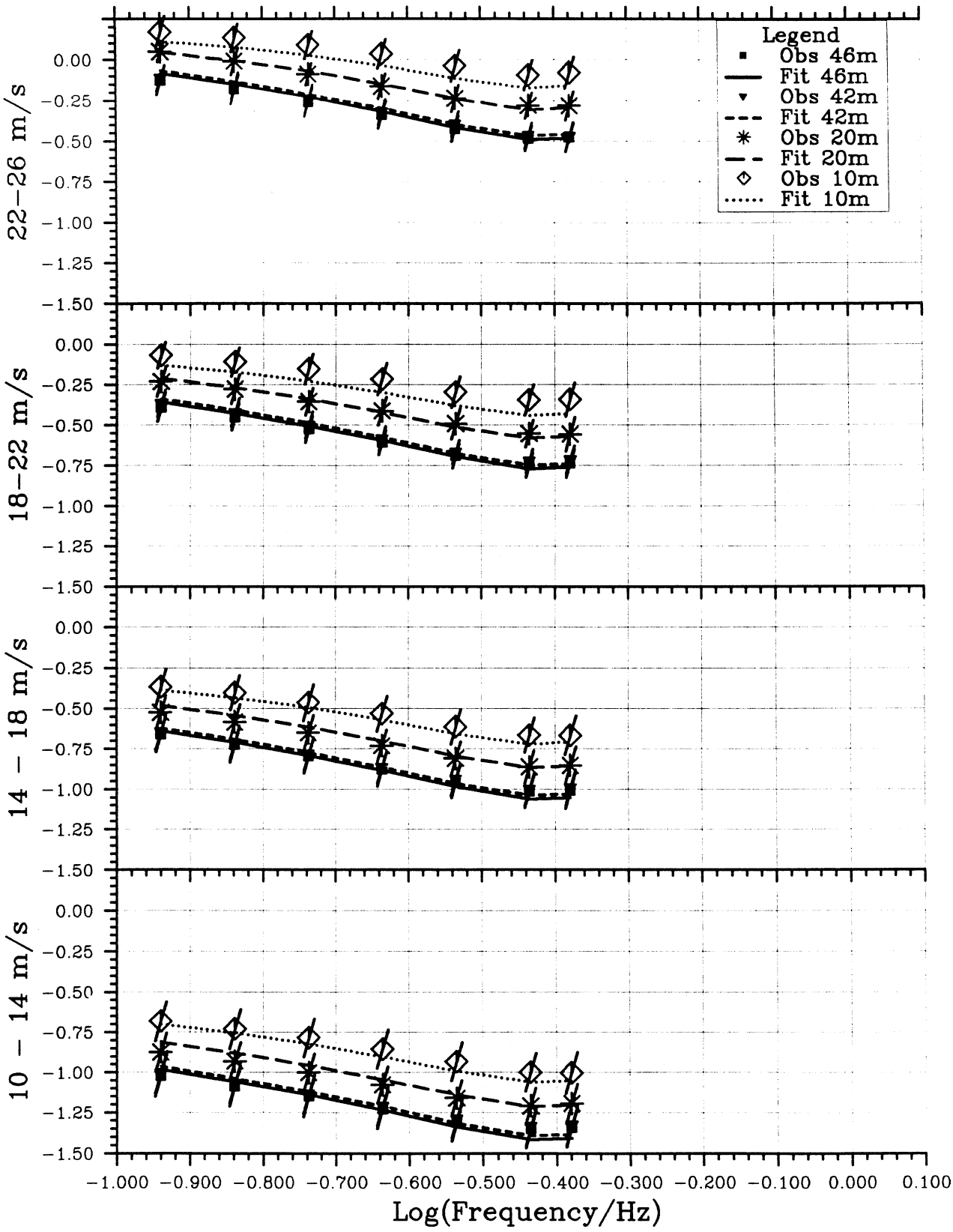

Fig. 4.3.1 DFT spectra versus frequency ($\log_{10}$[fS(f)] vs. $\log_{10}$f) for f > 0.1 Hz. Experimental data and a fit of the Kaimal model are shown for four wind speed classes, four heights and neutral stability (see text).

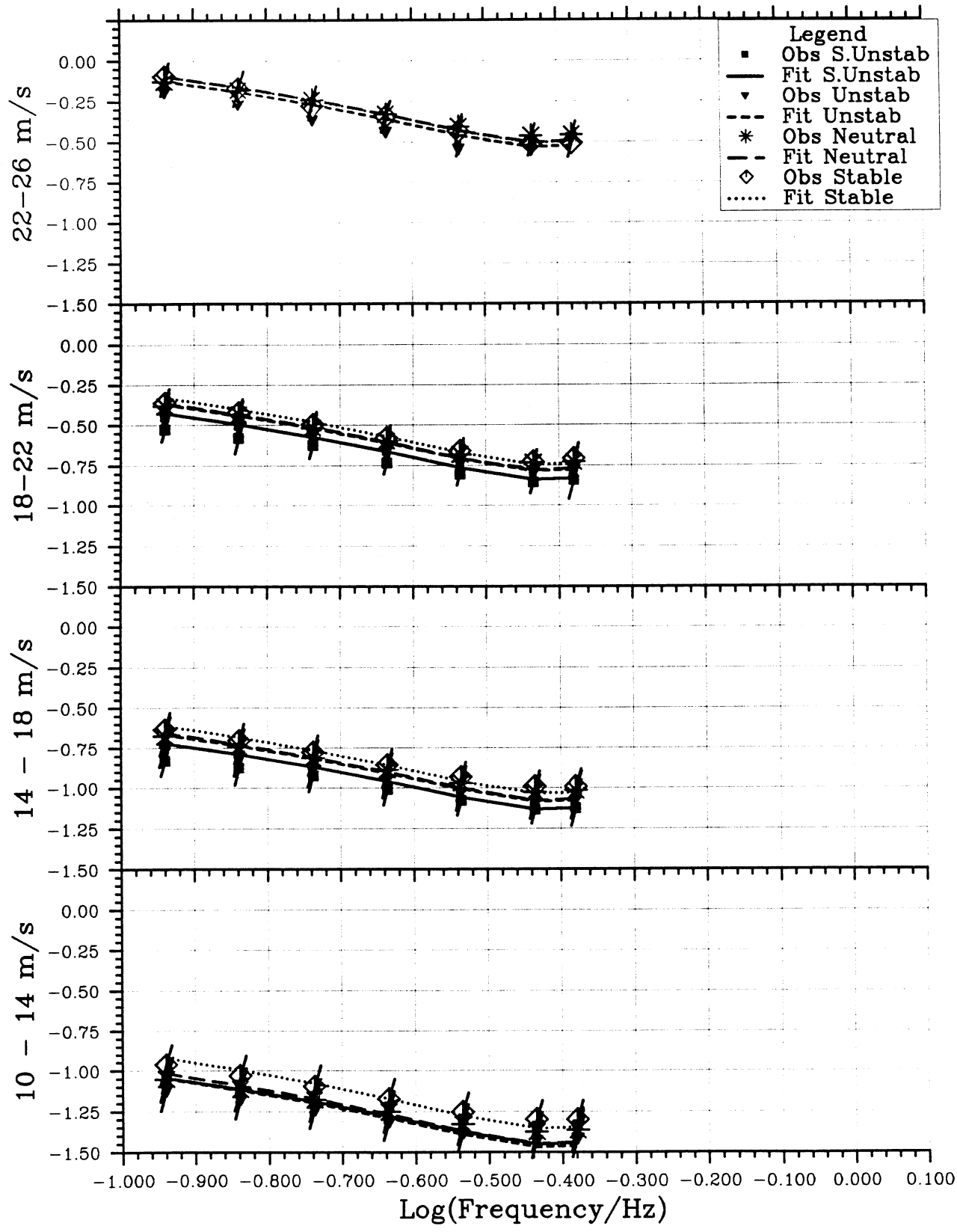

Fig. 4.3.2 As Fig. 4.3.1, but with mean results for the heights 42 and 44 m for four classes of atmospheric stability. The curves represent a fit an ad hoc Kaimal model.

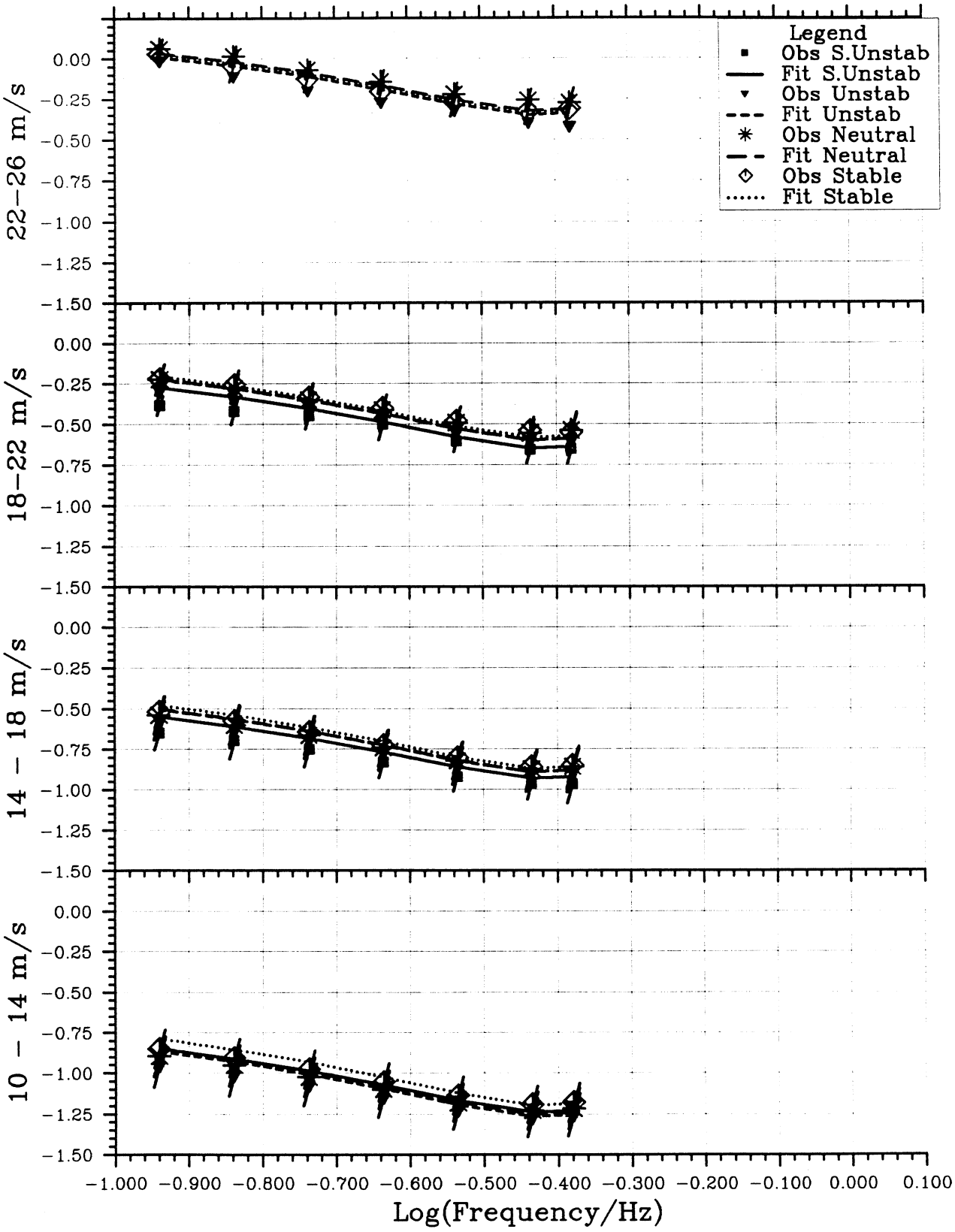

Fig. 4.3.3 As Fig. 4.3.2, but for 20 m height.

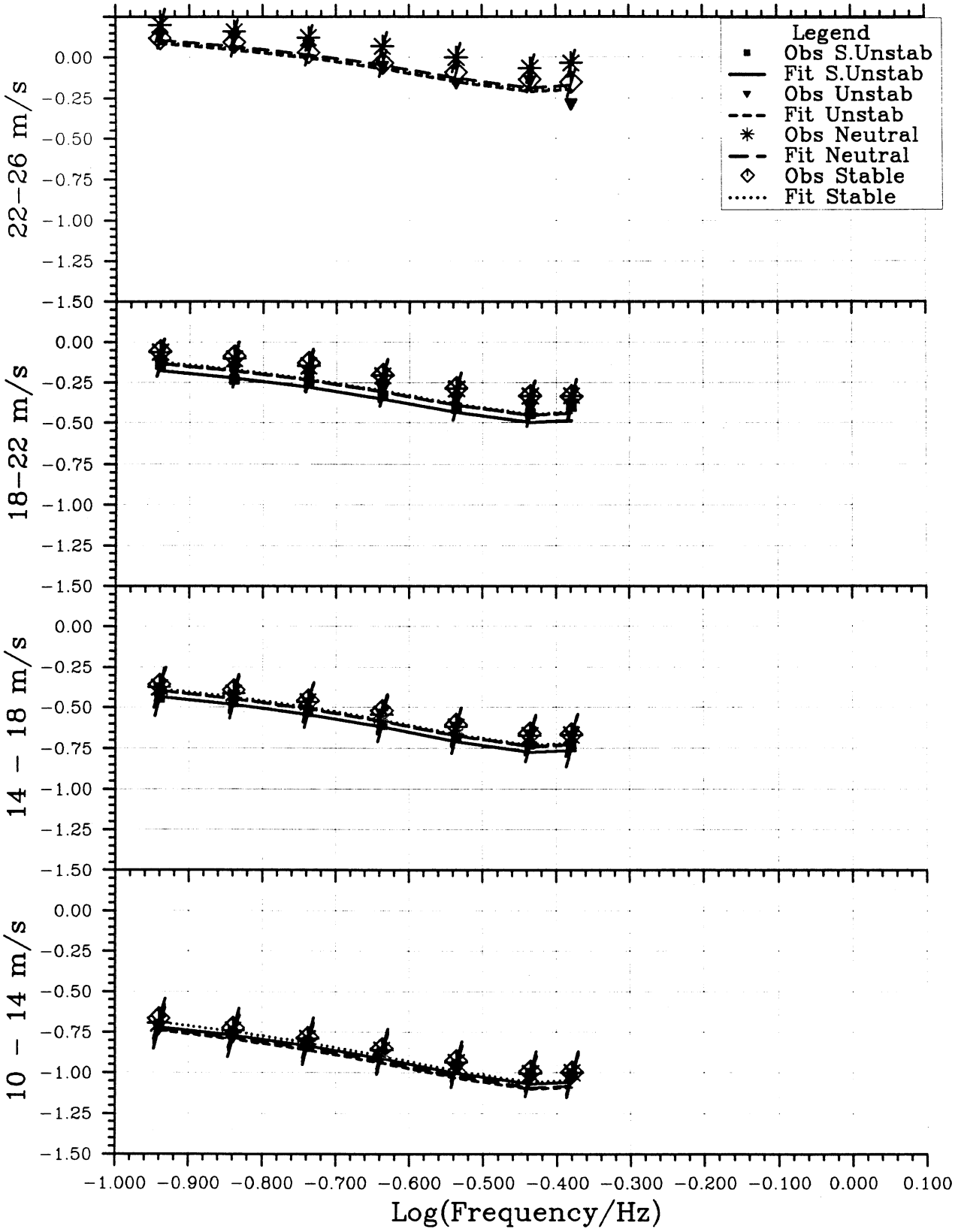

Fig. 4.3.4 As Fig. 4.3.2, but for 10 m height.

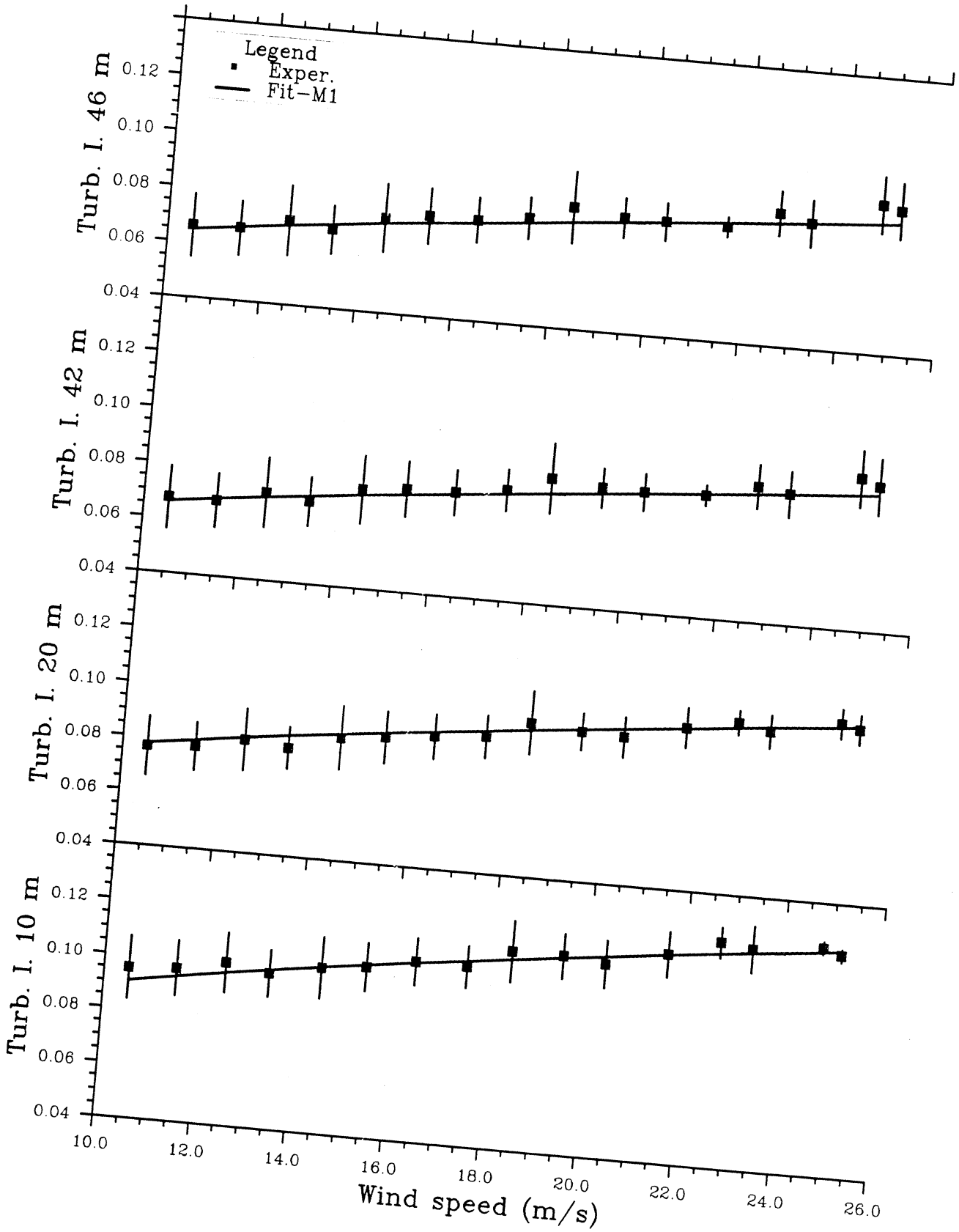

Fig. 5.1-M1 A least squares fit of the modified Vickery model, Eq. (5.1.2) to the "near" neutral turbulence intensity data.

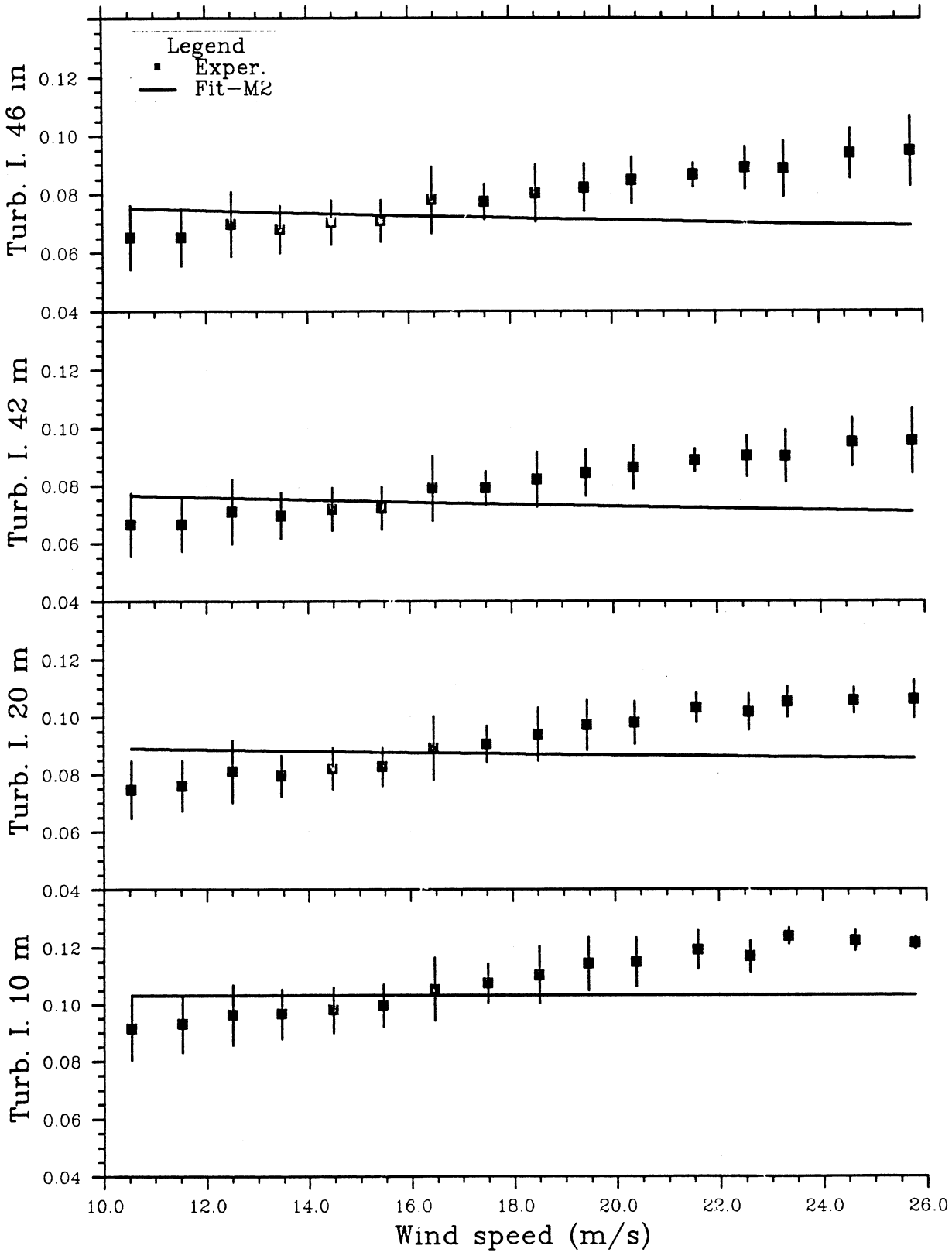

Fig. 5.1-M2 A least squares fit of the modified Standing model, Eq. (5.1.7) to the "truly" neutral turbulence intensity data.

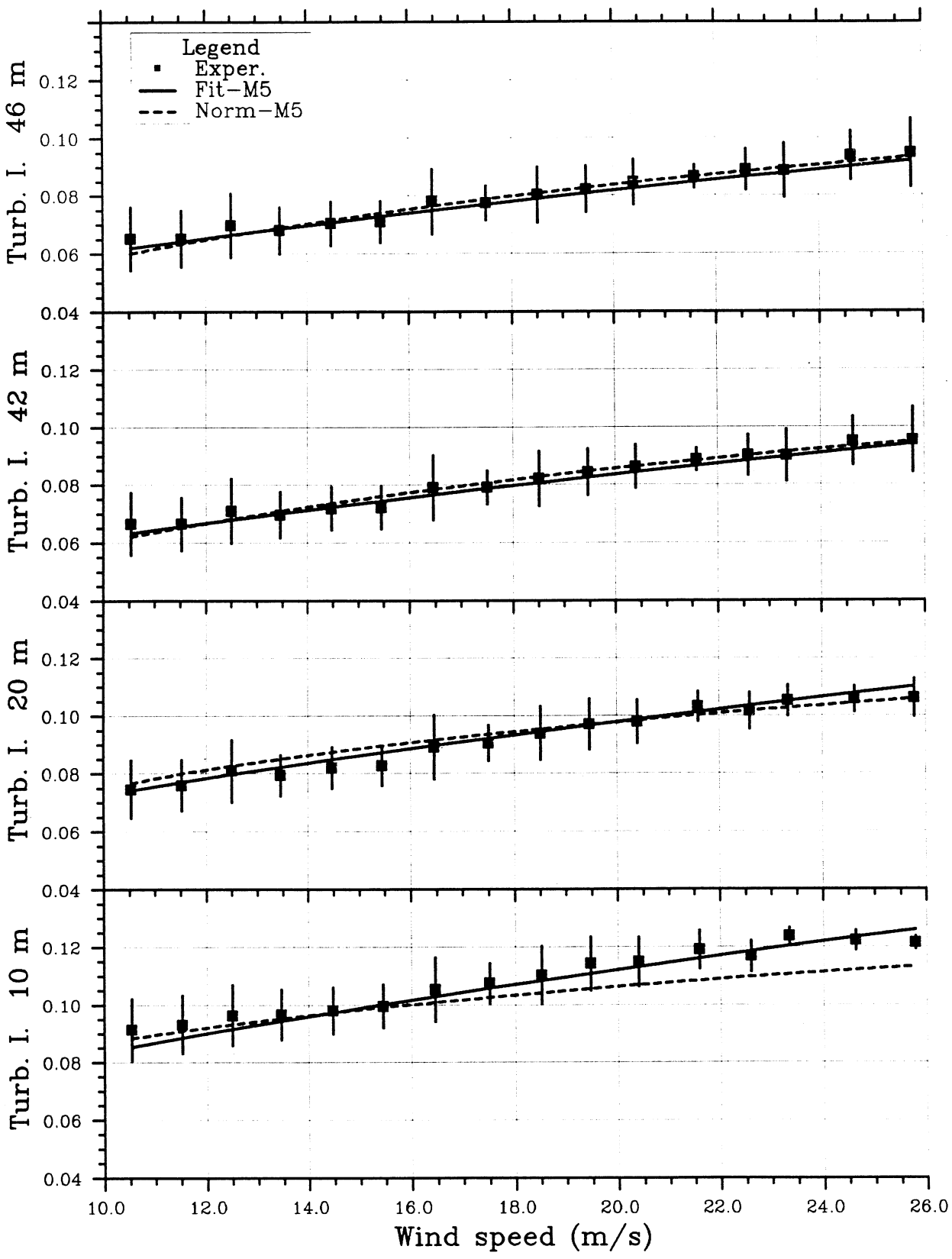

Fig. 5.1-M5 A least squares fit (full line) of the ESDU model, Eq. (5.1.12) to the "truly" neutral turbulence intensity data, and a normalized version of the same (dashed line, see text).

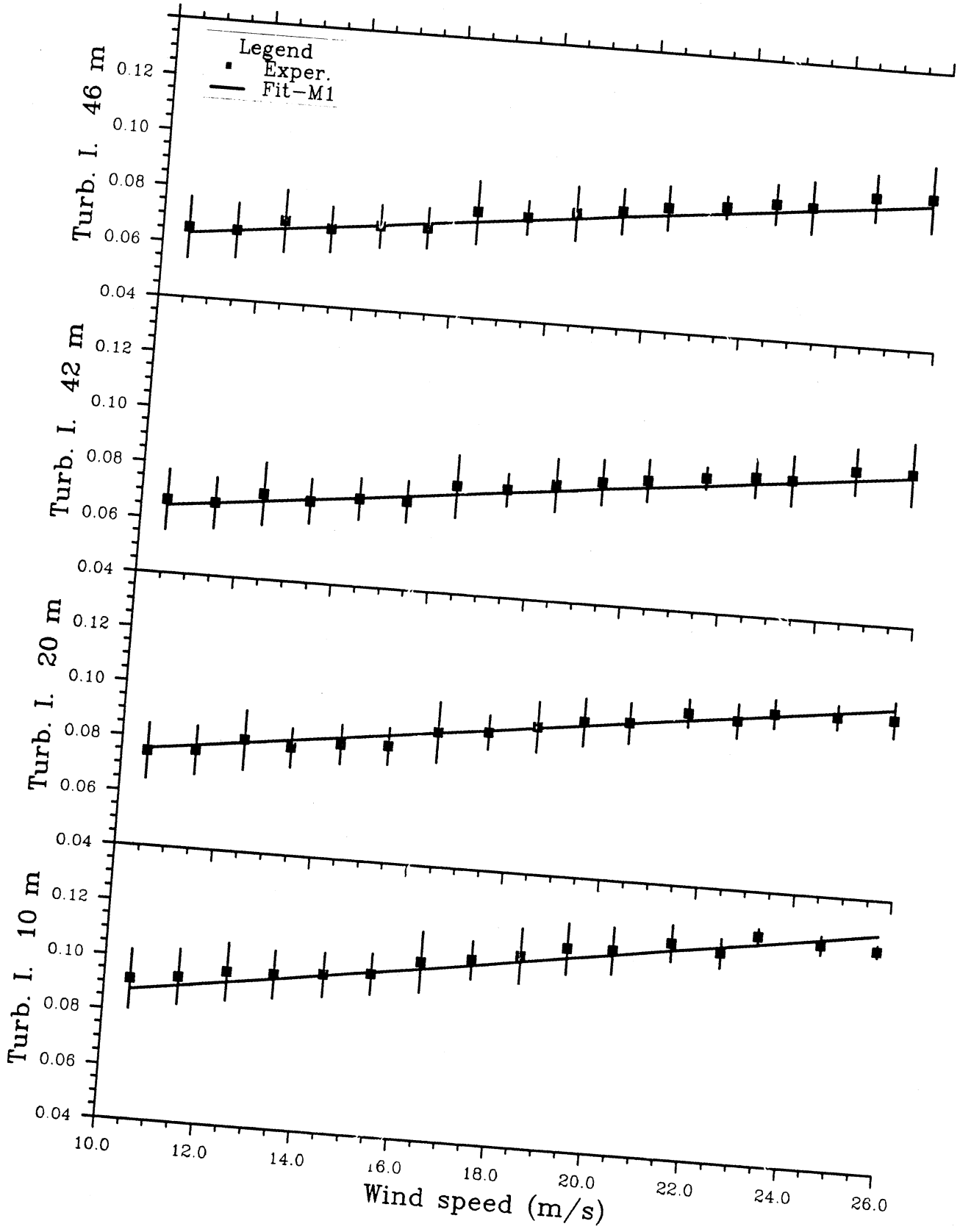

Fig. 5.1-M6 A least squares fit of the ad hoc model, Eq. (5.1.13) to the "truly" neutral turbulence intensity data.

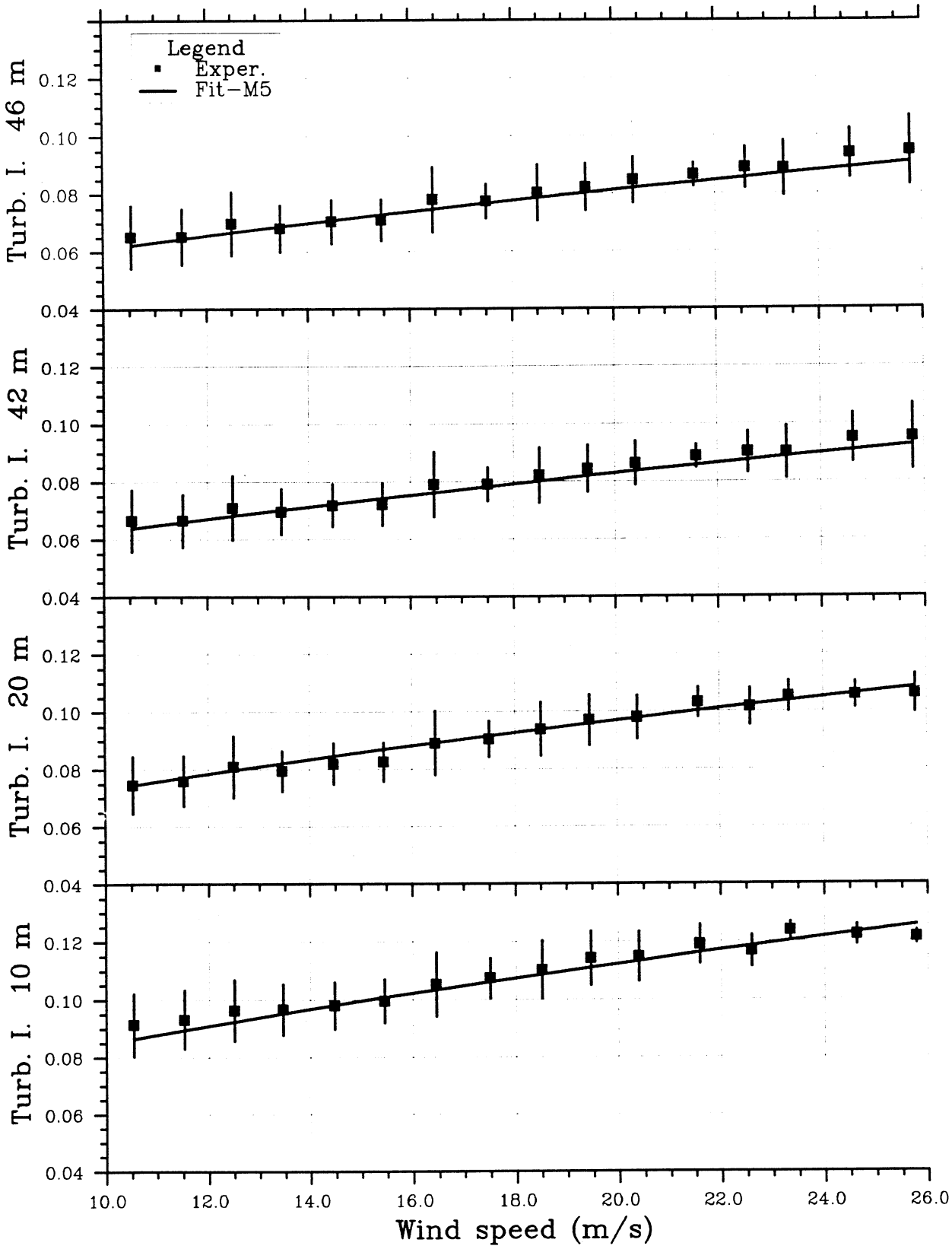

Fig. 5.1-M7 A least squares fit of the à la C_D model. Eq. (5.1.17) to the "truly" neutral turbulence intensity data.

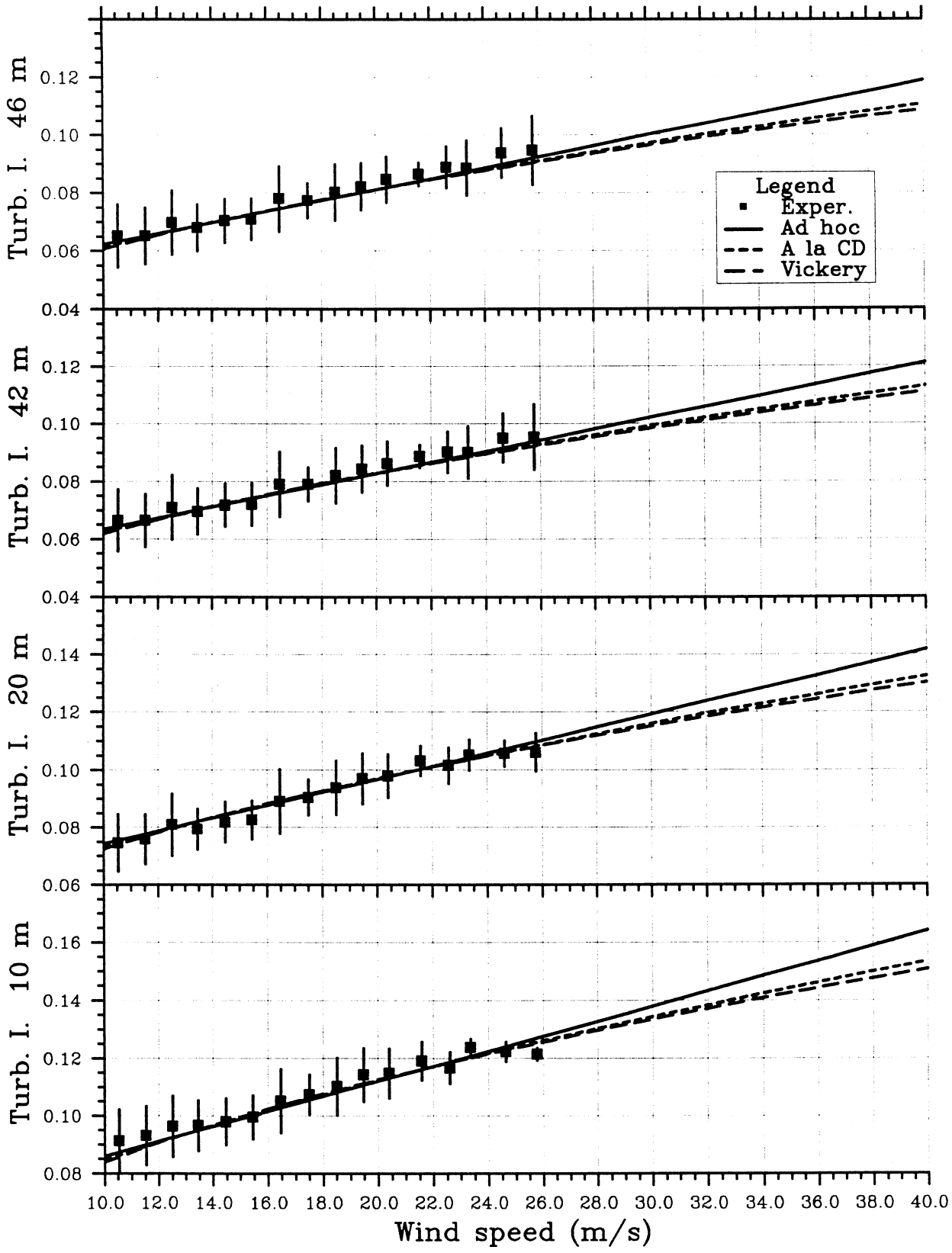

Fig. 5.1.8 The "truly" neutral turbulence intensity data versus wind speed, and a comparison of the fitted Vickery, ad hoc and à la C_d models extrapolated to u_r = 40 m/s.

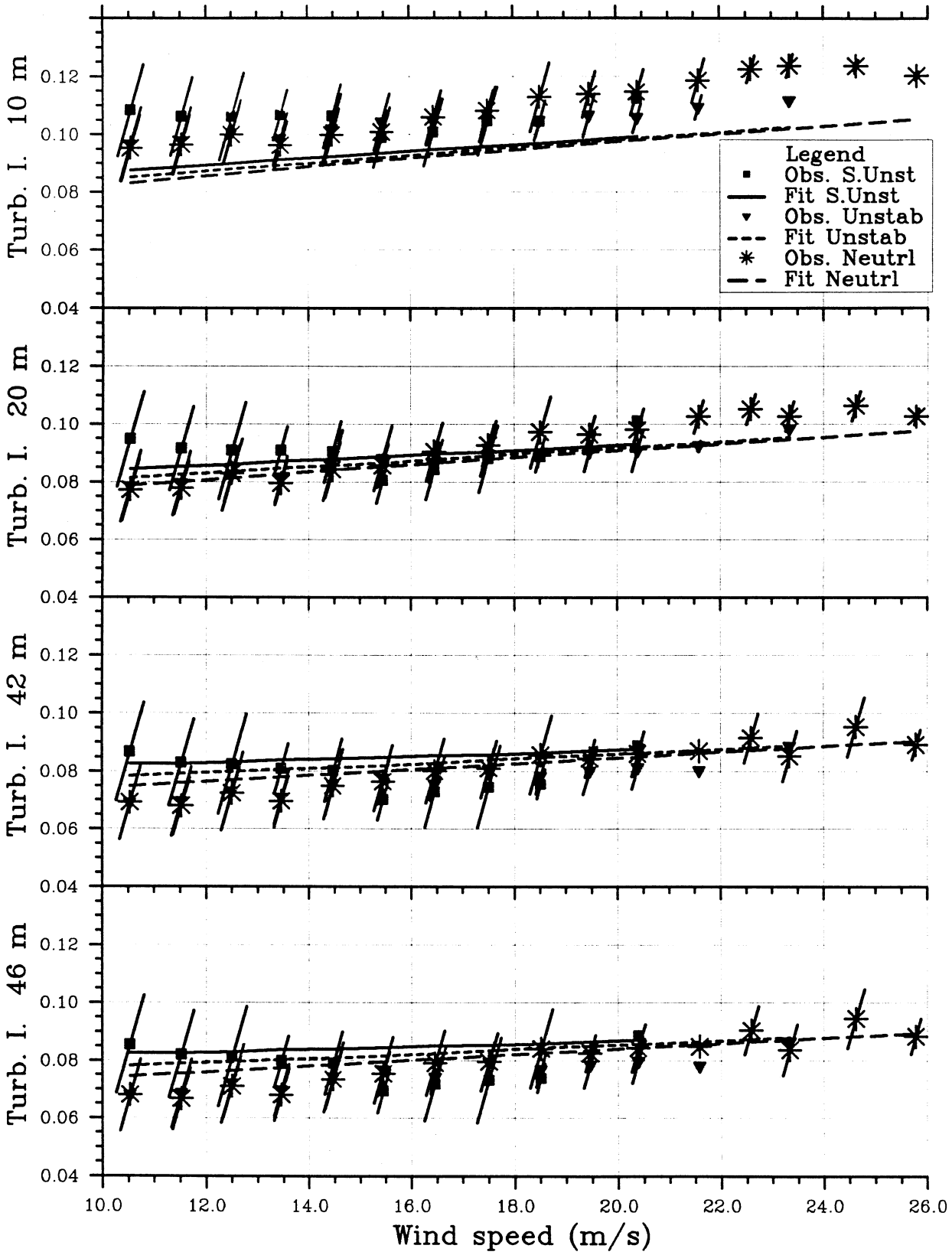

Fig. 5.2-M1.1 The Panofsky model, Eq. (5.2.1-2), compared to the turbulence intensity data for unstable atmospheric conditions. The normalizing parameter is fitted.

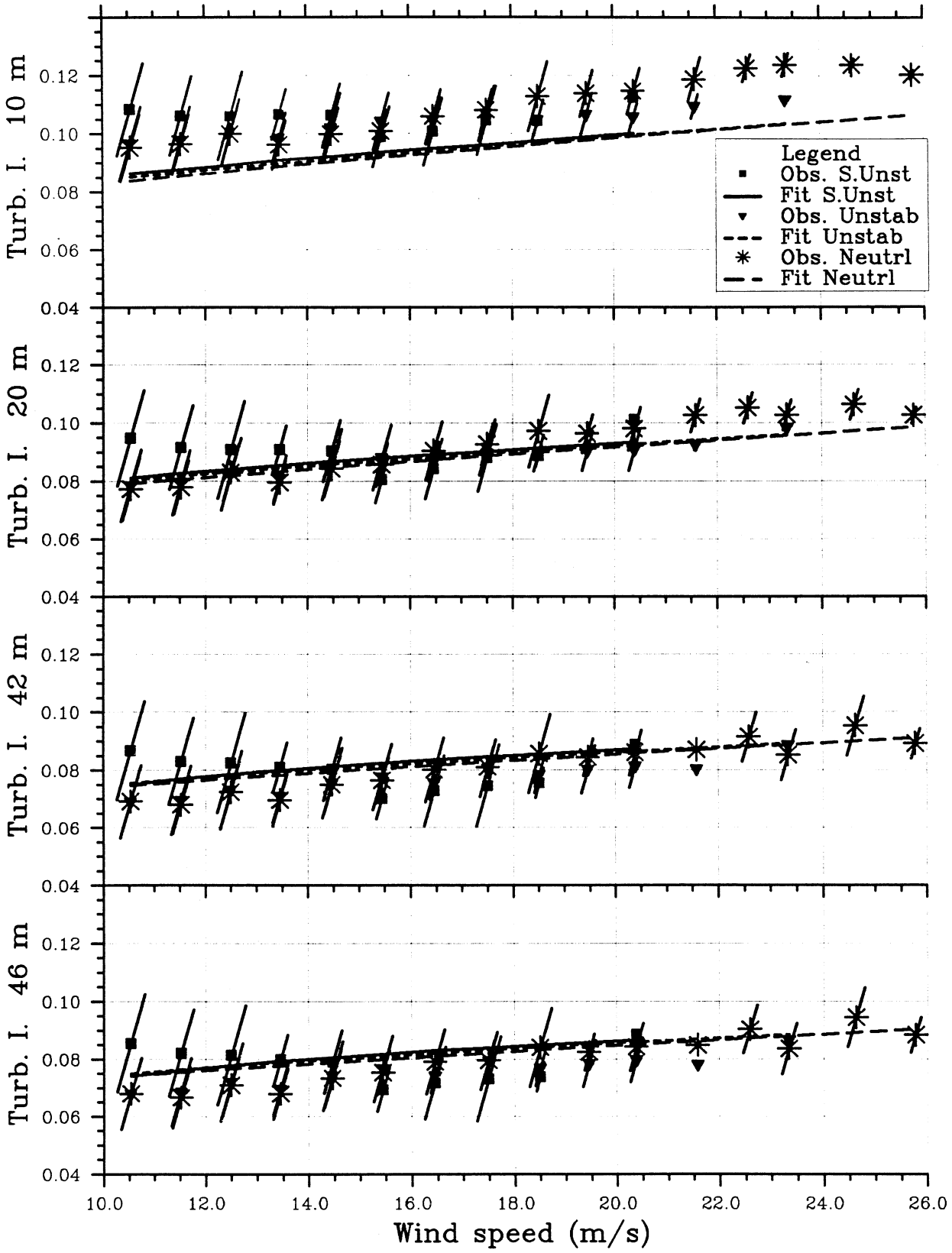

Fig. 5.2-M1.2 A least squares fit of the Panofsky model, Eq. (5.2.1-2), to the turbulence intensity data for unstable atmospheric conditions.

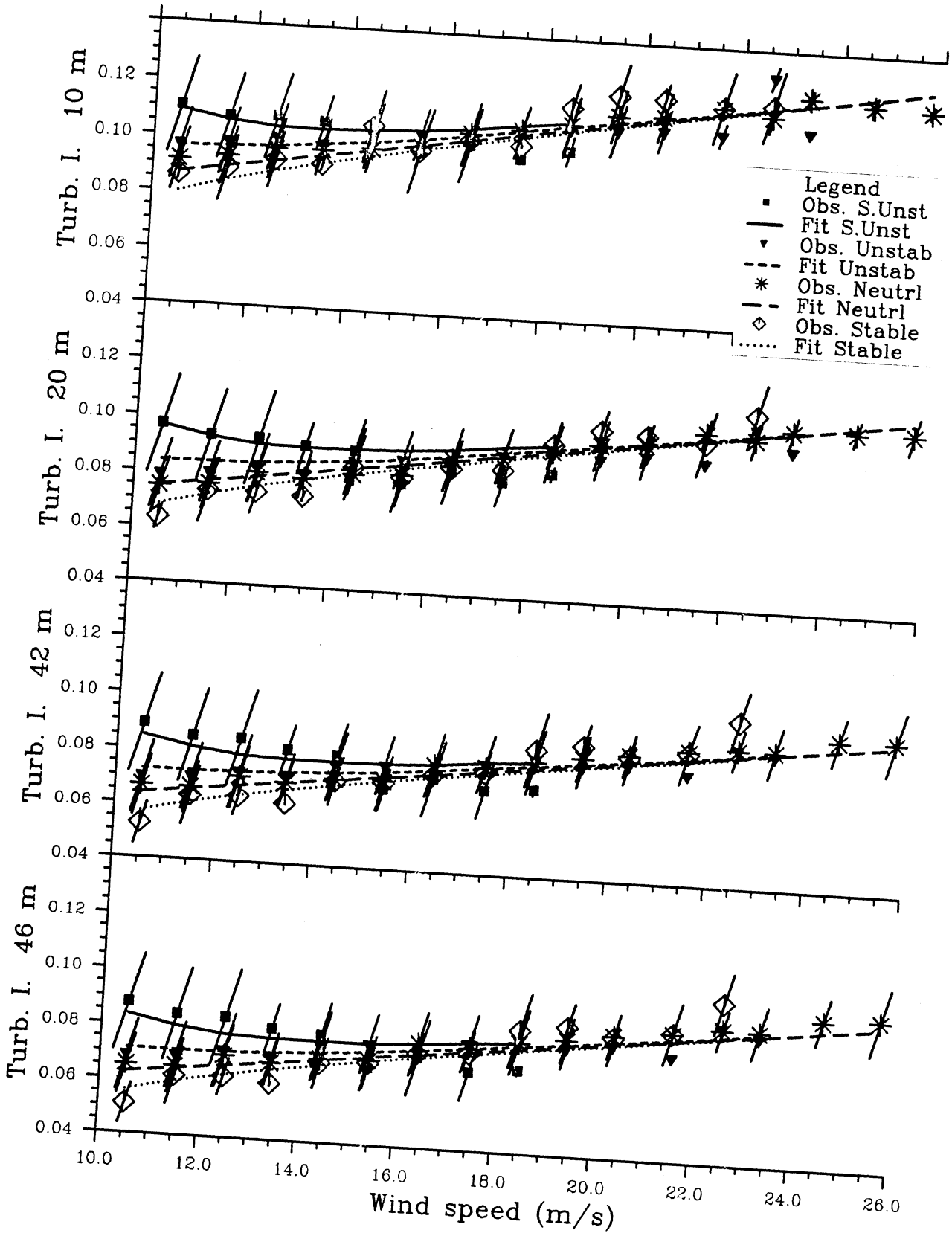

Fig. 5.2-M2 A least squares fit of the ad hoc model, Eq. (5.2.3) to the complete set of turbulence intensity data.

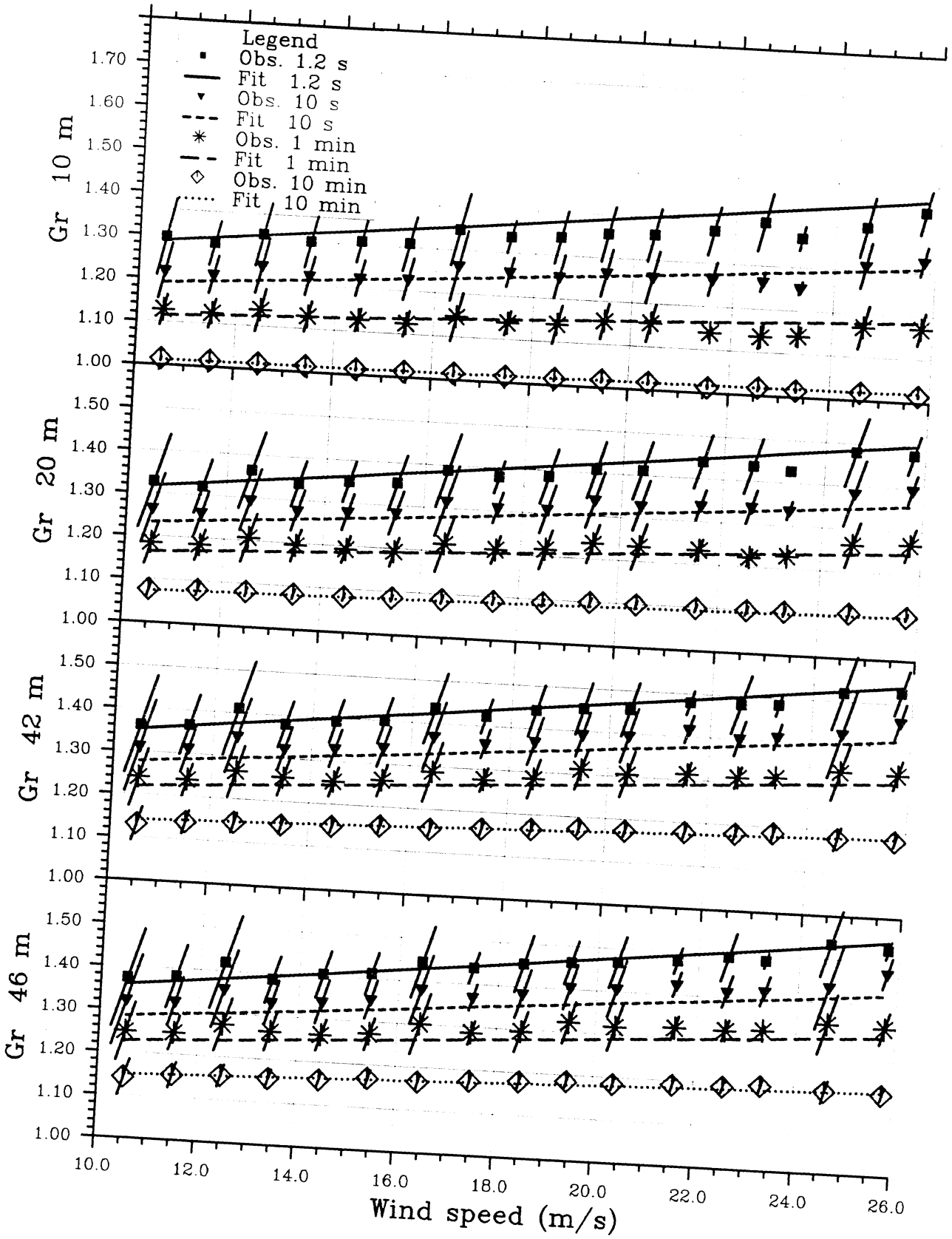

Fig. 6.1-M1 A least squares fit of the Mackey model, Eq. (6.1.5) to the "near" neutral data for reference gust factor.

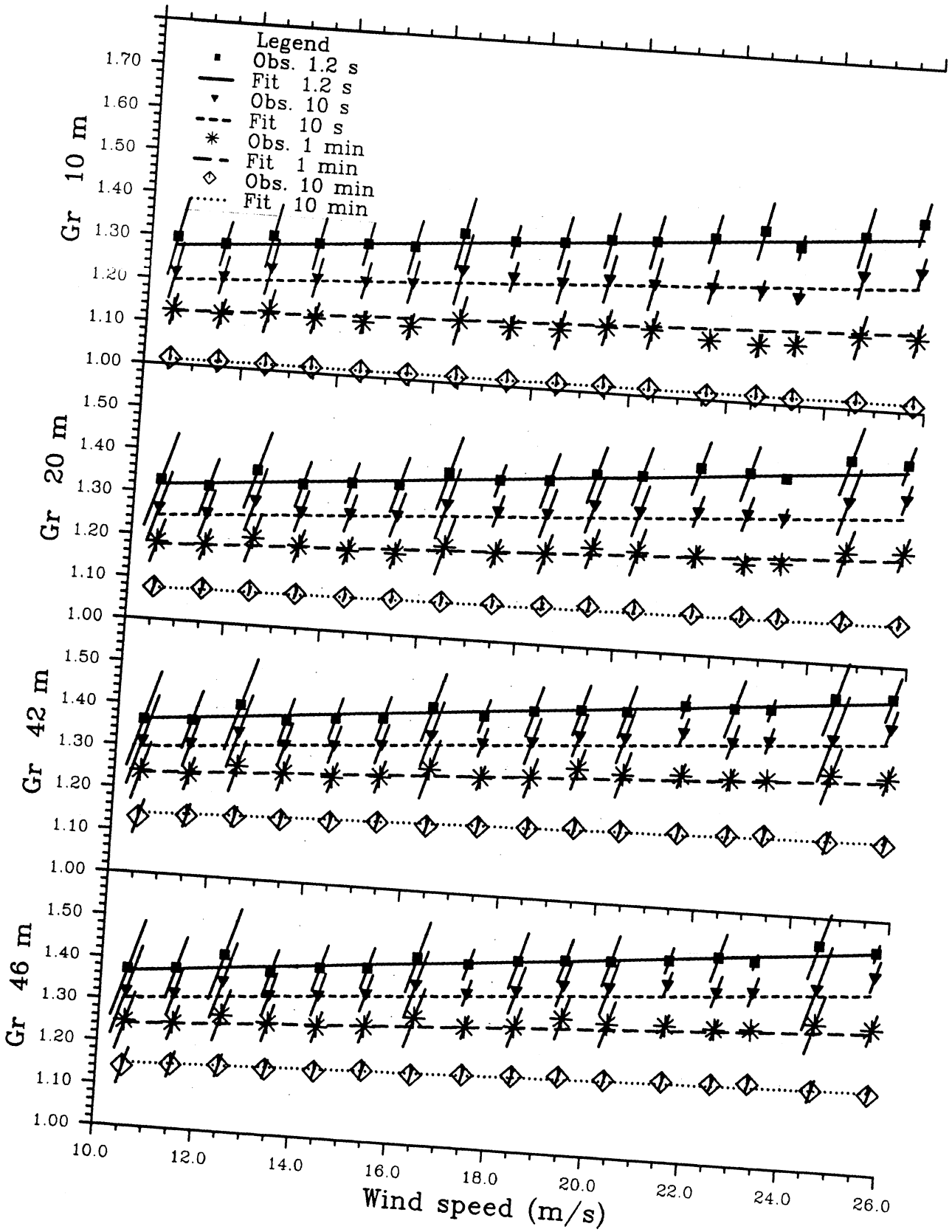

Fig. 6.1-M2 A least squares fit of the modified Mackey/Ishizaki model, Eq. (6.1.9) to the "near" neutral data for reference gust factor.

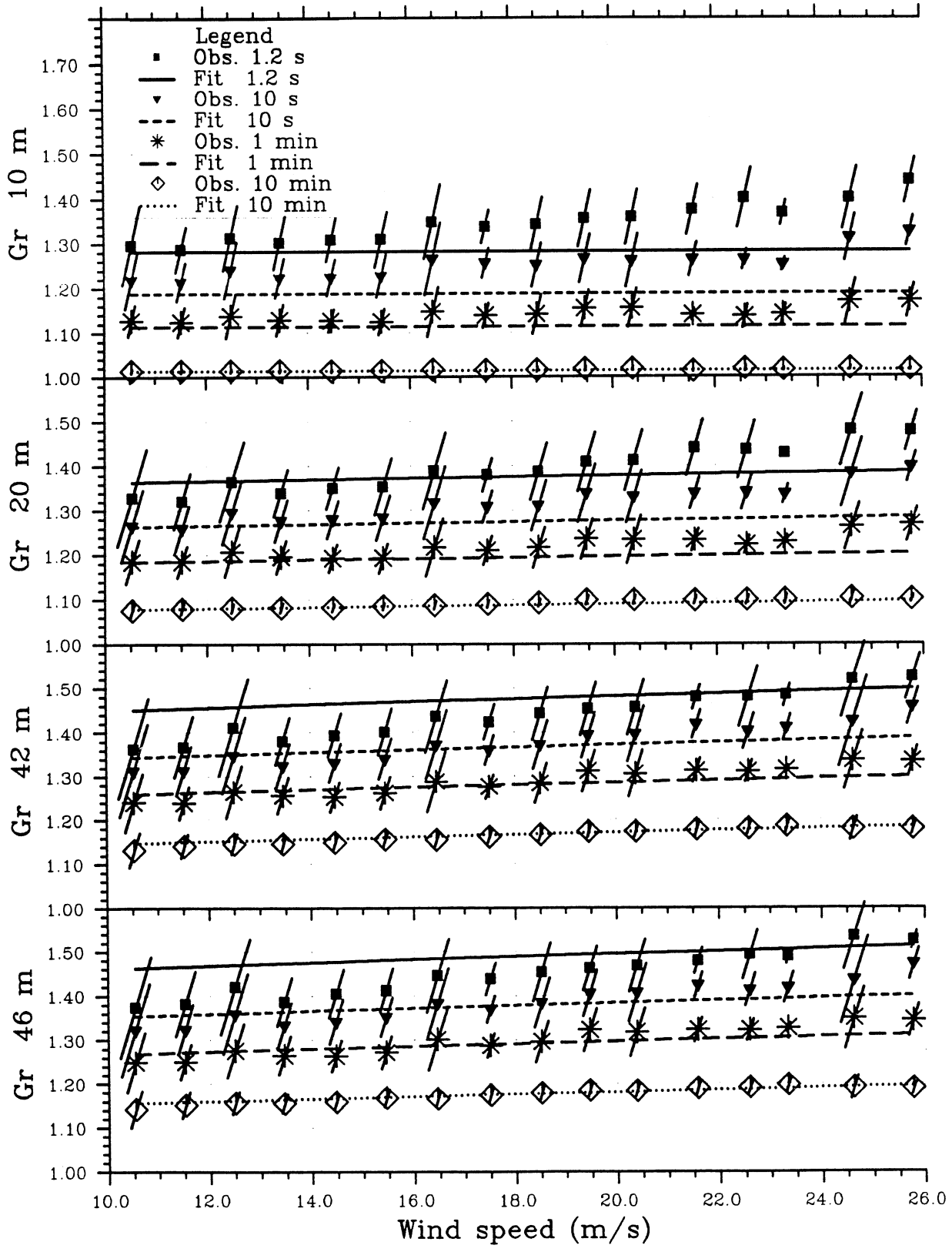

Fig. 6.1-M3 A least squares fit of the " a + b ln(t_g)" model, Eq. (6.1.12) to the "near" neutral data for reference gust factor.

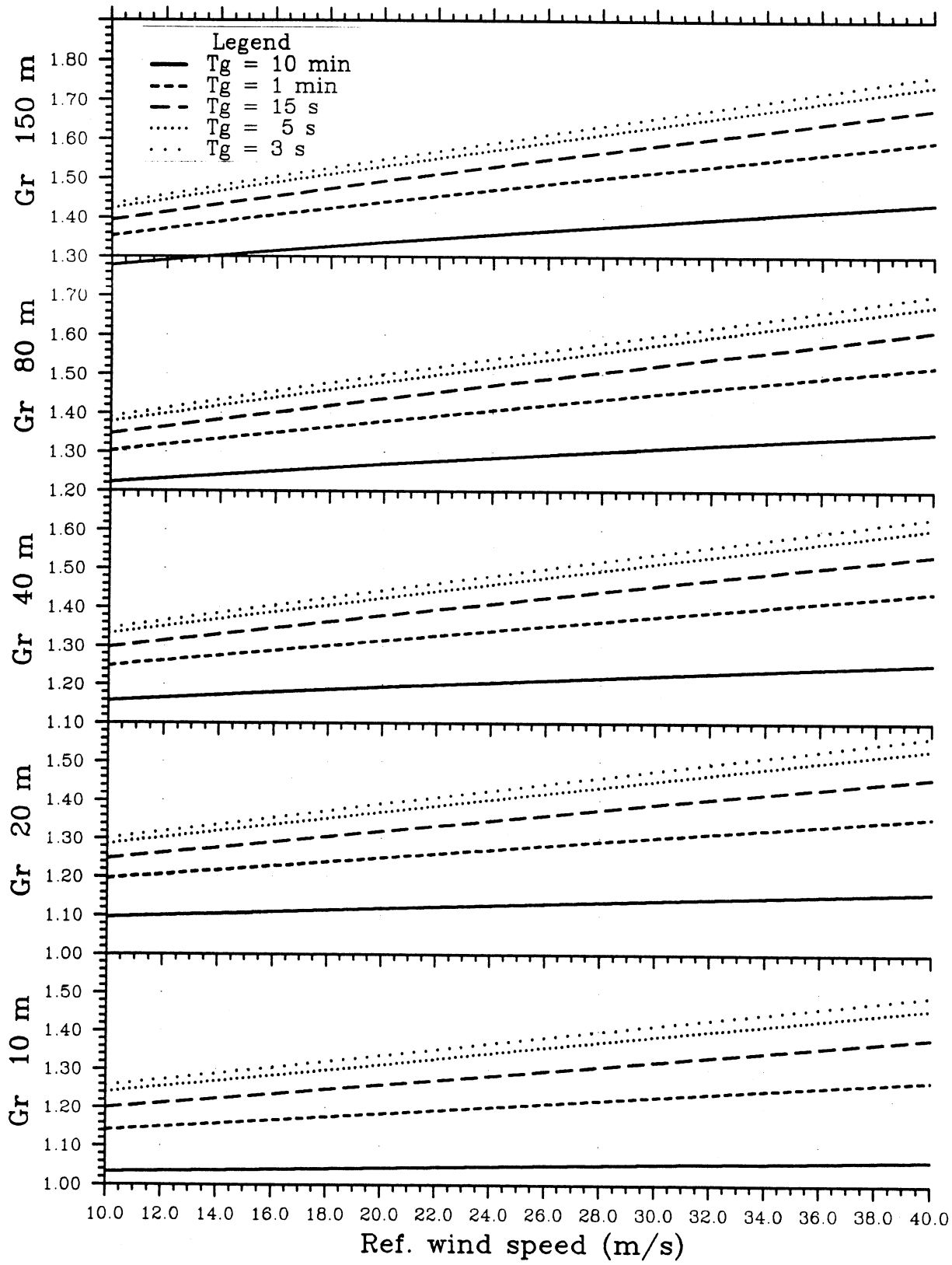

Fig. 6.1.4 Reference gust factor according to the model (6.1.9-10) versus reference wind speed. Curves are given for the heights 10, 20, 40, 80 and 150 m, and for gust intervals 3, 5, 15, 60 and 600 s. See text for comments on validity.

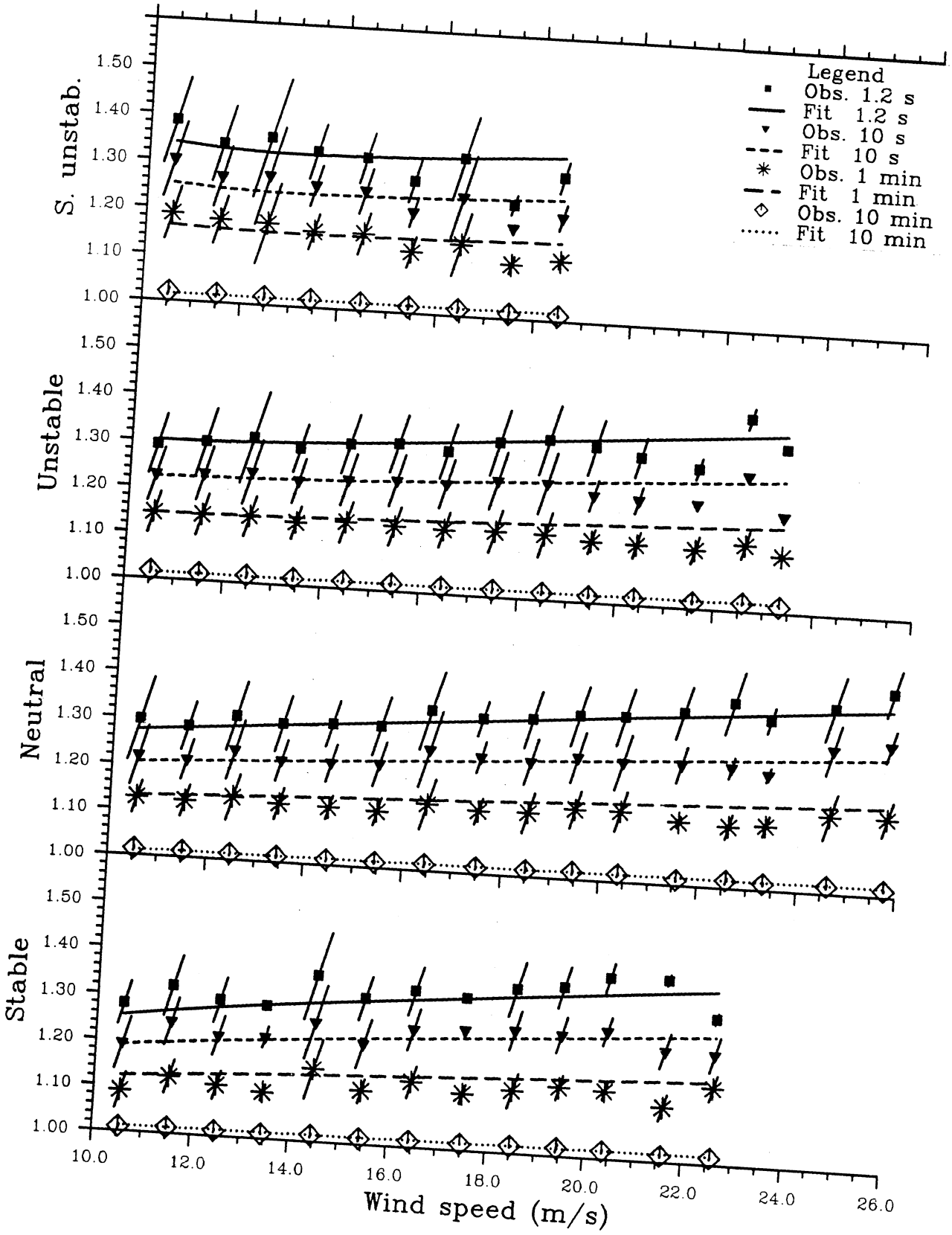

Fig. 6.2.1 A least squares fit of the model (6.1.9) to reference gust factor values for general atmospheric stability. The data are shown for 10 m height and for 4 stability classes.

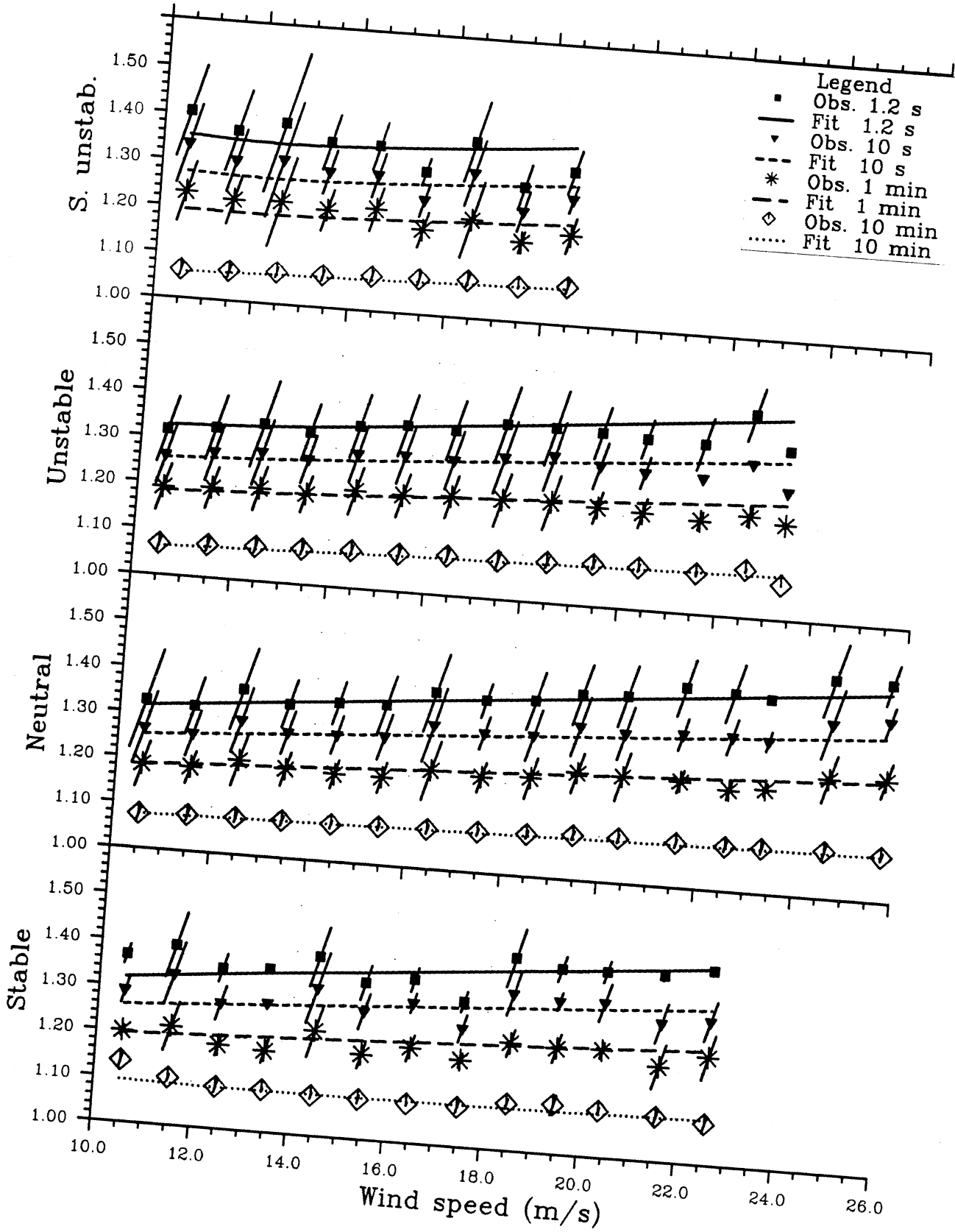

Fig. 6.2.2 As Fig. 6.2.1, but for 20 m height.

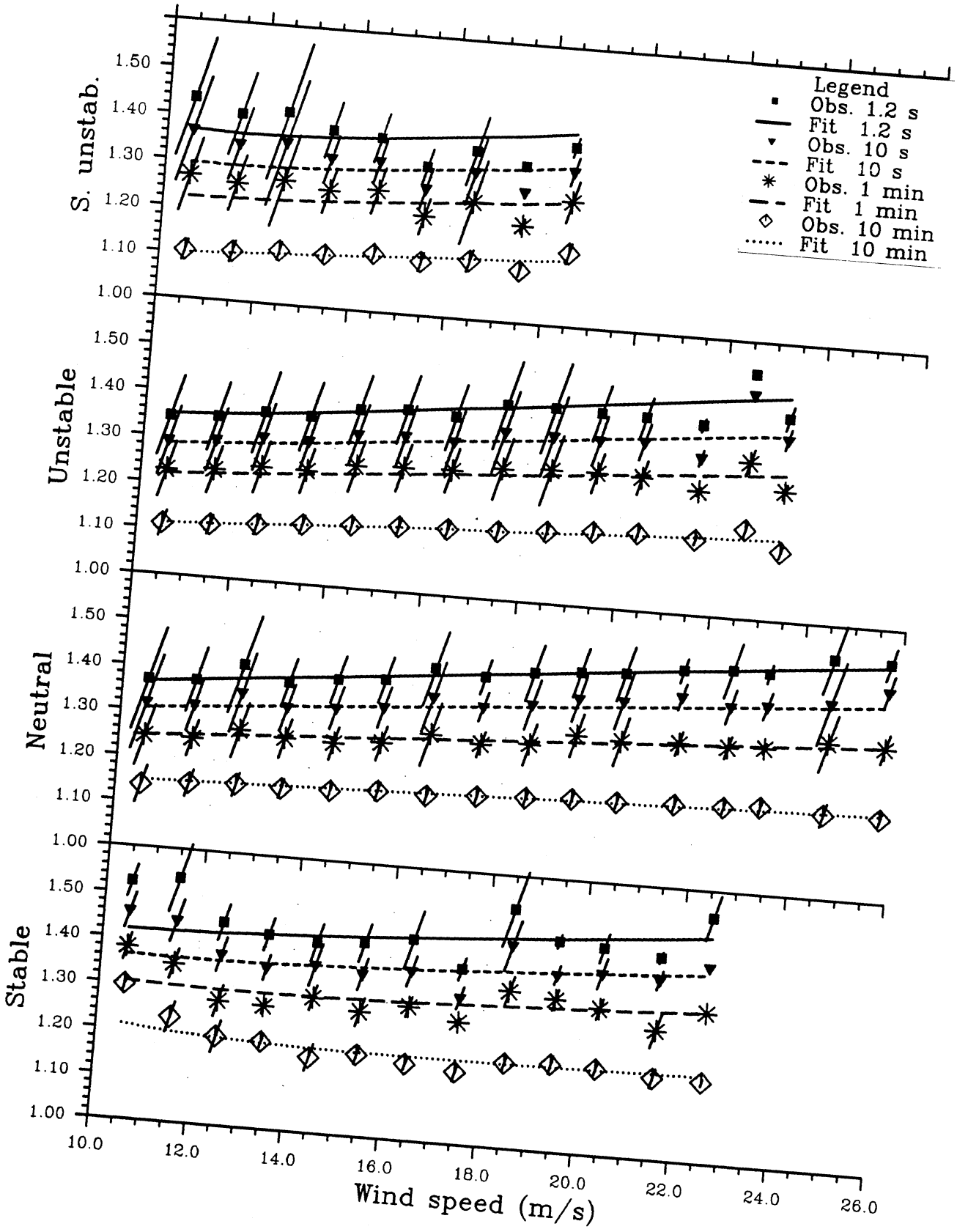

Fig. 6.2.3 As Fig. 6.2.1, but for mean values of data from 42 and 46 m height.

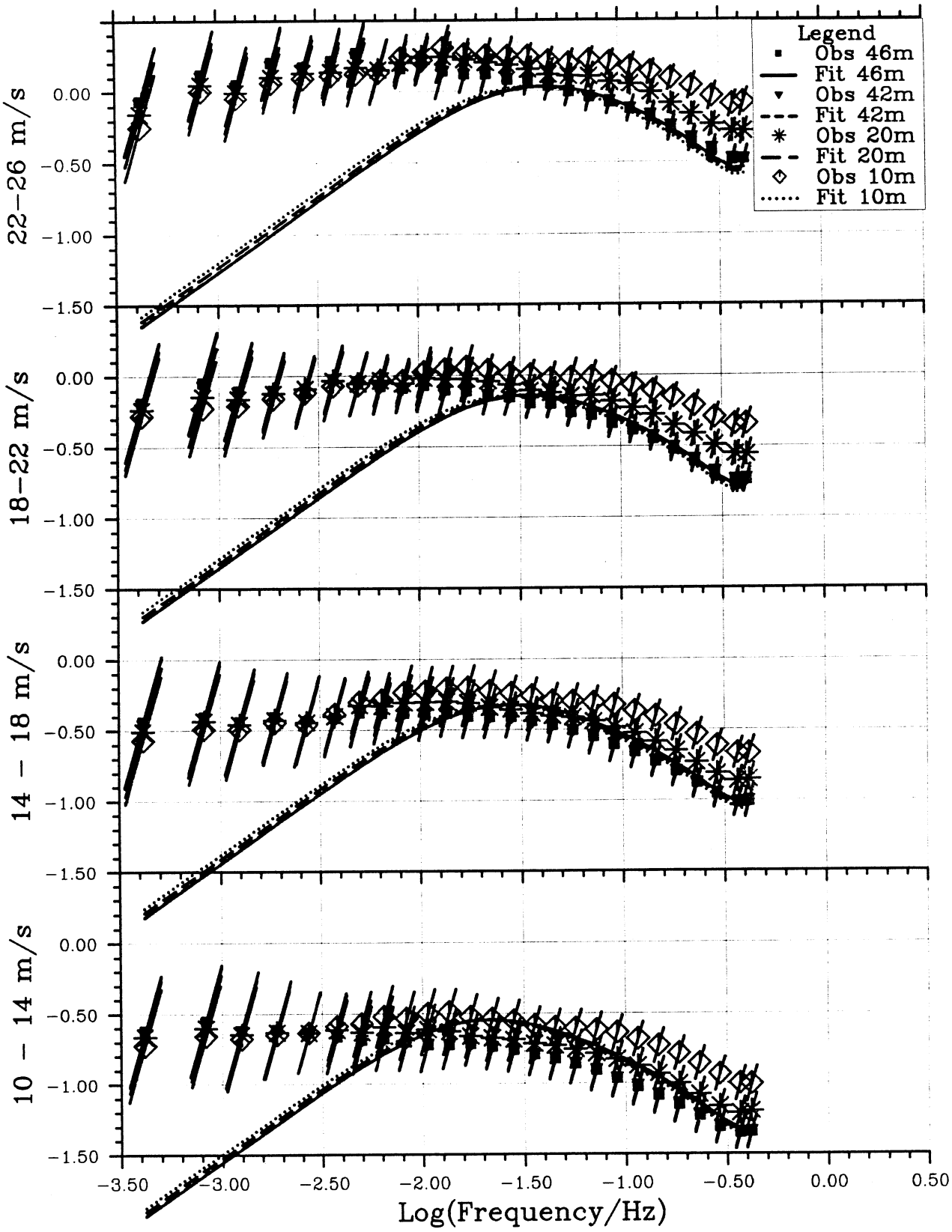

Fig. 7.2-M1 Spectra for four wind speed classes, four heights and neutral stability versus frequency ($\log_{10}$[fS(f)] versus $\log_{10}$f) with a fit of the Harris/NPD model (see text, SI units understood).

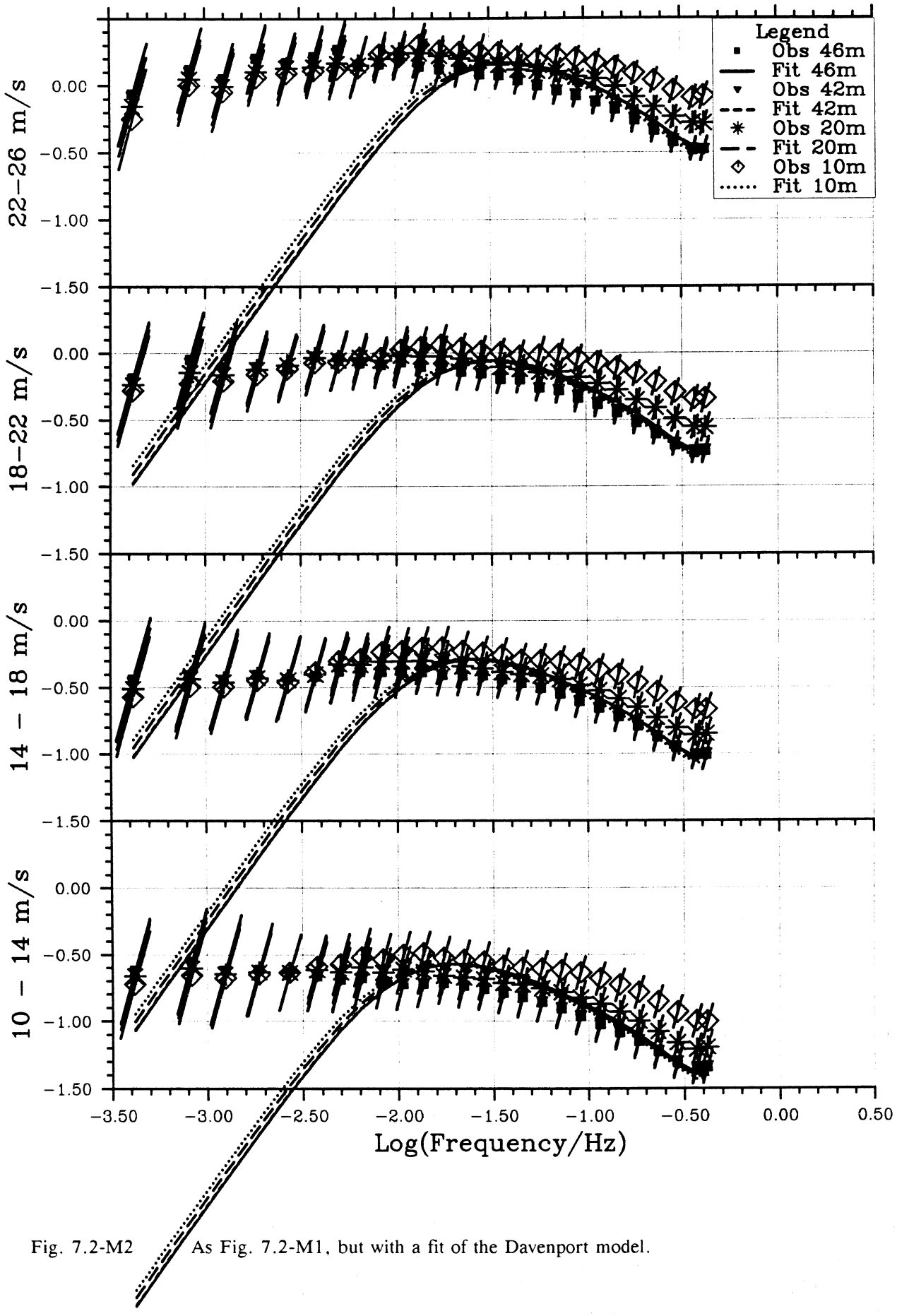

Fig. 7.2-M2 As Fig. 7.2-M1, but with a fit of the Davenport model.

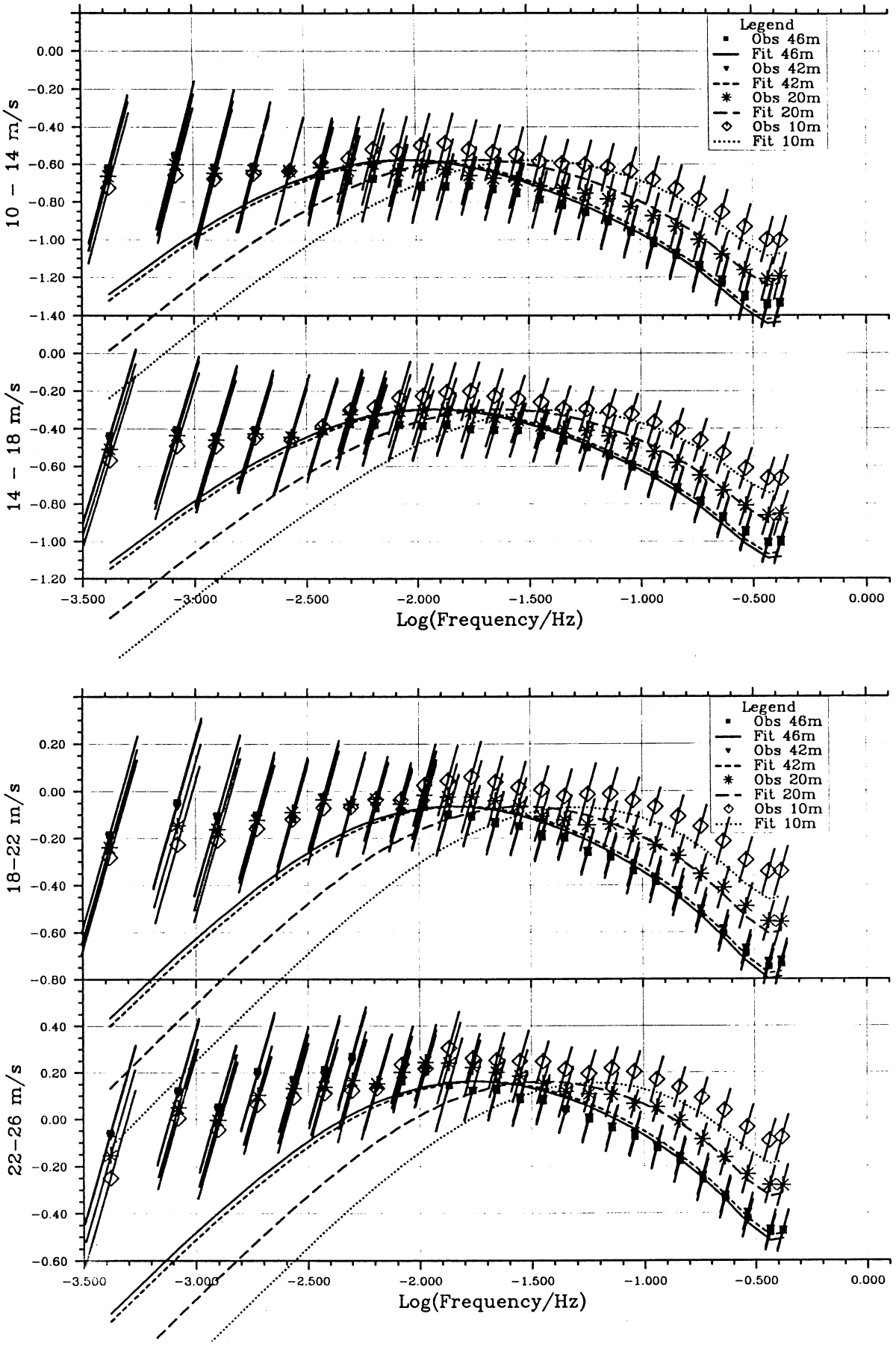

Fig. 7.2-M3 As Fig. 7.2-M1, but with a fit of the Kaimal model.

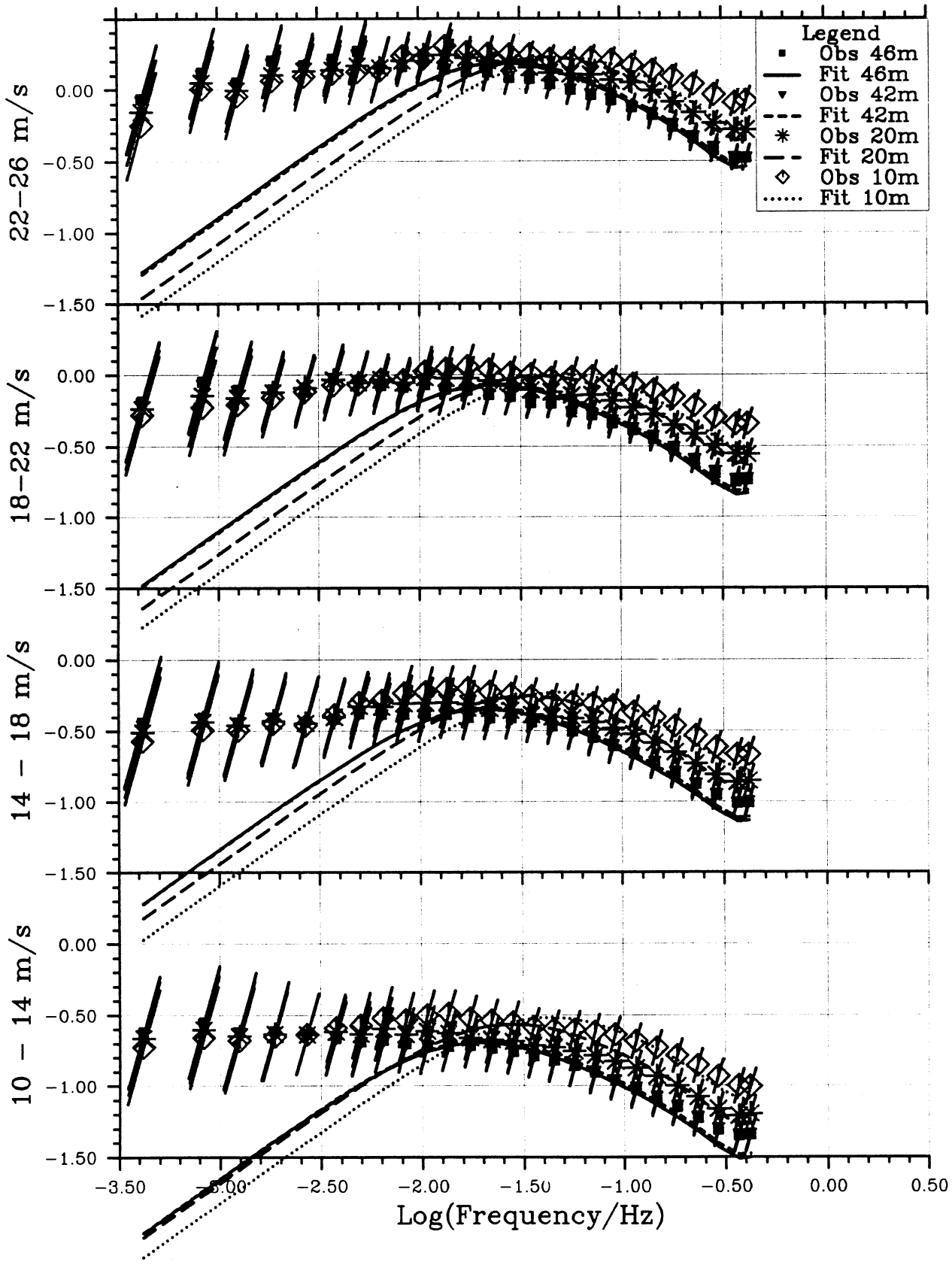

Fig. 7.2-M4 As Fig. 7.2-M1, but with a fit of the Deaves & Harris model.

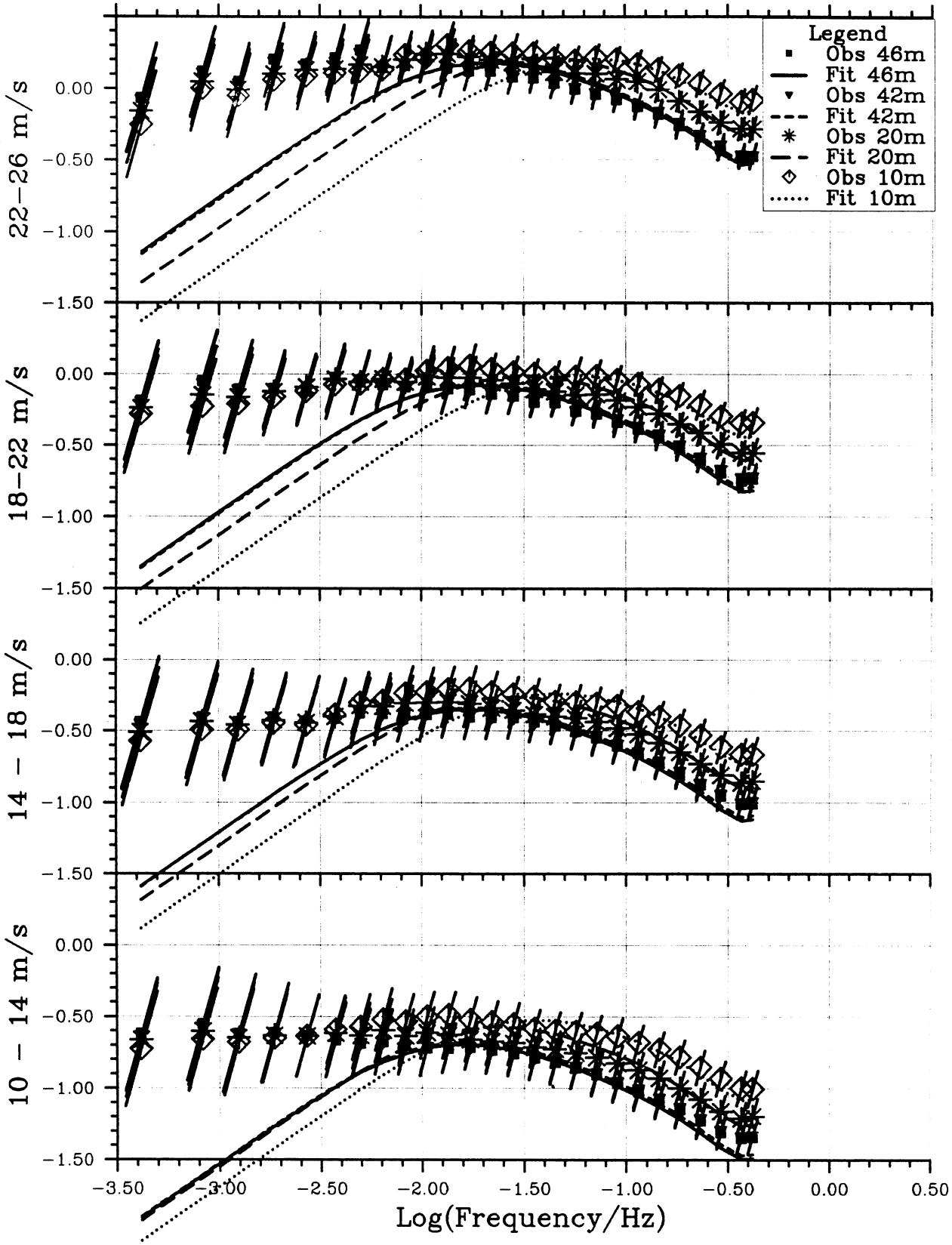

Fig. 7.2-M5 As Fig. 7.2-M1, but with a fit of the ESDU model.

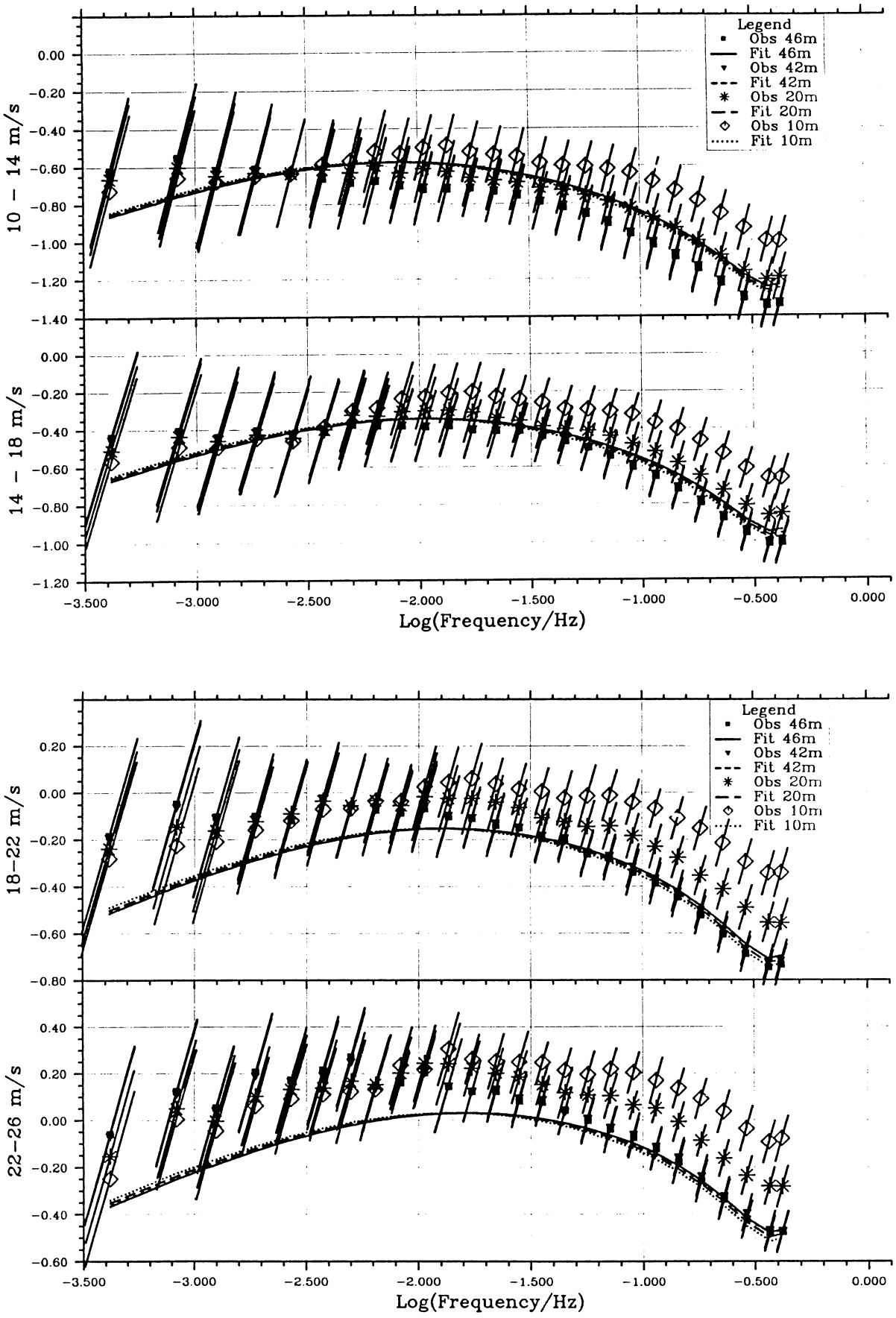

Fig. 7.2-M6 As Fig. 7.2-M1, but with a fit of the Standing model.

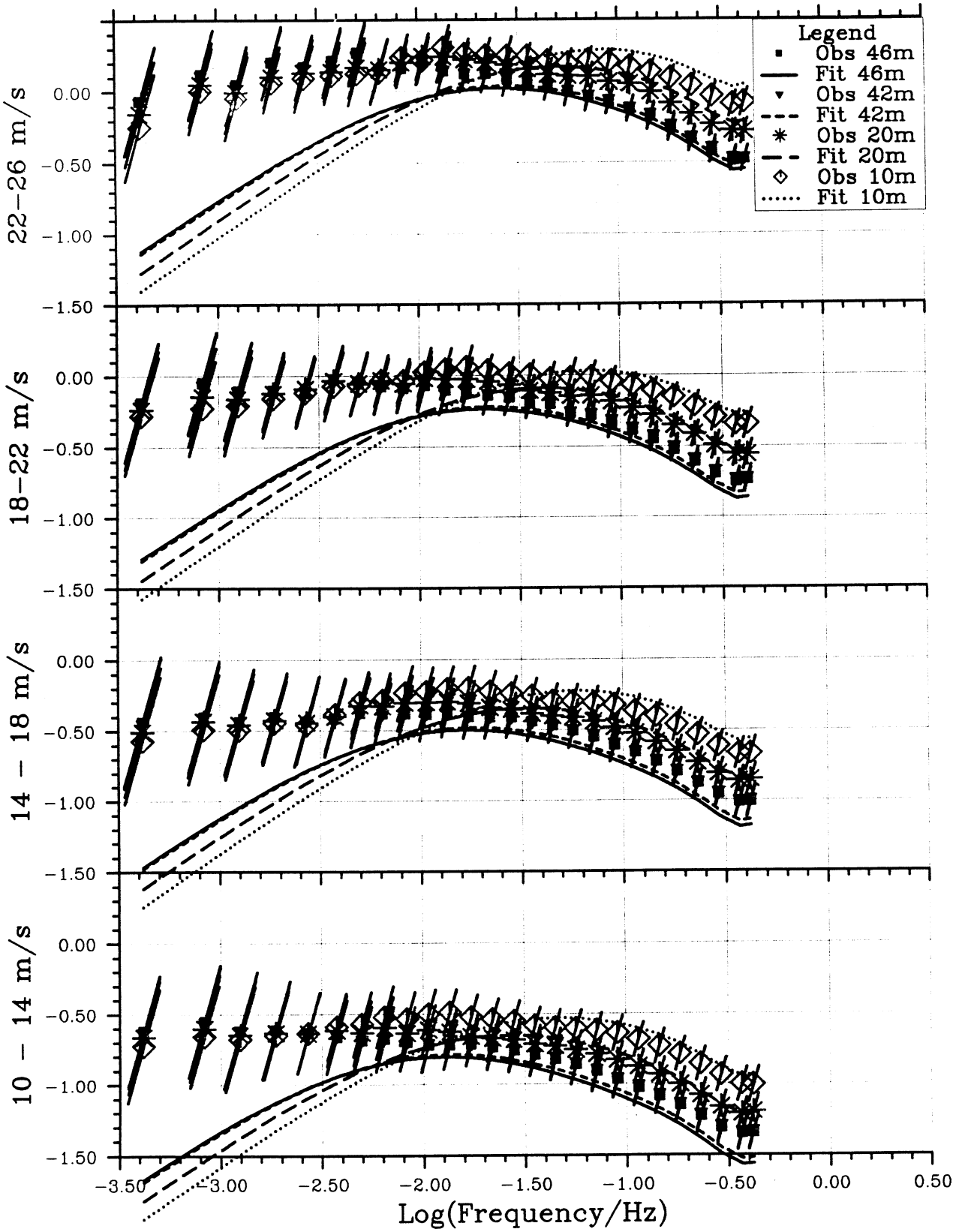

Fig. 7.2-M7 As Fig. 7.2-M1, but with a fit of the Naito/Kaimal model.

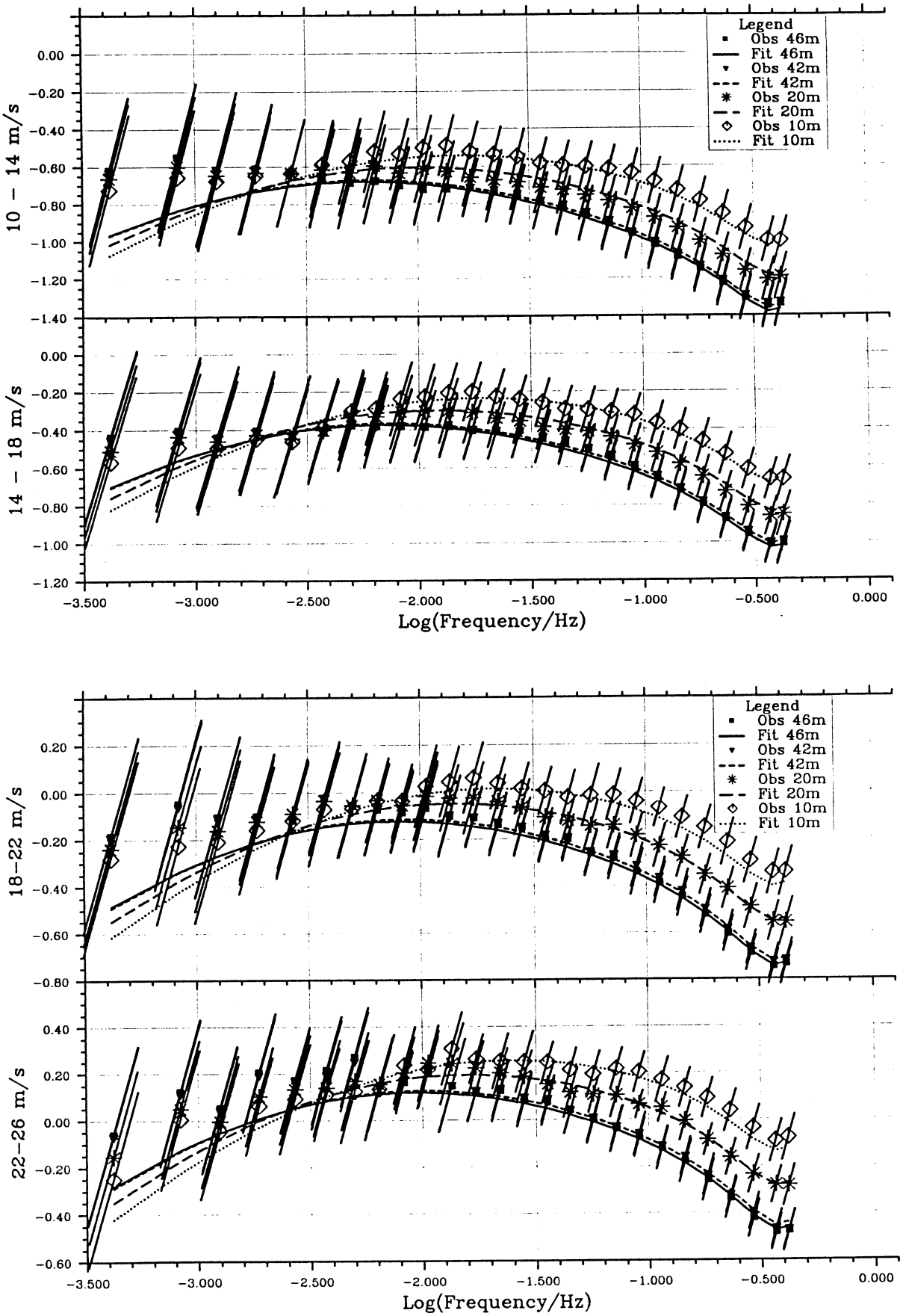

Fig. 7.2-M8 As Fig. 7.2-M1, but with a fit of the Phase 1 model.

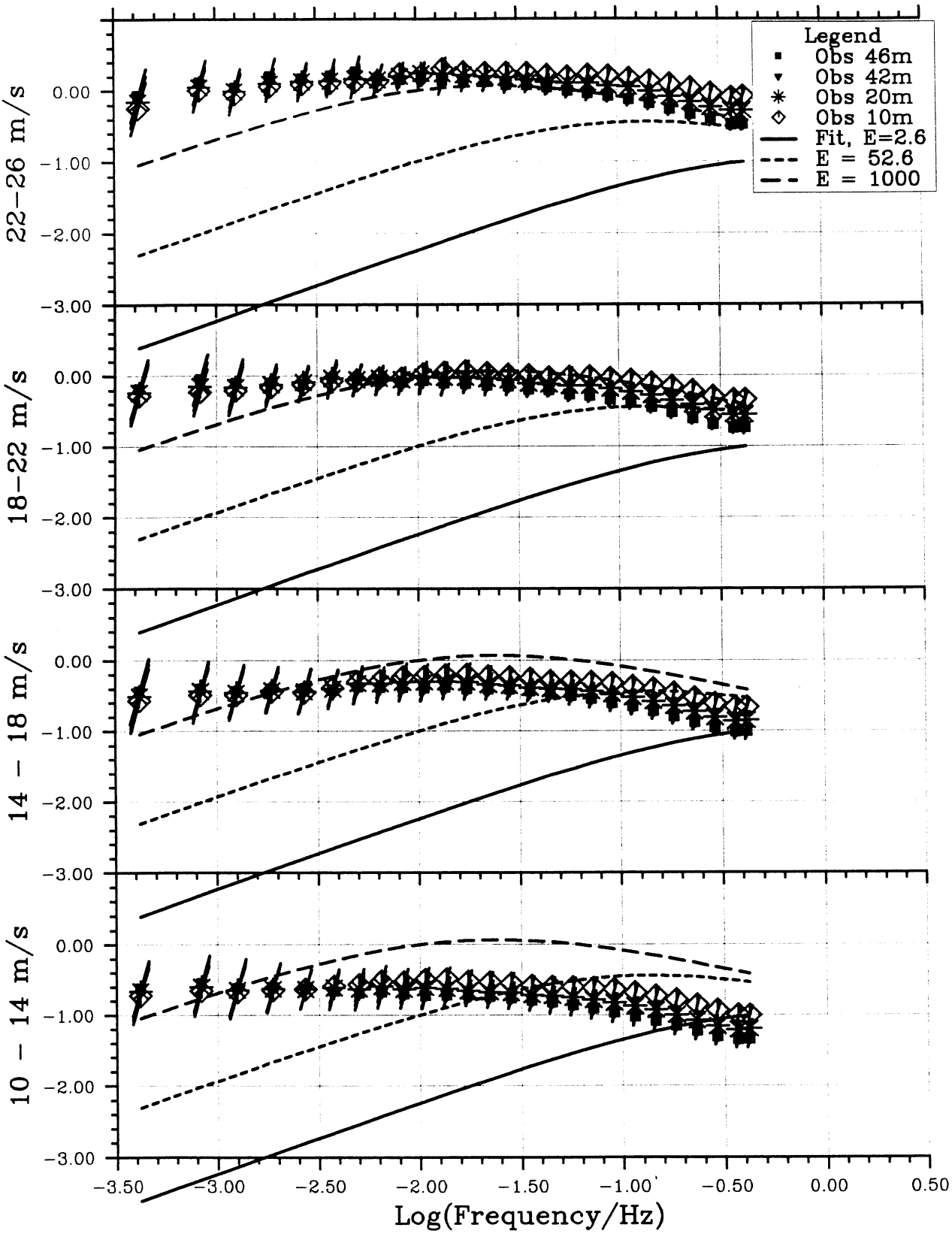

Fig. 7.2-M10 As Fig. 7.2-M1, but with a fit of the Lacour model and curves for parameter values E = 50 and E = 1000 of the same model.

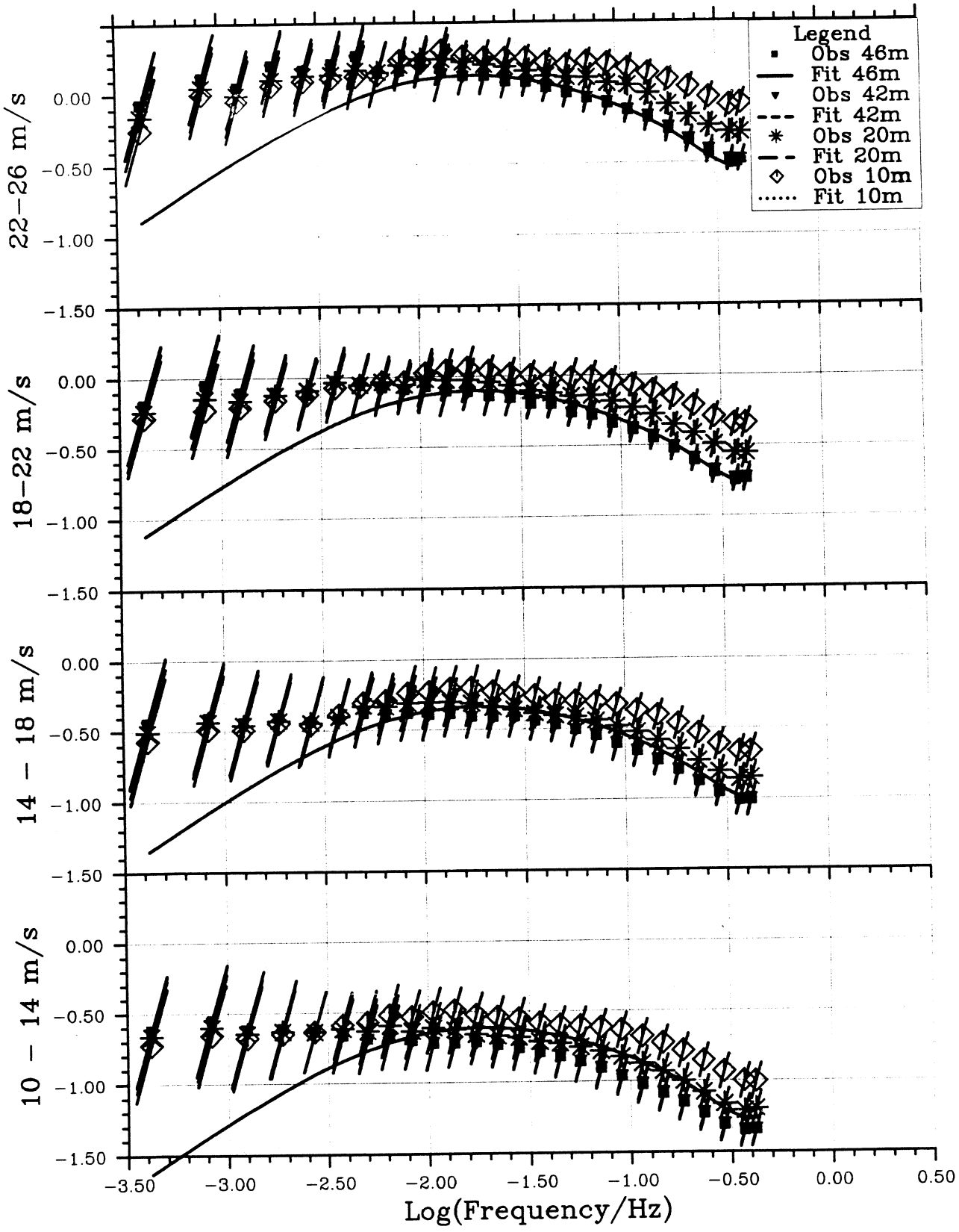

Fig. 7.2-M11 As Fig. 7.2-M1, but with a fit of the "blunt" spectrum.

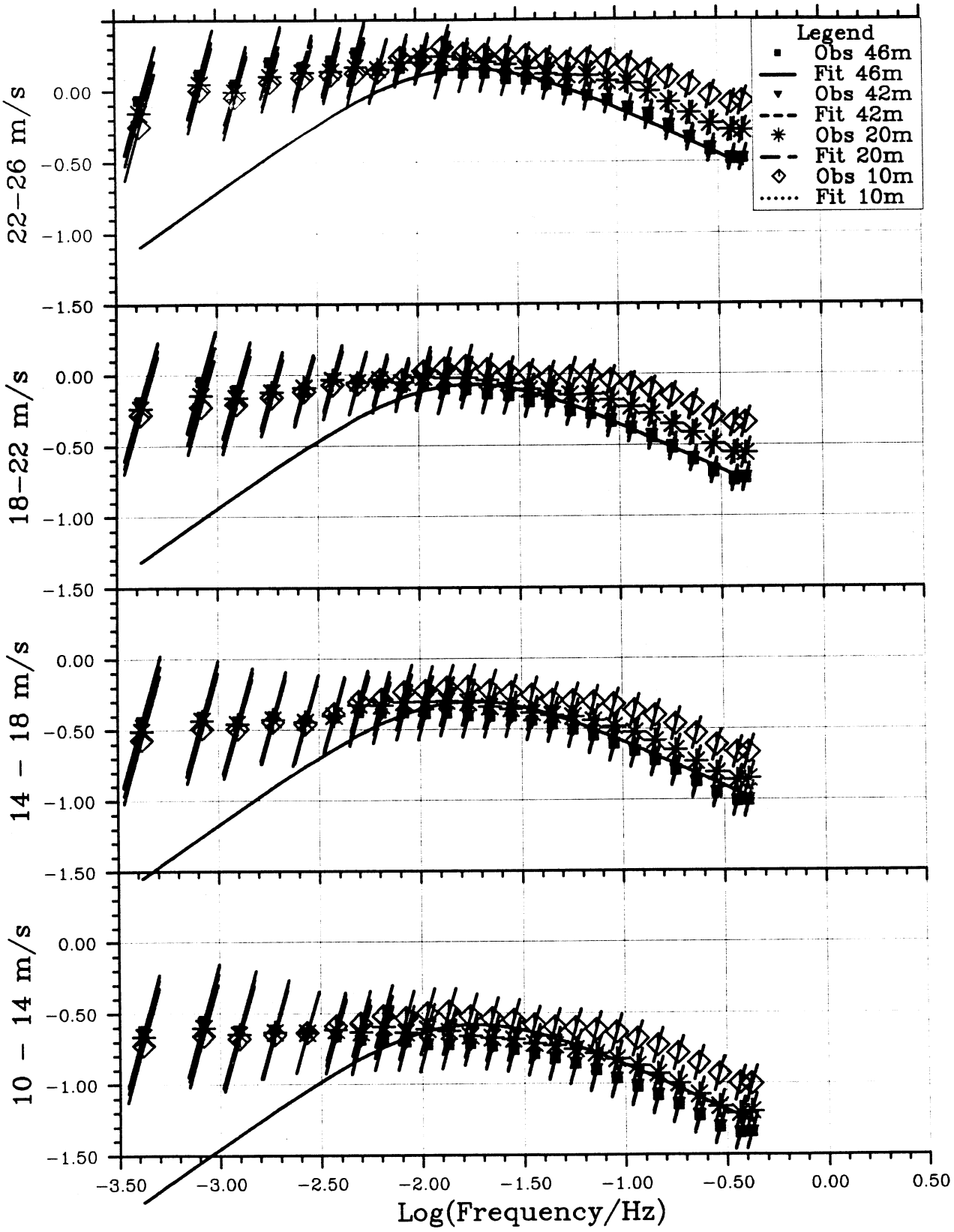

Fig. 7.2-M12 As Fig. 7.2-M1, but with a fit of the "pointed" spectrum.

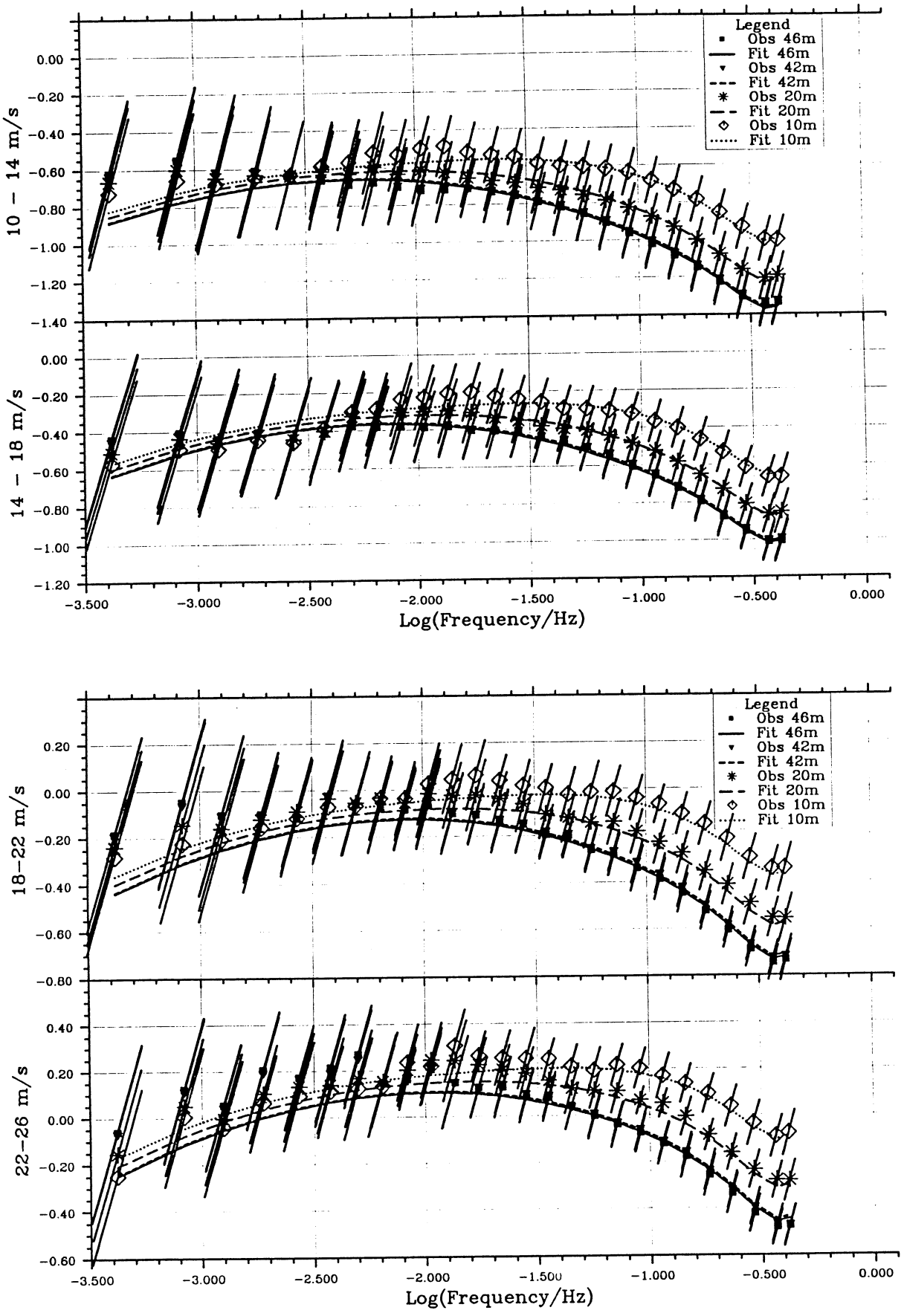

Fig. 7.2-M13 As Fig. 7.2-M1, but with a fit of the Phase 2 neutral spectrum.

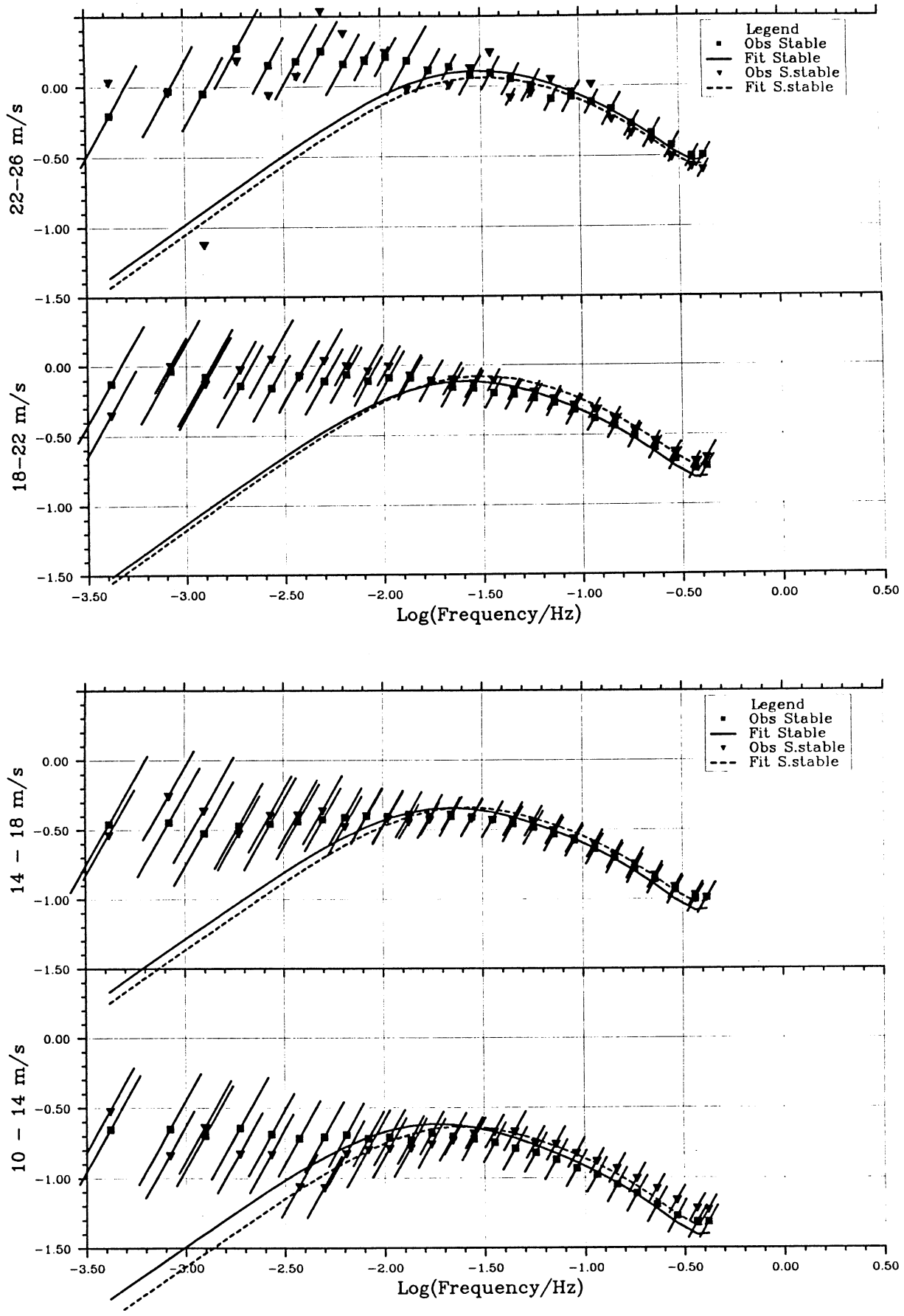

Fig. 7.3-M2a As Fig. 7.2-M1, but for the mean of the heights 42 and 46 m and two classes of stable atmospheric conditions. The curves represent a fit of the Moraes & Epstein model.

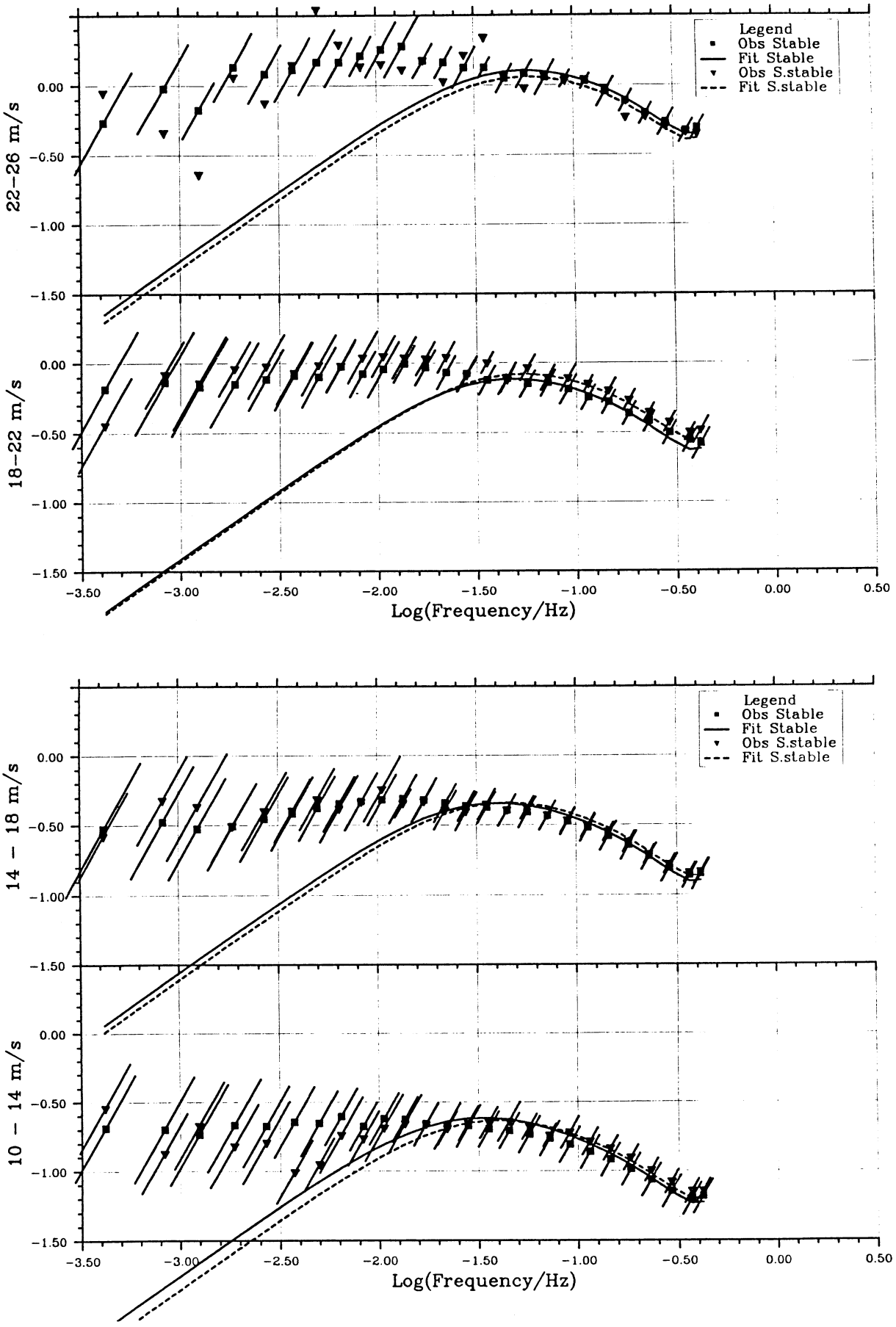

Fig. 7.3-M2b As Fig. 7.3-M2a, but for 20 m height.

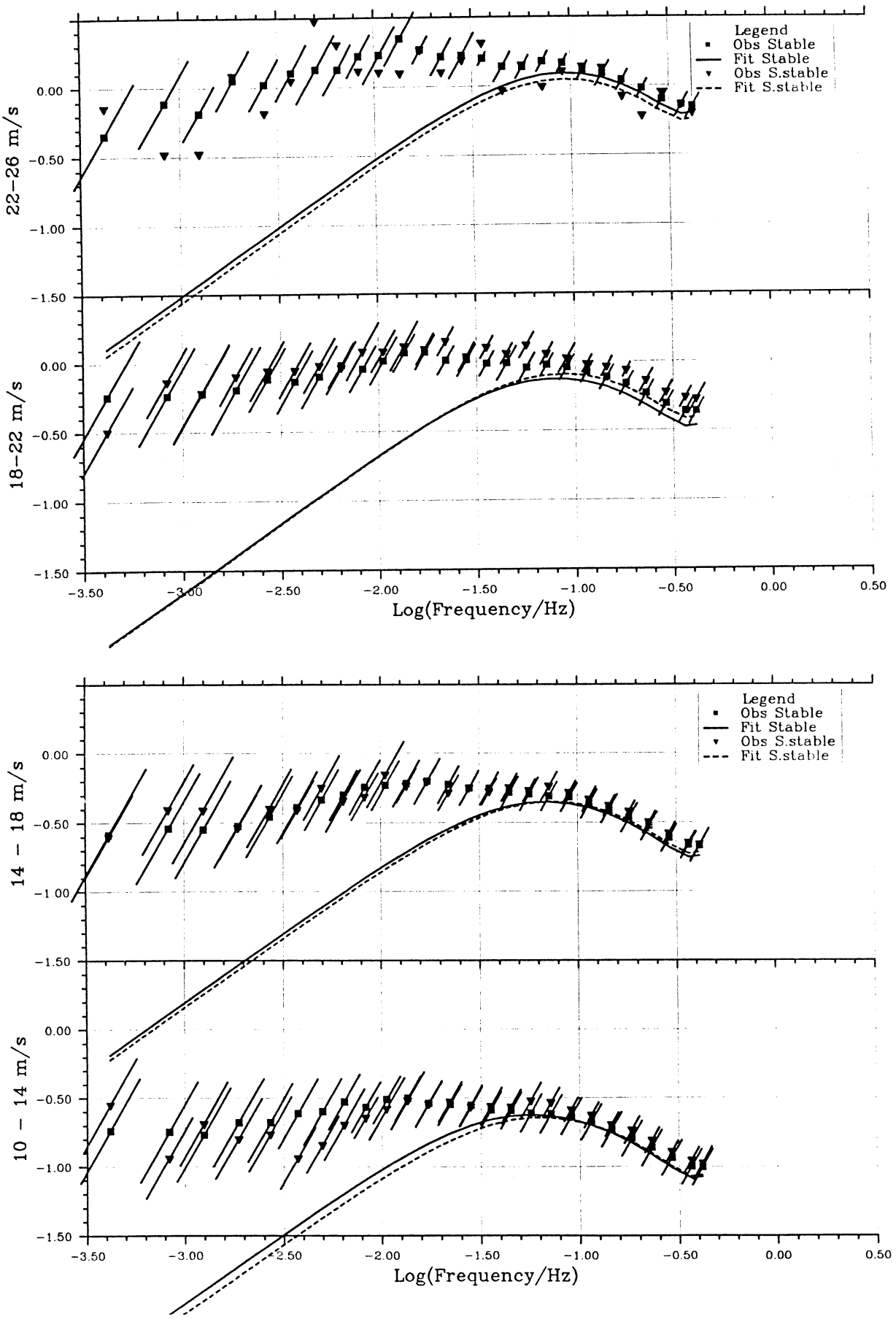

Fig. 7.3-M2c As Fig. 7.3-M2a, but for 10 m height.

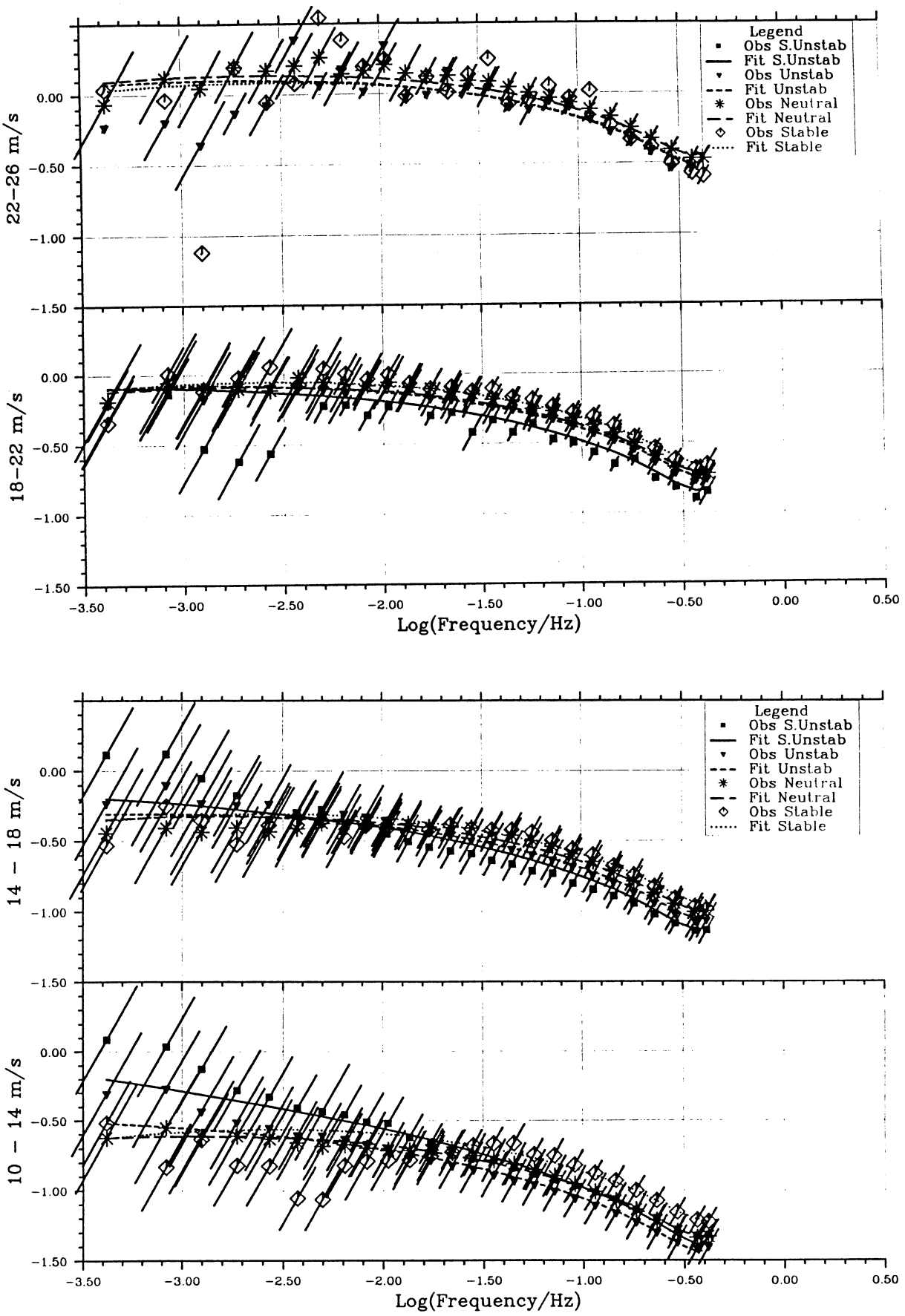

Fig. 7.3-M3a As Fig. 7.3-M2a, but for 4 classes of atmospheric stability and a fit of the Phase 2 model.

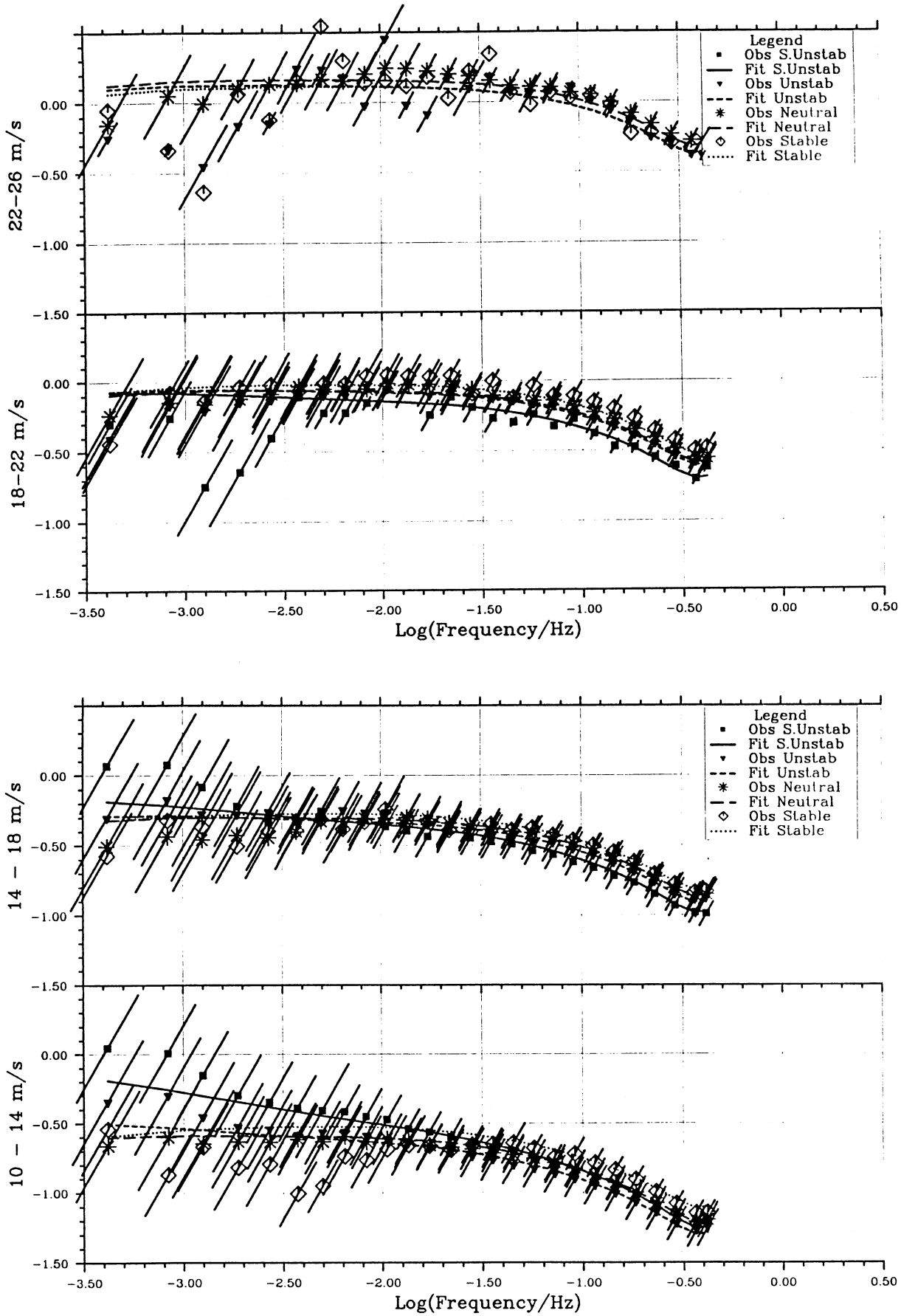

Fig. 7.3-M3b As Fig. 7.3-M3a, but for 20 m height.

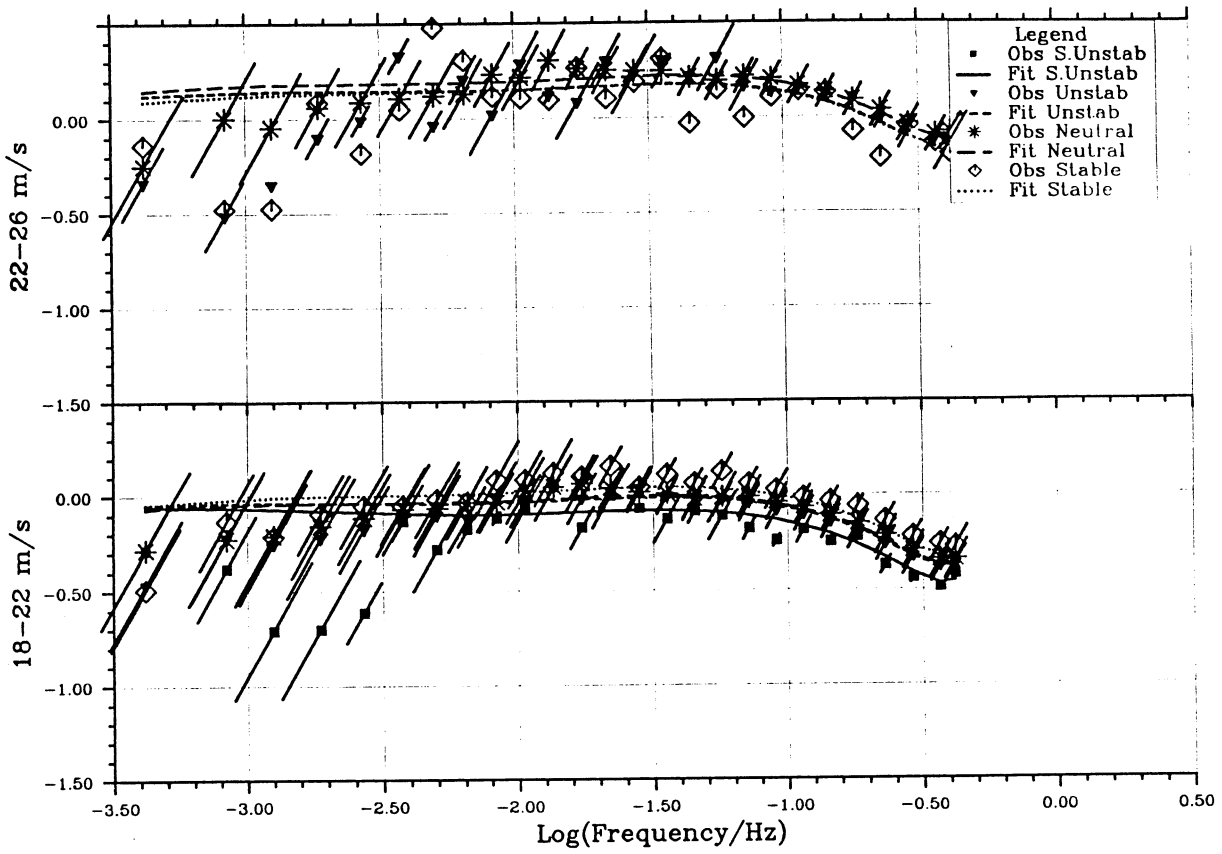

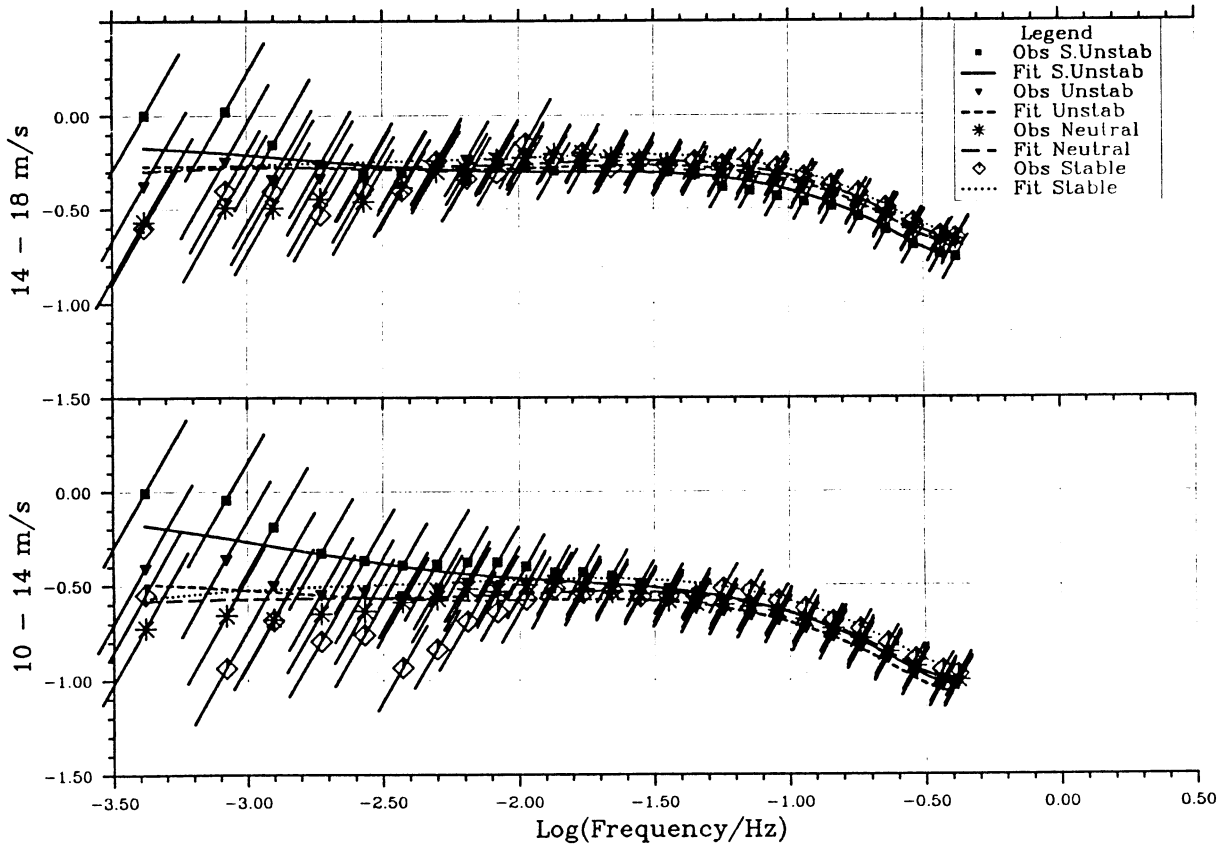

Fig. 7.3-M3c As Fig. 7.3-M3a, but for 10 m height.

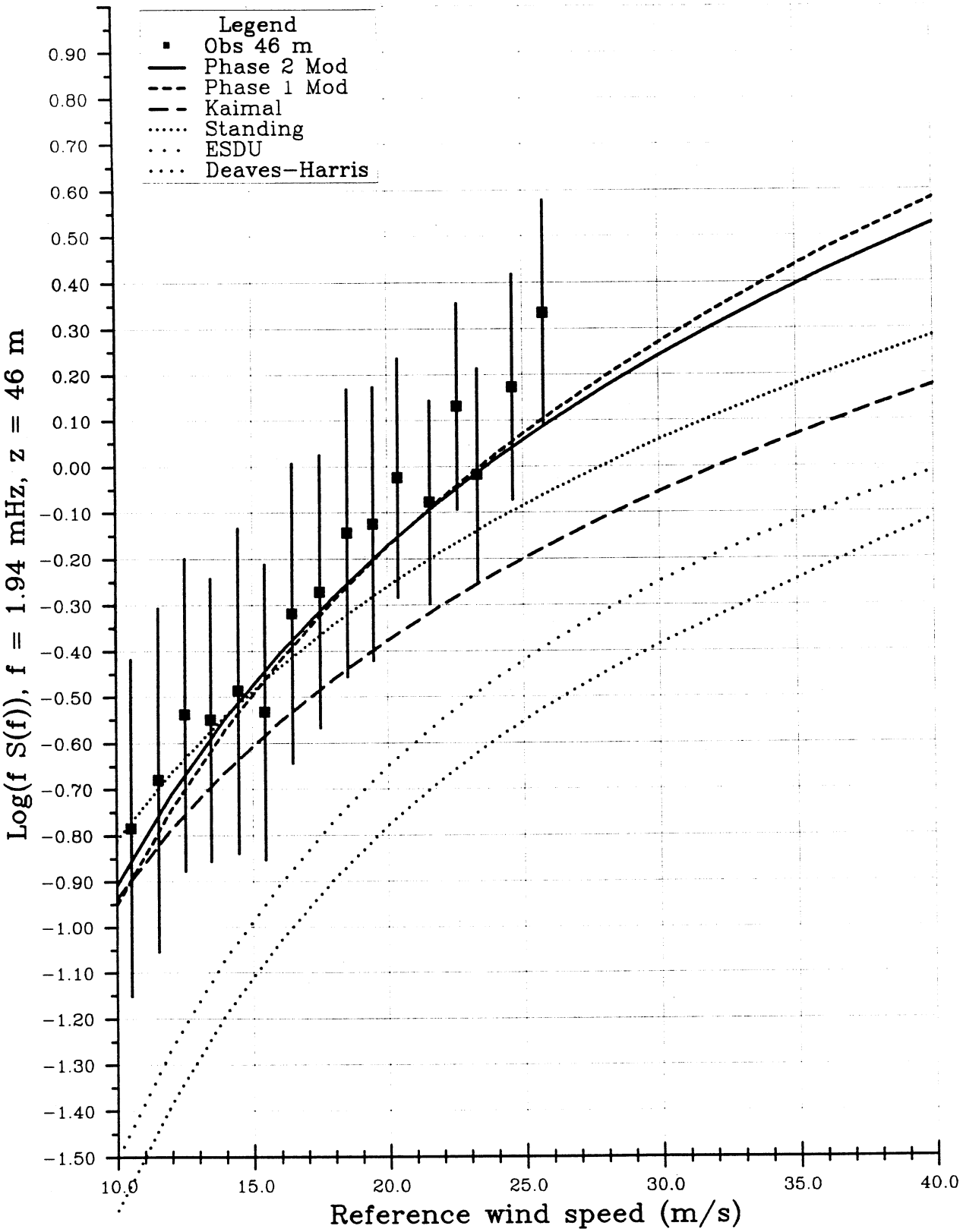

Fig. 7.4.1 Observed and model spectra versus wind speed for a height of 46 m. The observation represent mean values for 3 frequency intervals, mean frequency f = 0.00194 Hz.

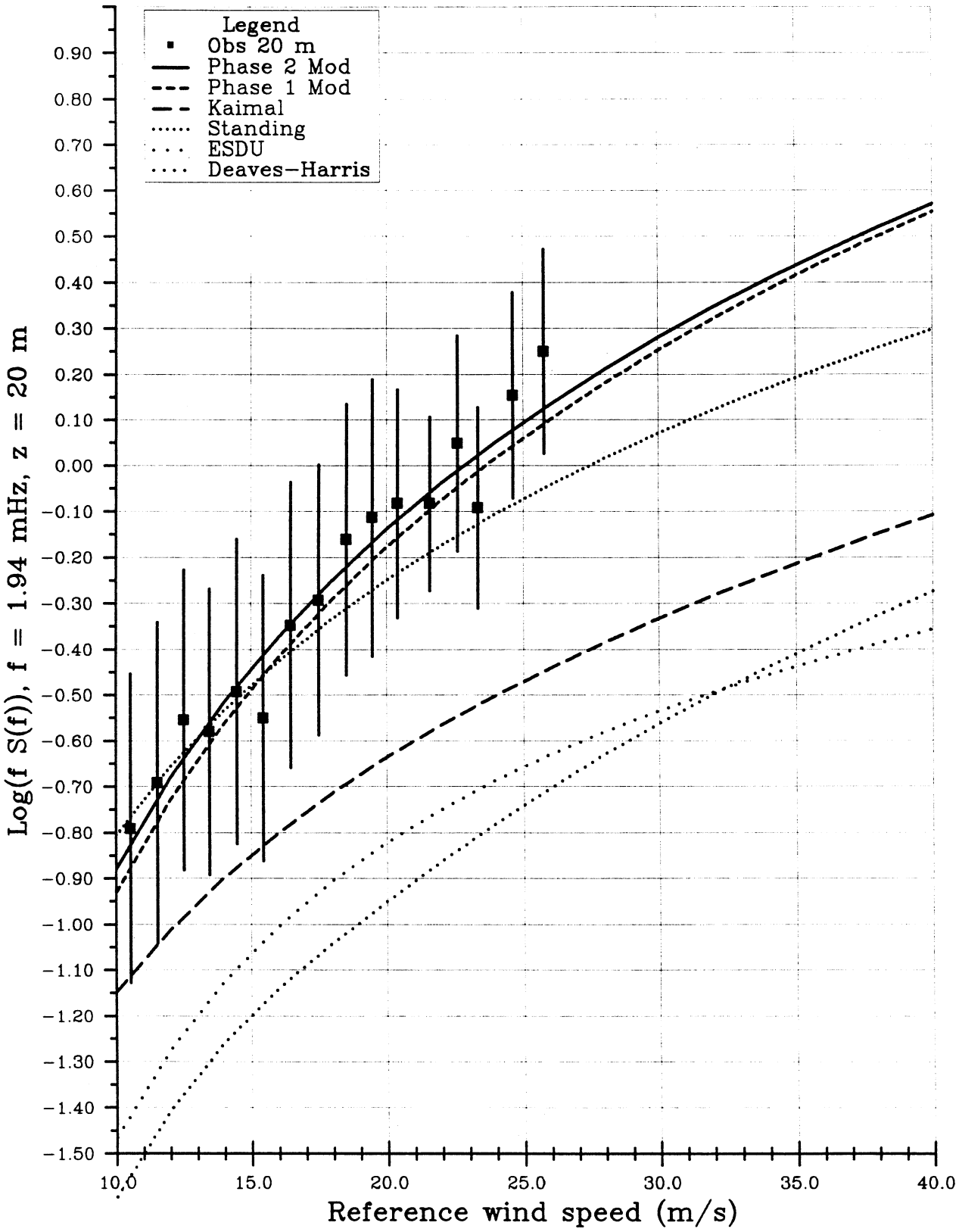

Fig. 7.4.2 As Fig. 7.4.1, but for 20 m height.

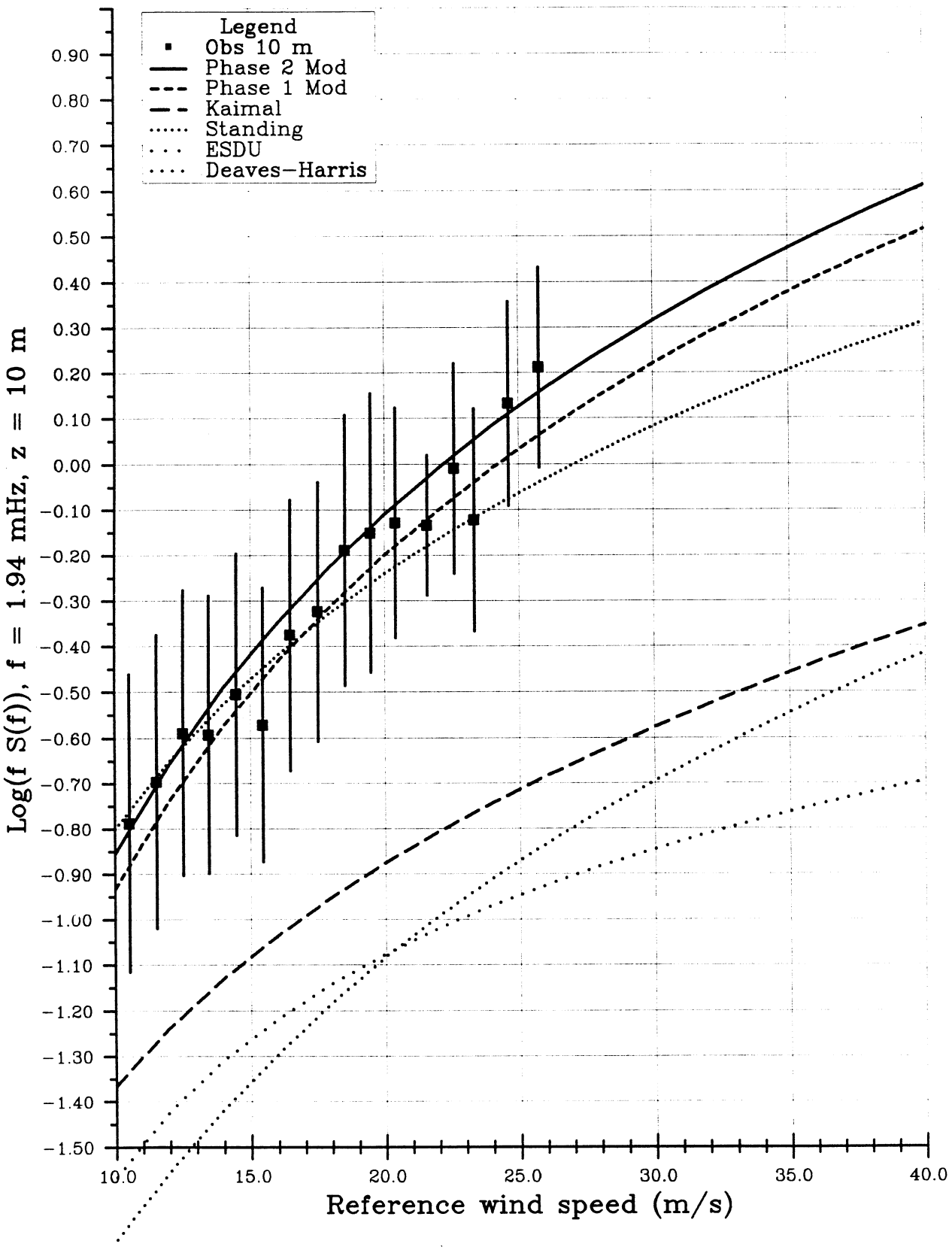

Fig. 7.4.3 As Fig. 7.4.1, but for 10 m height.

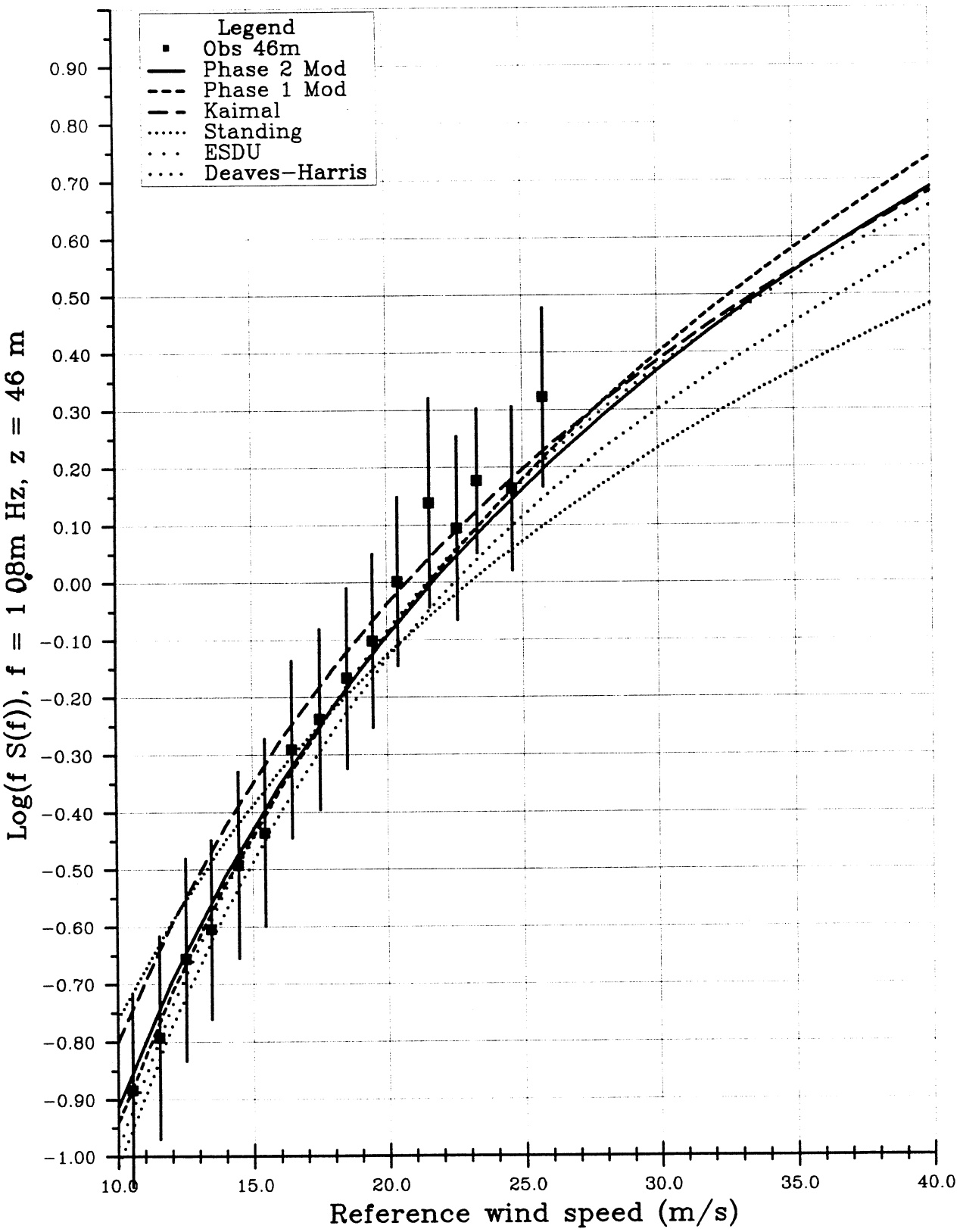

Fig. 7.4.4 As Fig. 7.4.1, but for a mean frequency of 0.0108 Hz.

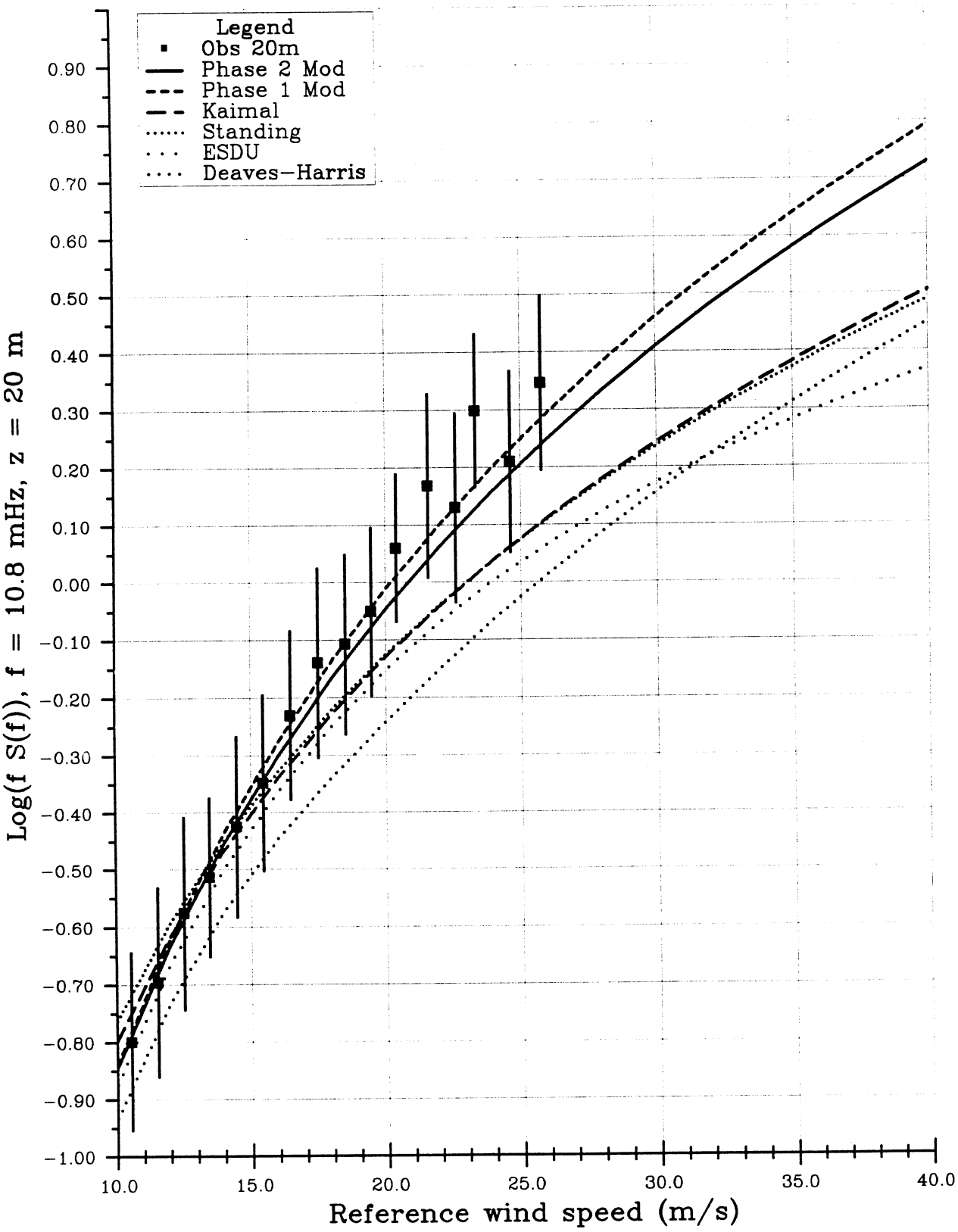

Fig. 7.4.5 As Fig. 7.4.4, but for 20 m height.

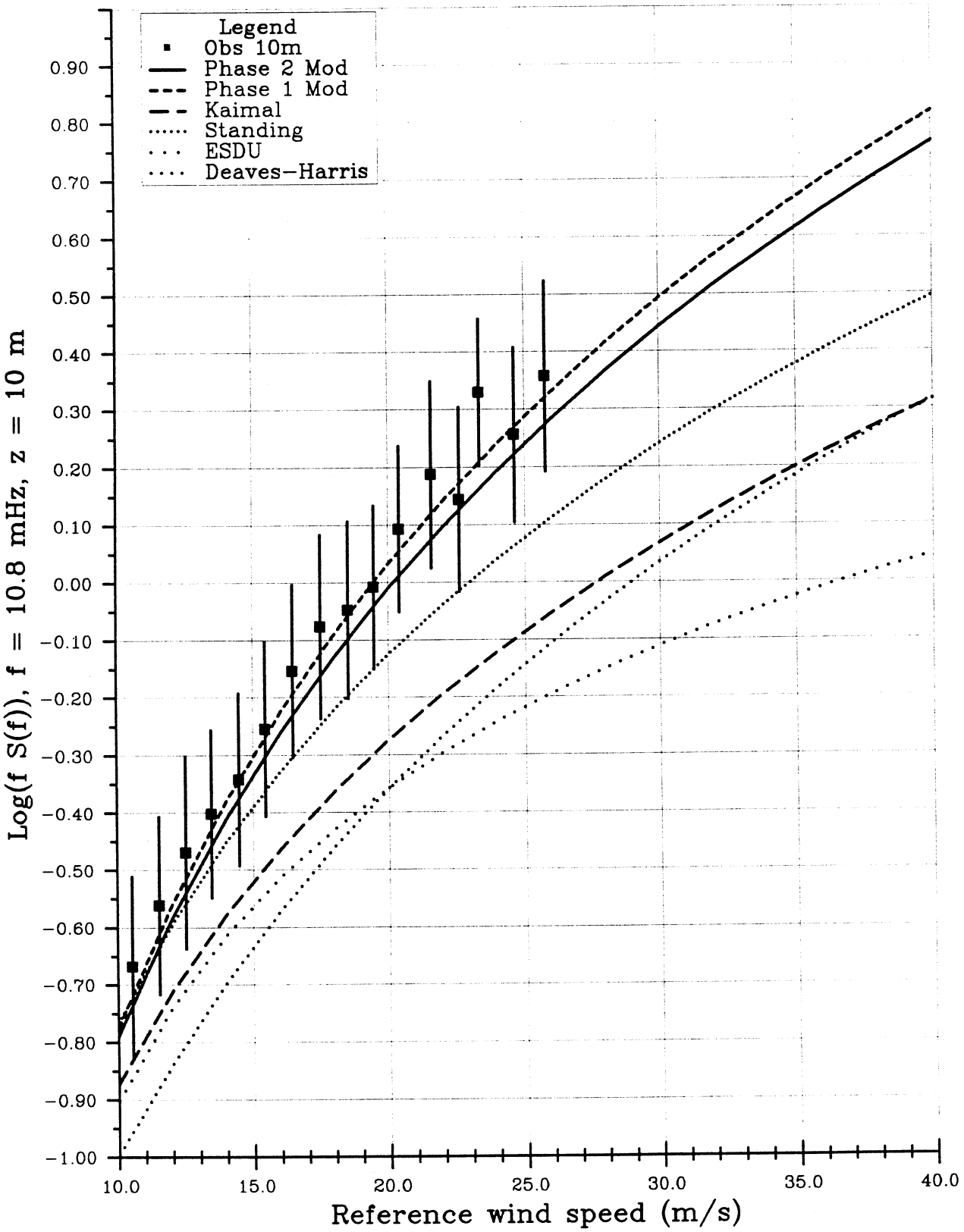

Fig. 7.4.6 As Fig. 7.4.4, but for 10 m height.

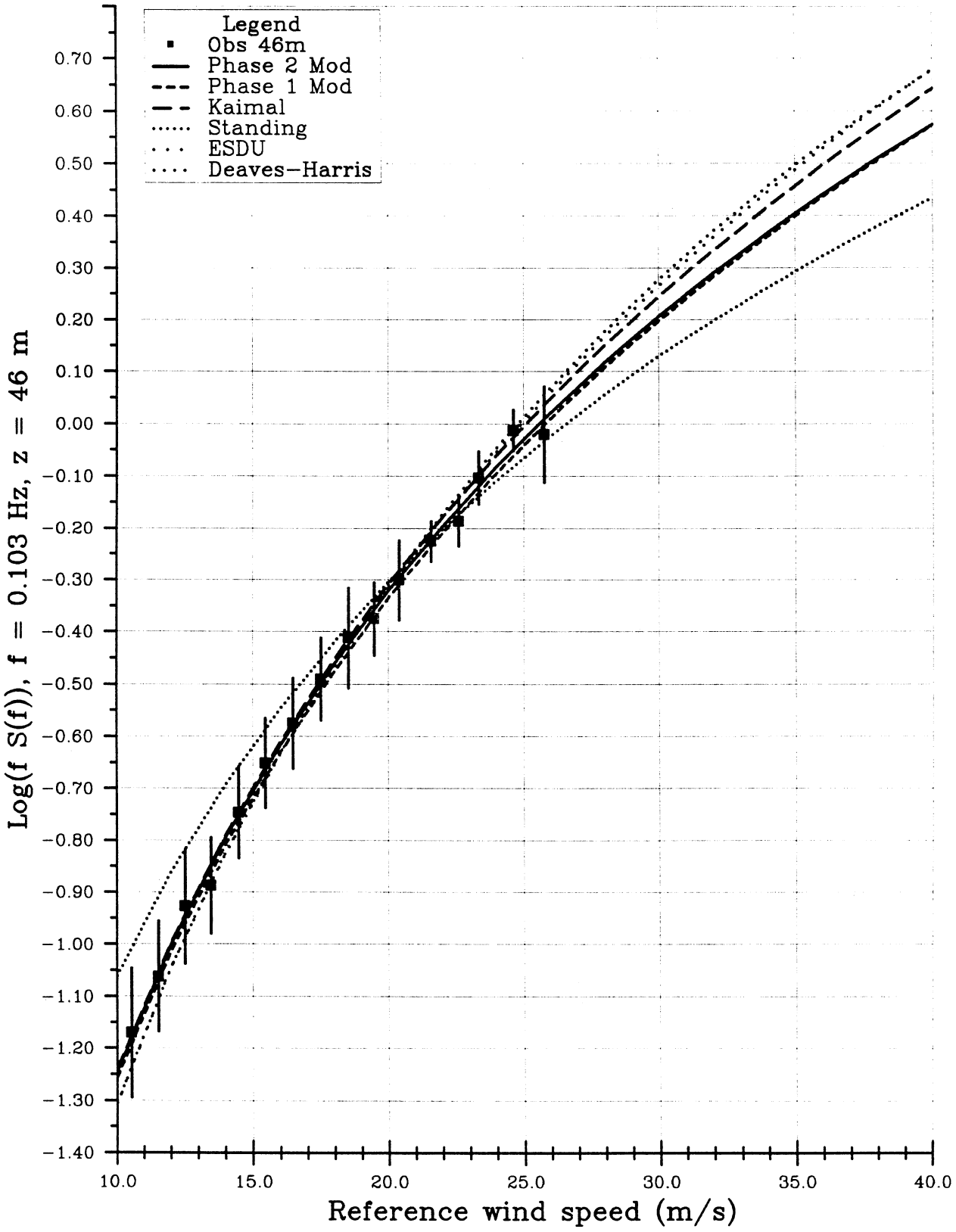

Fig. 7.4.7 As Fig. 7.4.1, but mean values for 2 frequency intervals with a mean frequency of 0.103 Hz.

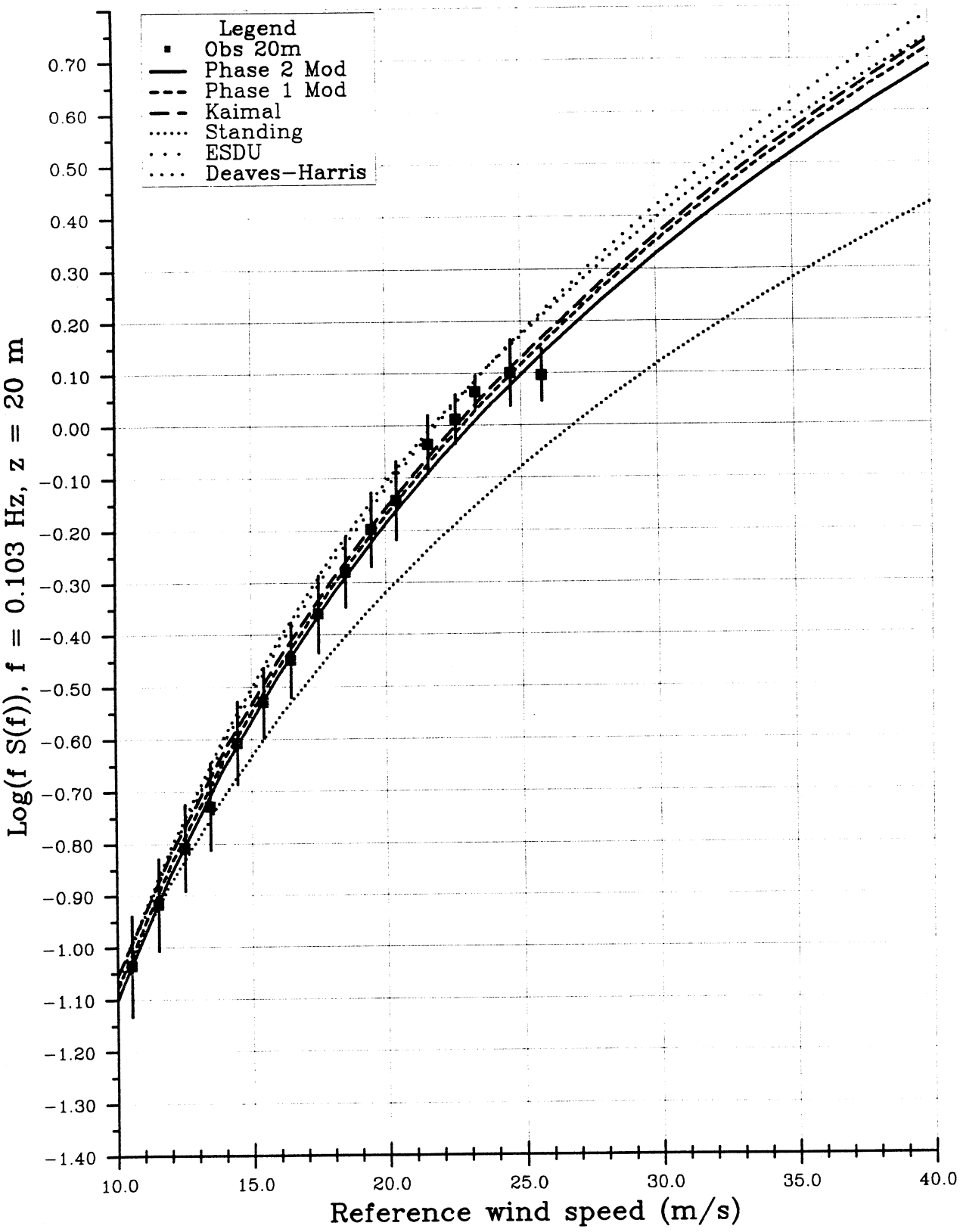

Fig. 7.4.8 As Fig. 7.4.7, but for 20 m height.

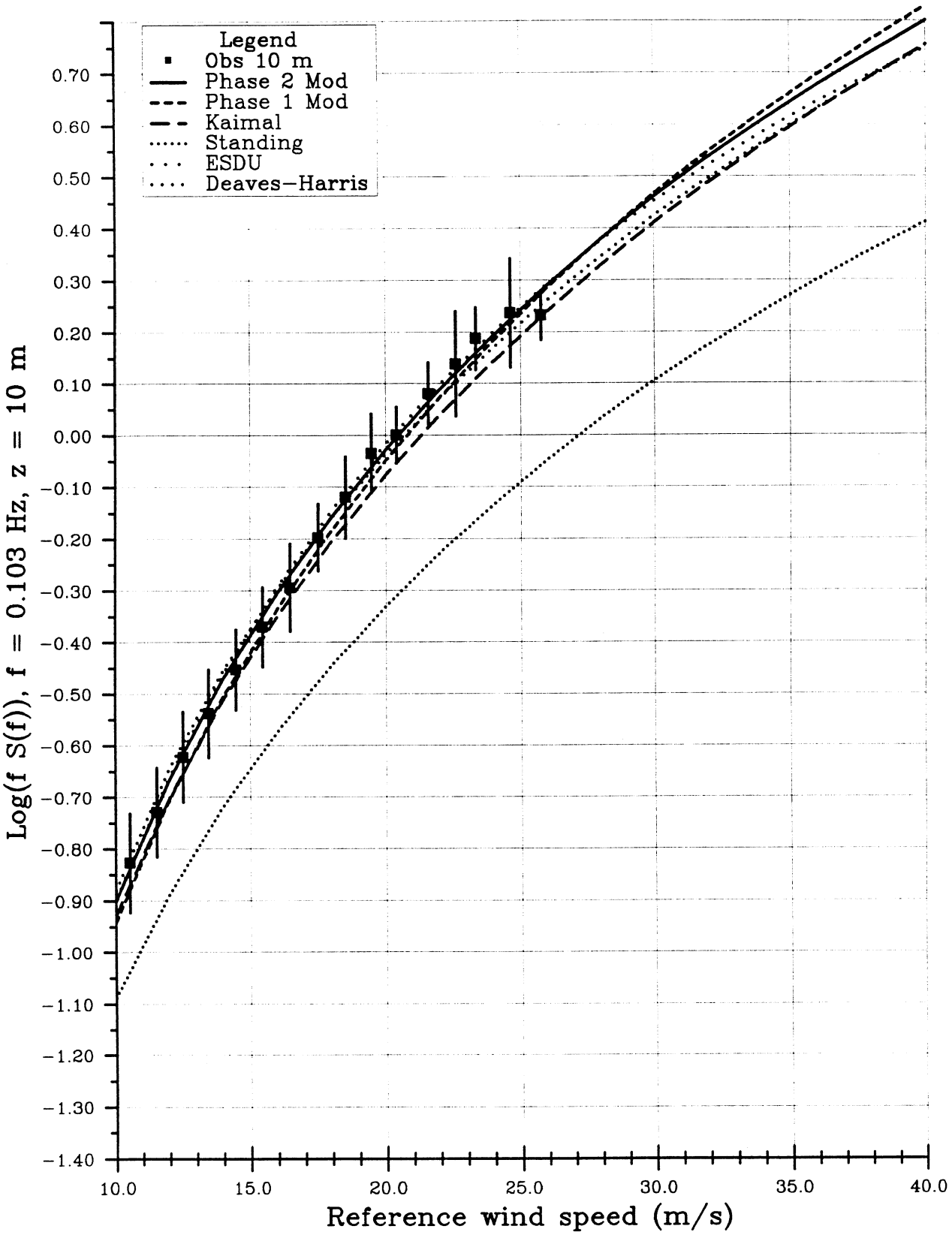

Fig. 7.4.9 As Fig. 7.4.7, but for 10 m height.

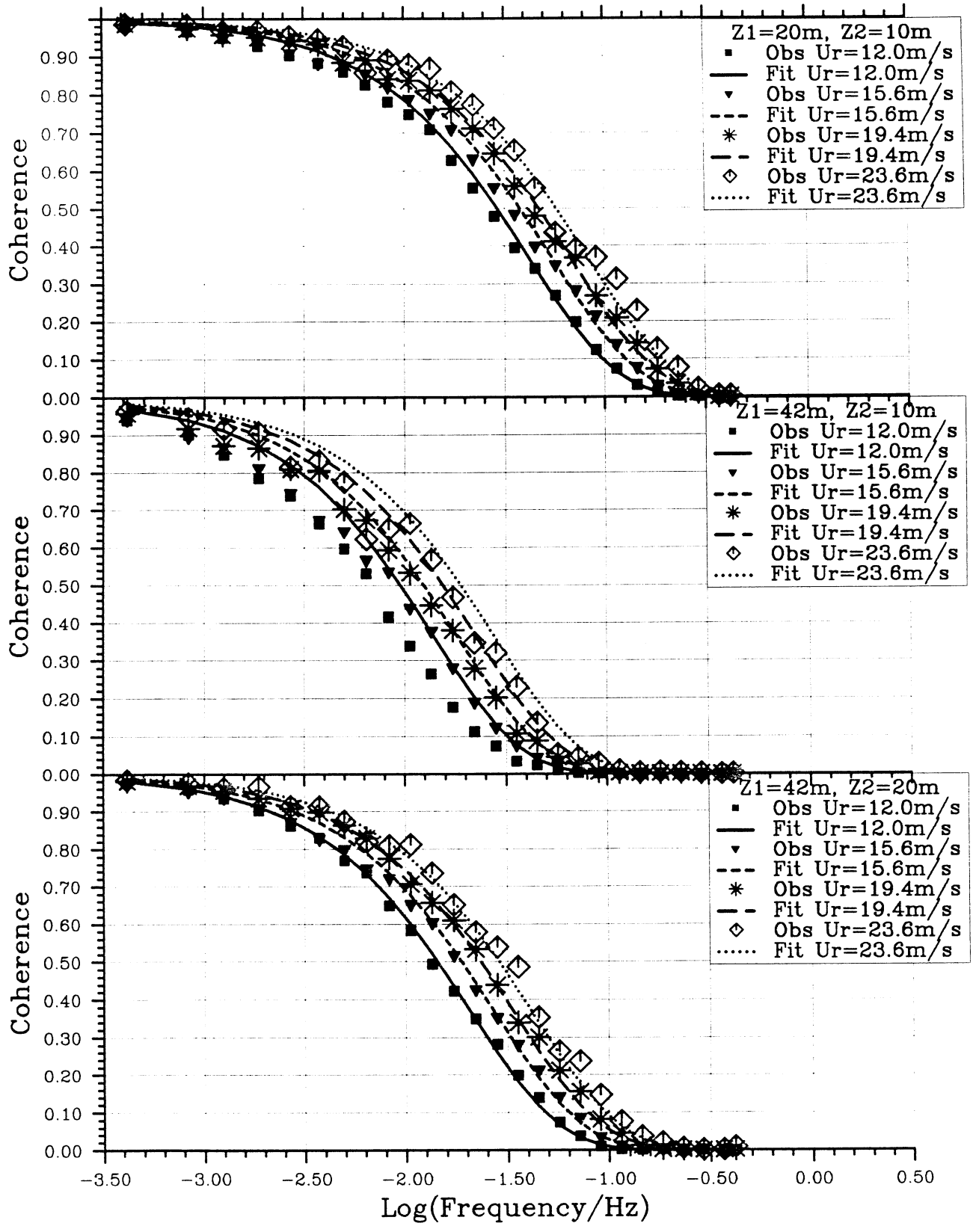

Fig. 8.2-M1a Coherence spectra for the height combinations 20/10, 42/10 and 42/20 m, four wind speed classes and neutral stability versus frequency ($\log_{10}$[fS(f)] vs. $\log_{10}$f) with a fit of the Davenport model (see text).

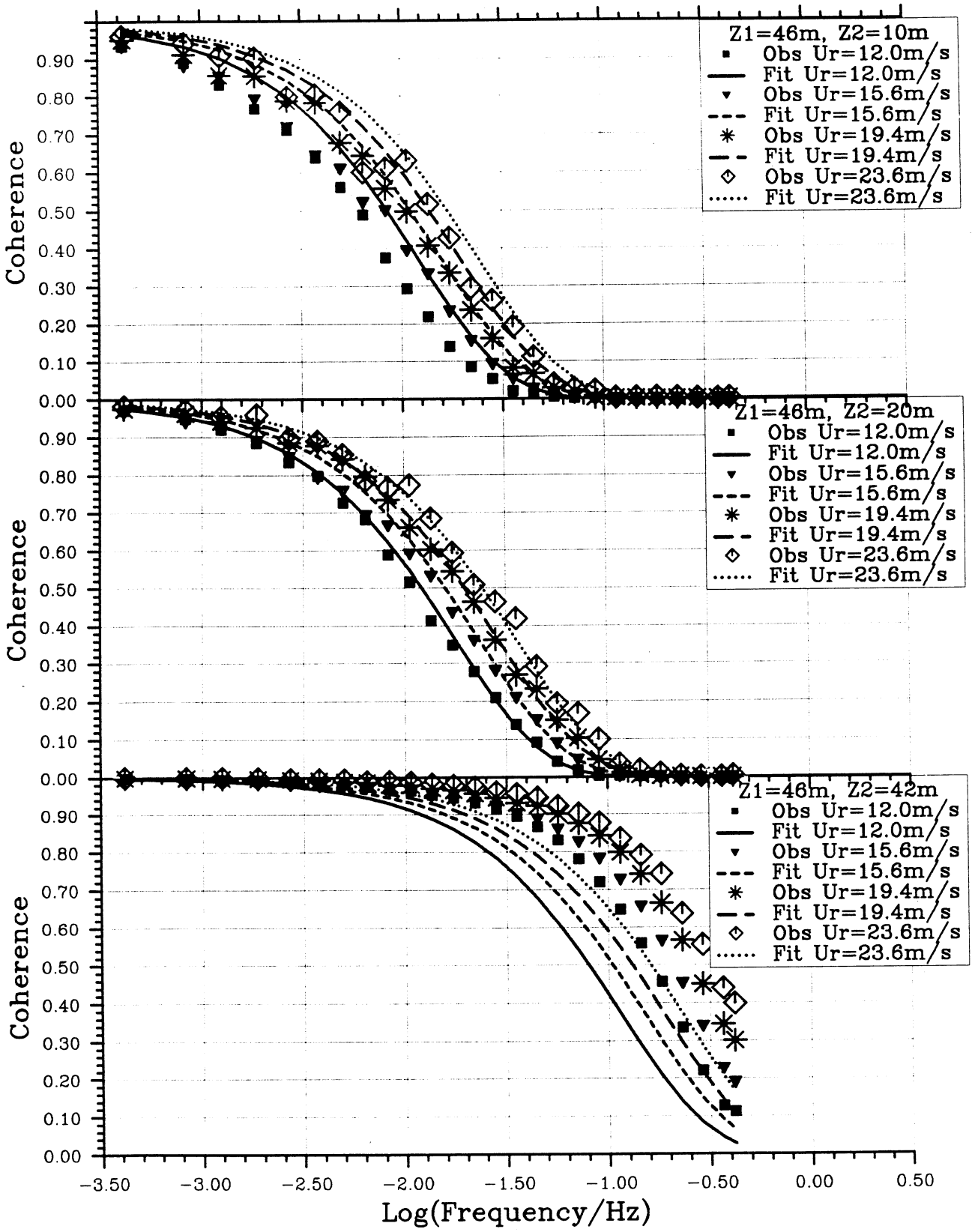

Fig. 8.2-M1b As Fig. 8.2-M1a, but for the height combinations 46/10, 46/20 and 46/42 m.

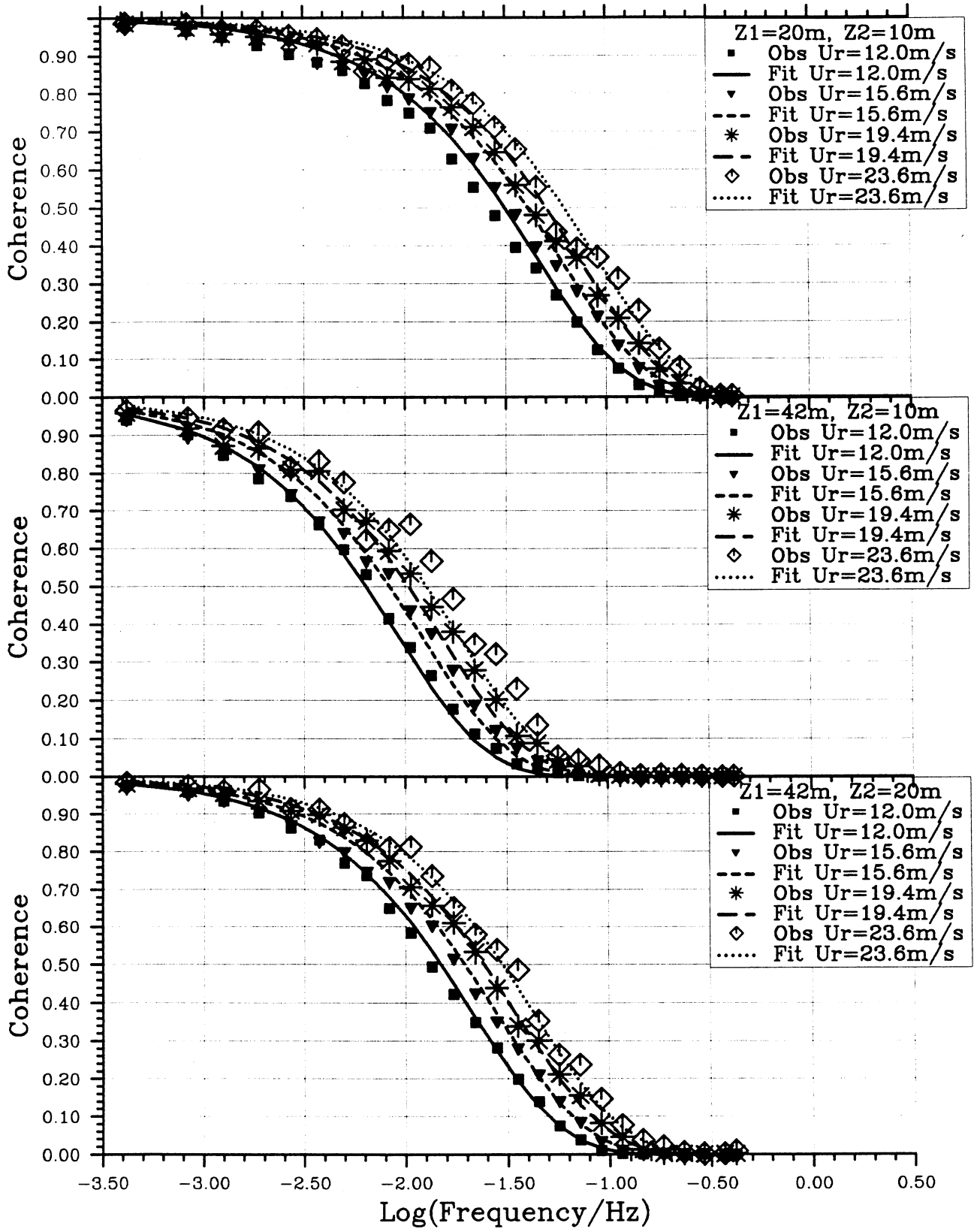

Fig. 8.2-M2a As Fig. 8.2-M1a, but with a fit of the Shiotani model.

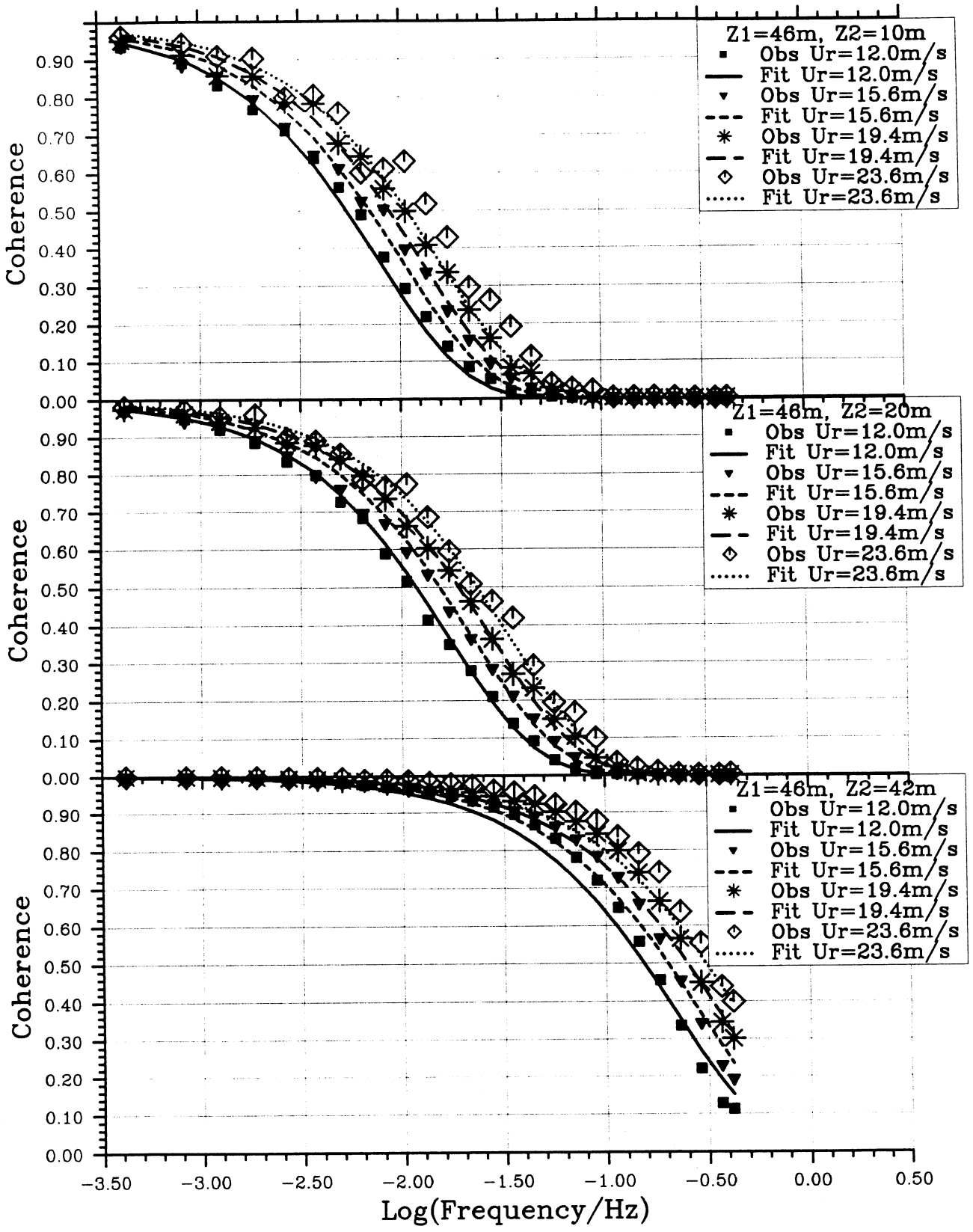

Fig. 8.2-M2b As Fig. 8.2-M1a, but for the height combinations 46/10, 46/20 and 46/42 m, and with a fit of the Shiotani model.

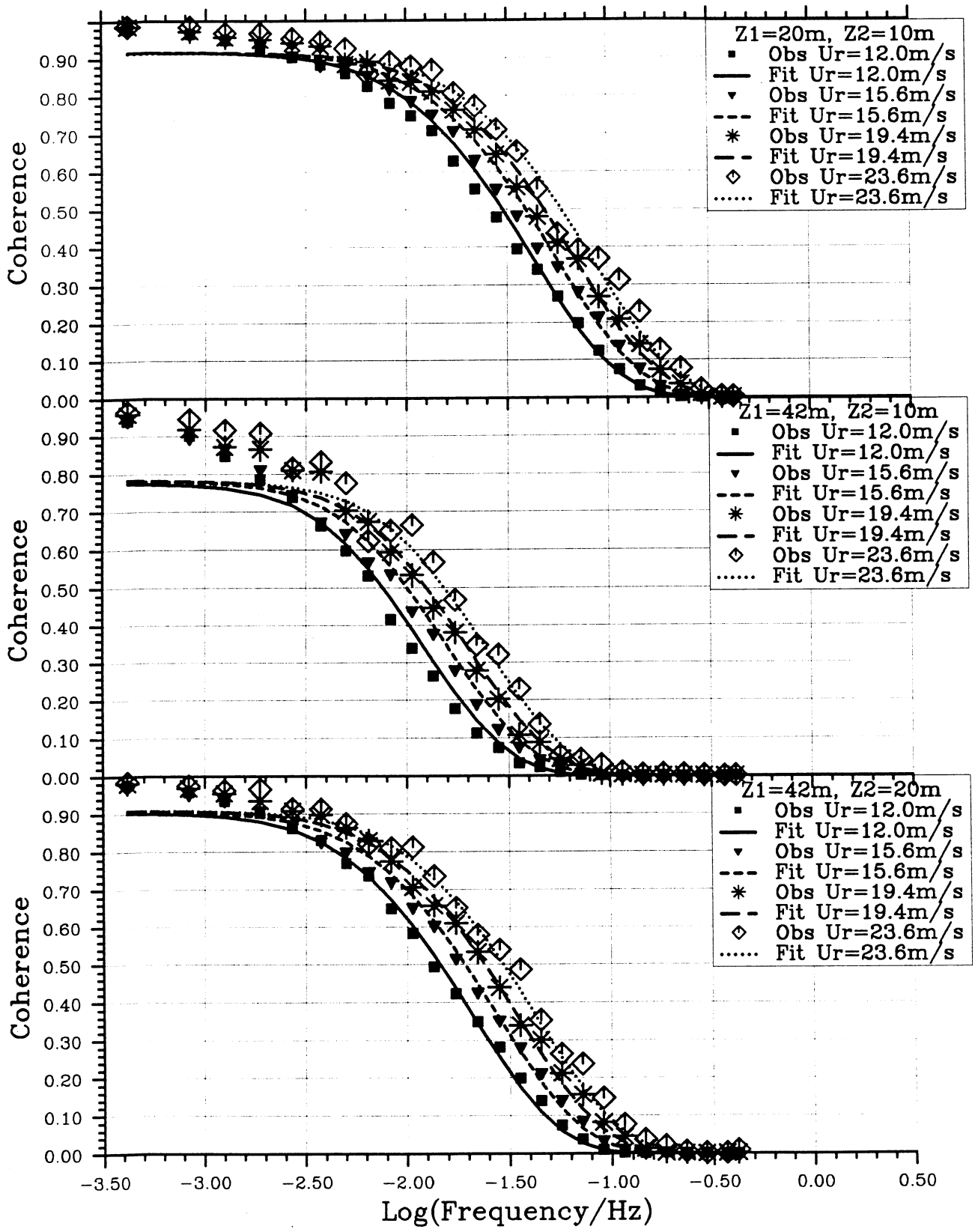

Fig. 8.2-M3a As Fig. 8.2-M1a, but with a fit of the ESDU model.

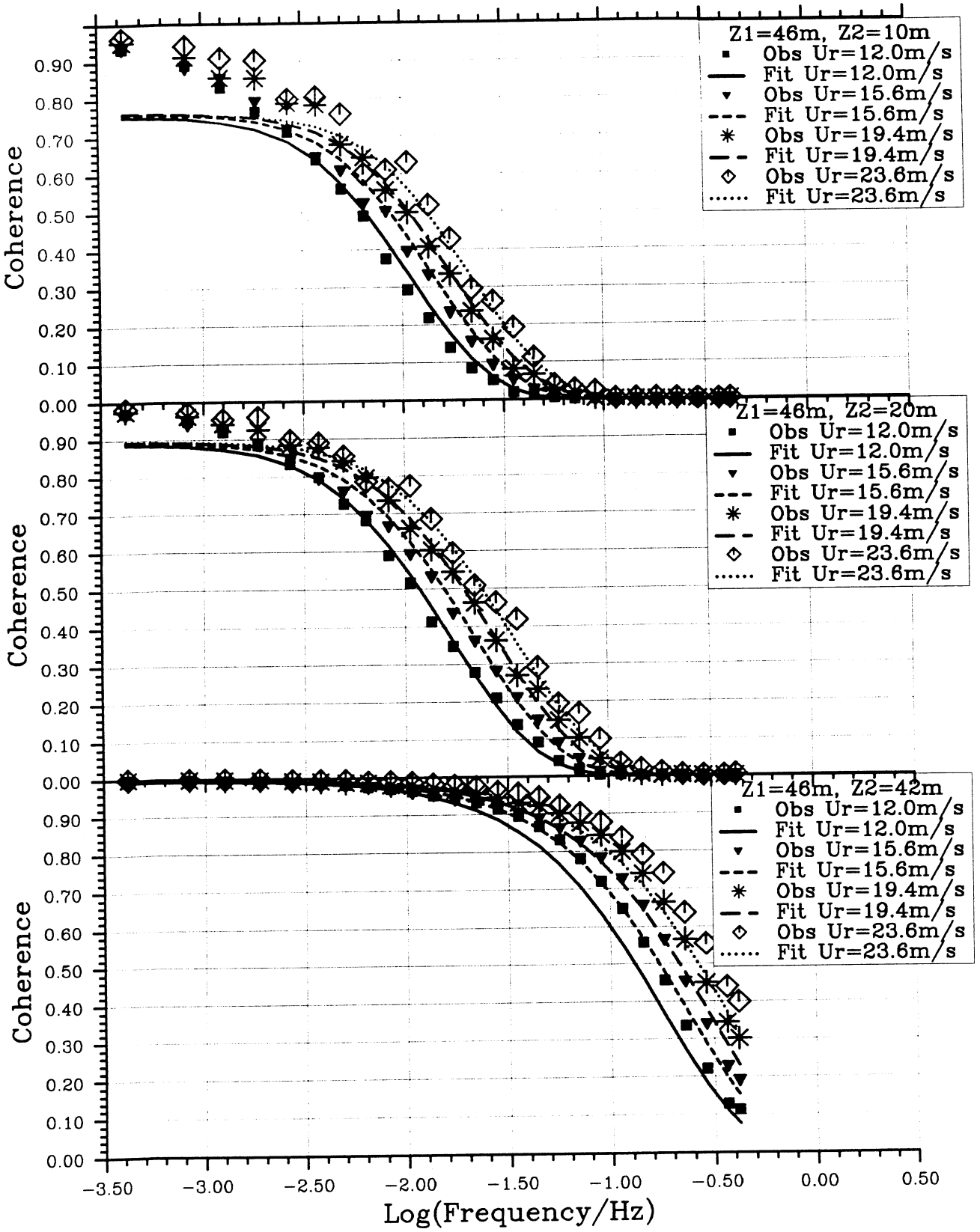

Fig. 8.2-M3b As Fig. 8.2-M1a, but for the height combinations 46/10, 46/20 and 46/42 m, and with a fit of the ESDU model.

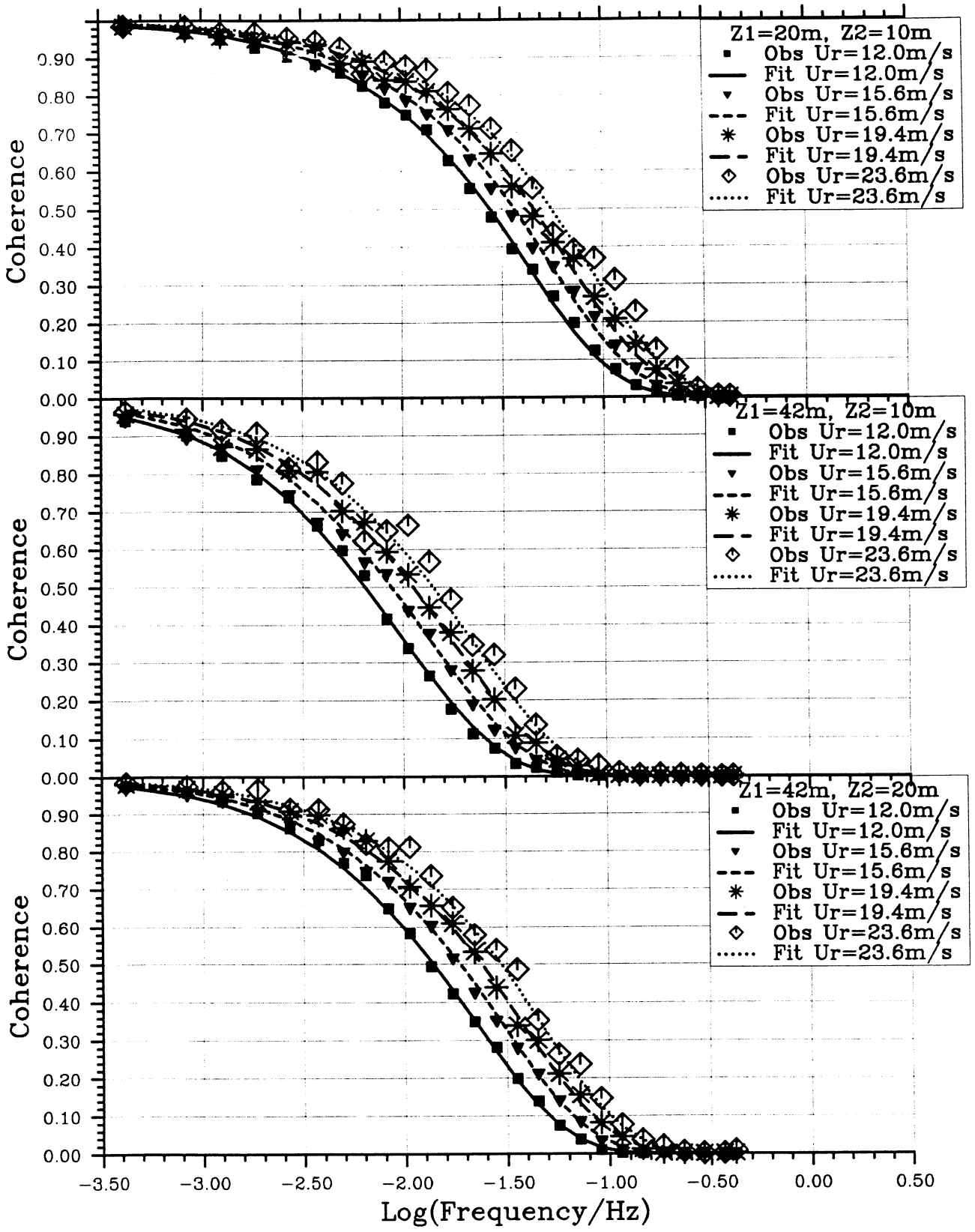

Fig. 8.2-M4a As Fig. 8.2-M1a, but with a fit of the Phase 2 model.

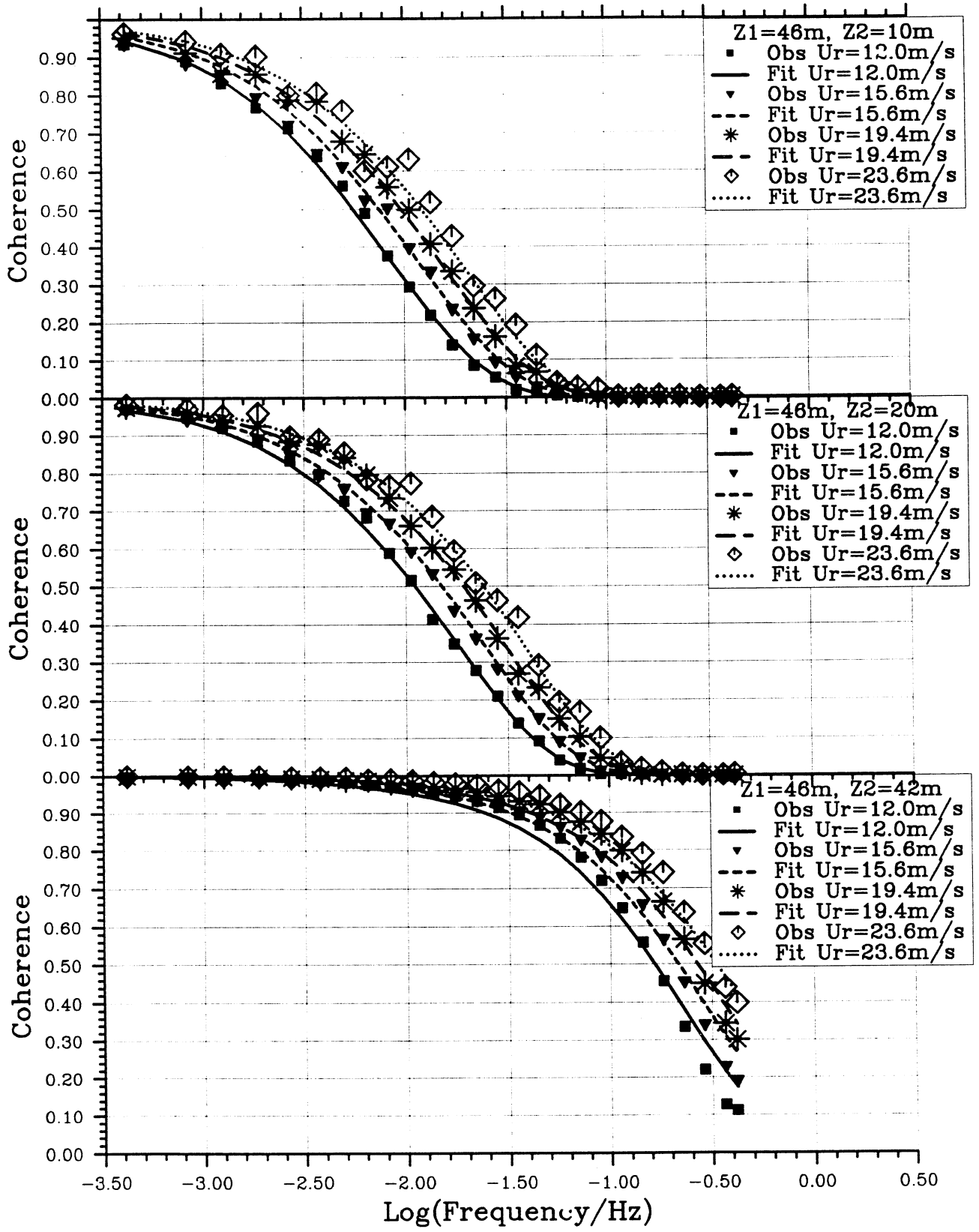

Fig. 8.2-M4b As Fig. 8.2-M1a, but for the height combinations 46/10, 46/20 and 46/42 m, and with a fit of the Phase 2 model.

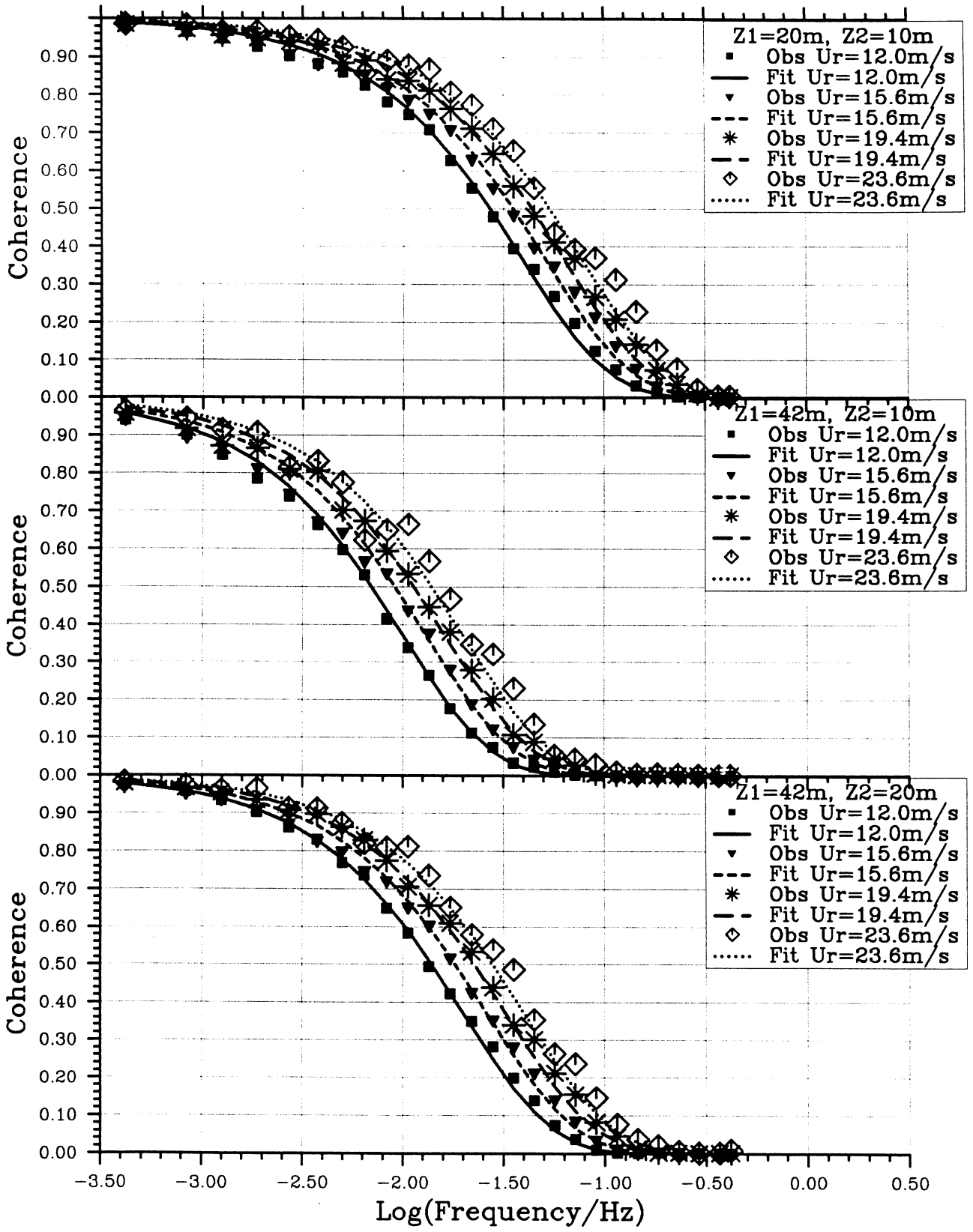

Fig. 8.2-M4c As Fig. 8.2-M1a, but with a fit of a simplified Phase 2 model, Eq. (8.2.13).

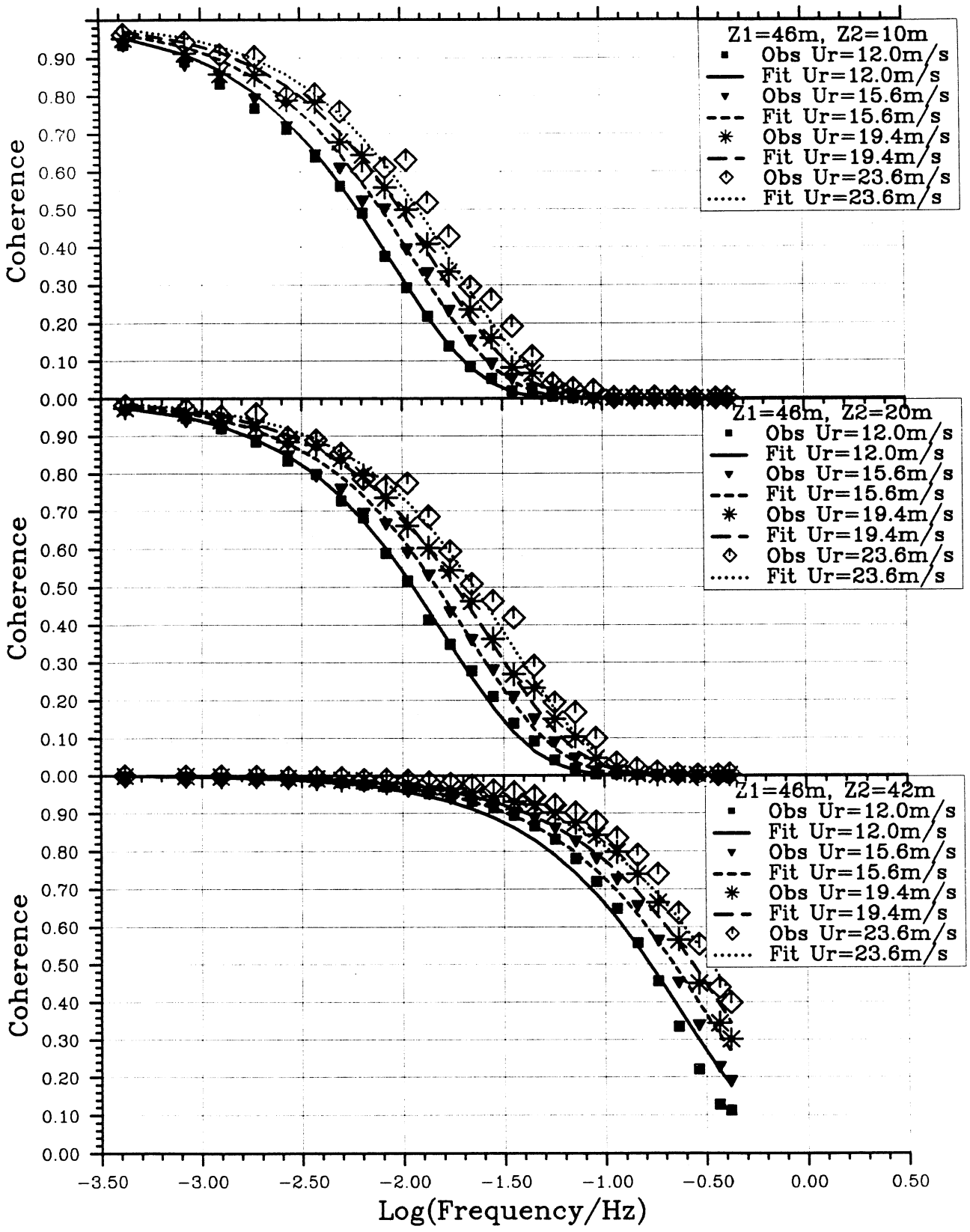

Fig. 8.2-M4d As Fig. 8.2-M1a, but for the height combinations 46/10, 46/20 and 46/42 m, and with a fit of a simplified Phase 2 model, Eq. (8.2.13).

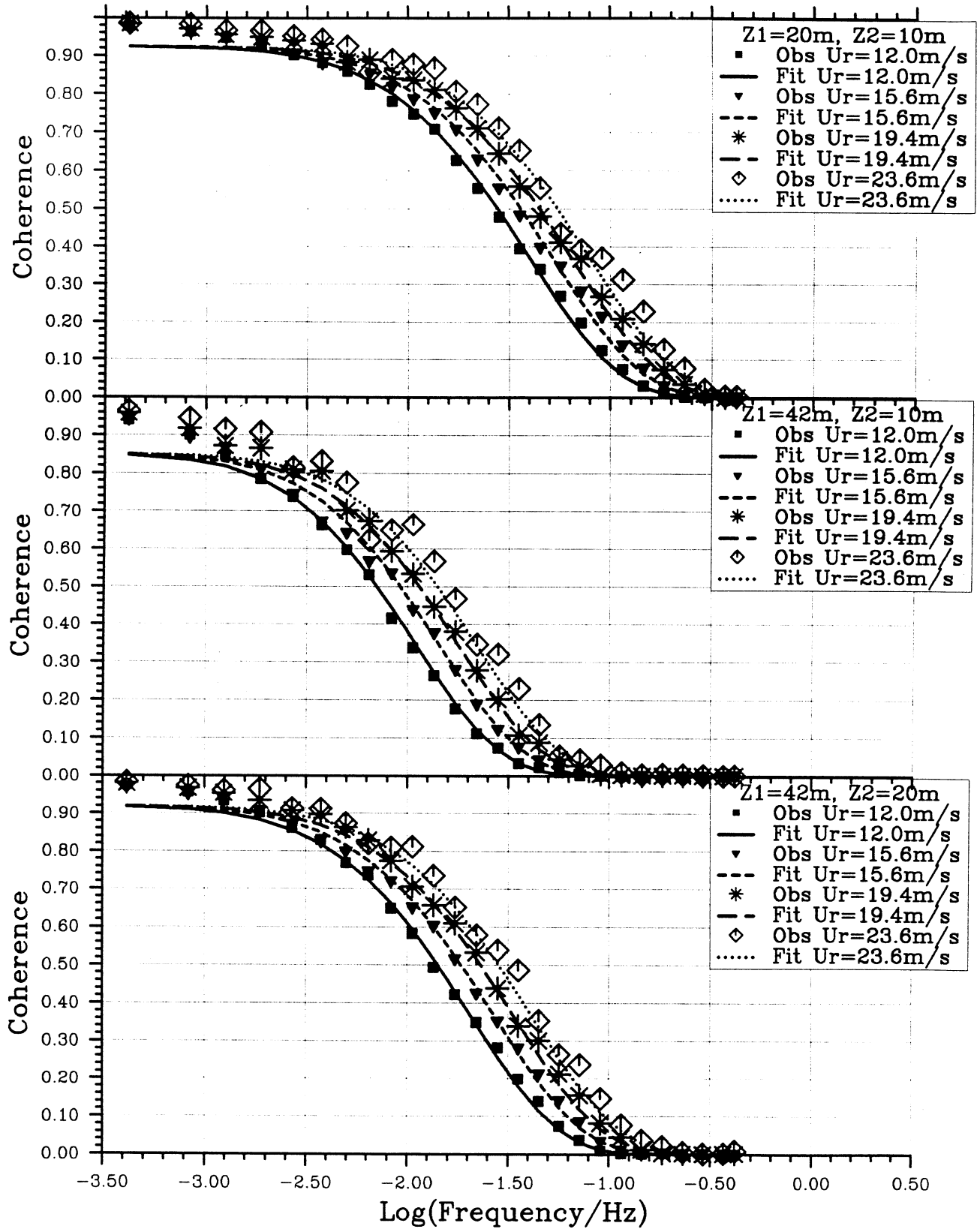

Fig. 8.2-M4e As Fig. 8.2-M1a, but with a fit of a modified Phase 2 model, Eq. (8.2.15).

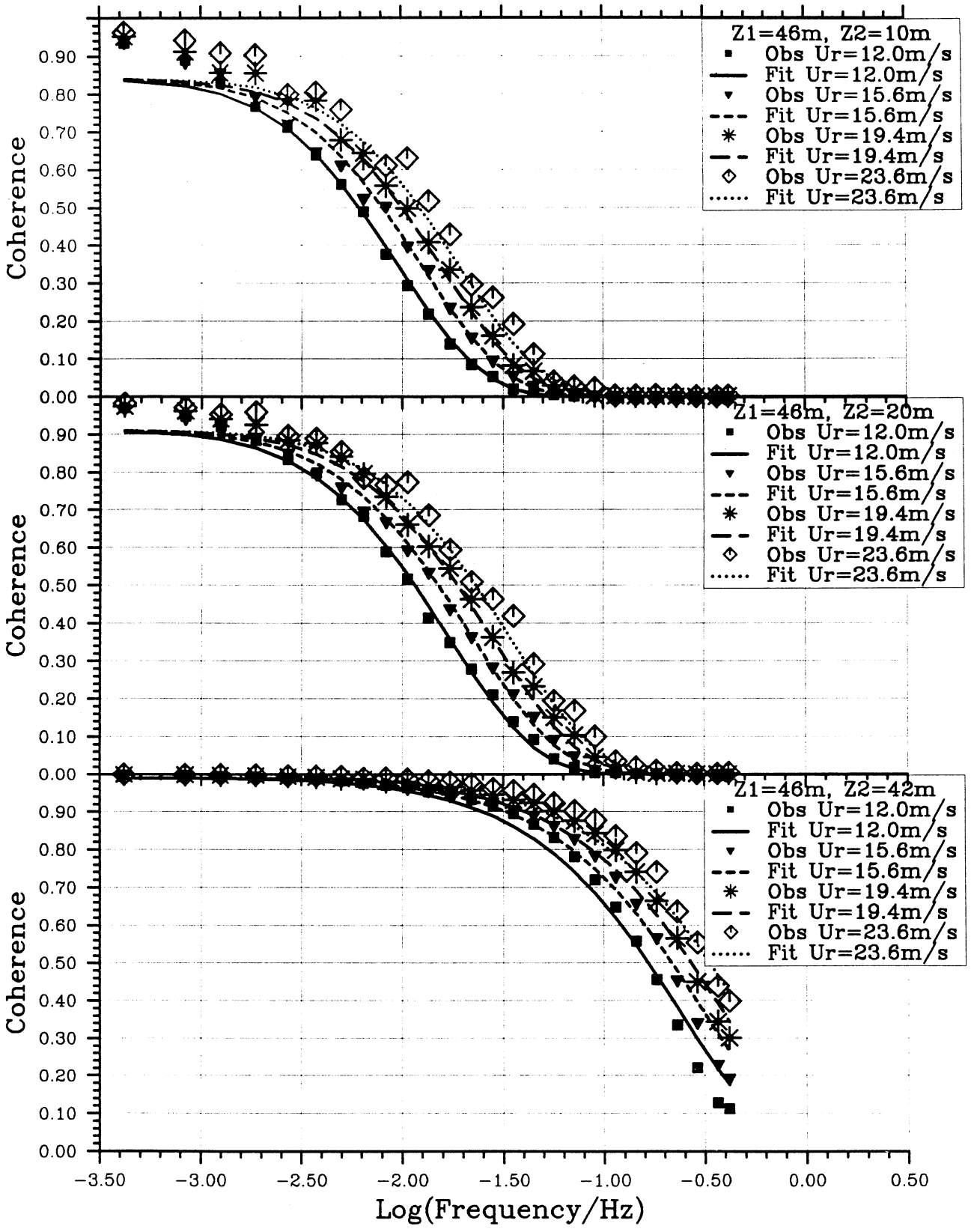

Fig. 8.2-M4f As Fig. 8.2-M1a, but for the height combinations 46/10, 46/20 and 46/42 m, and with a fit of a modified Phase 2 model, Eq. (8.2.15).

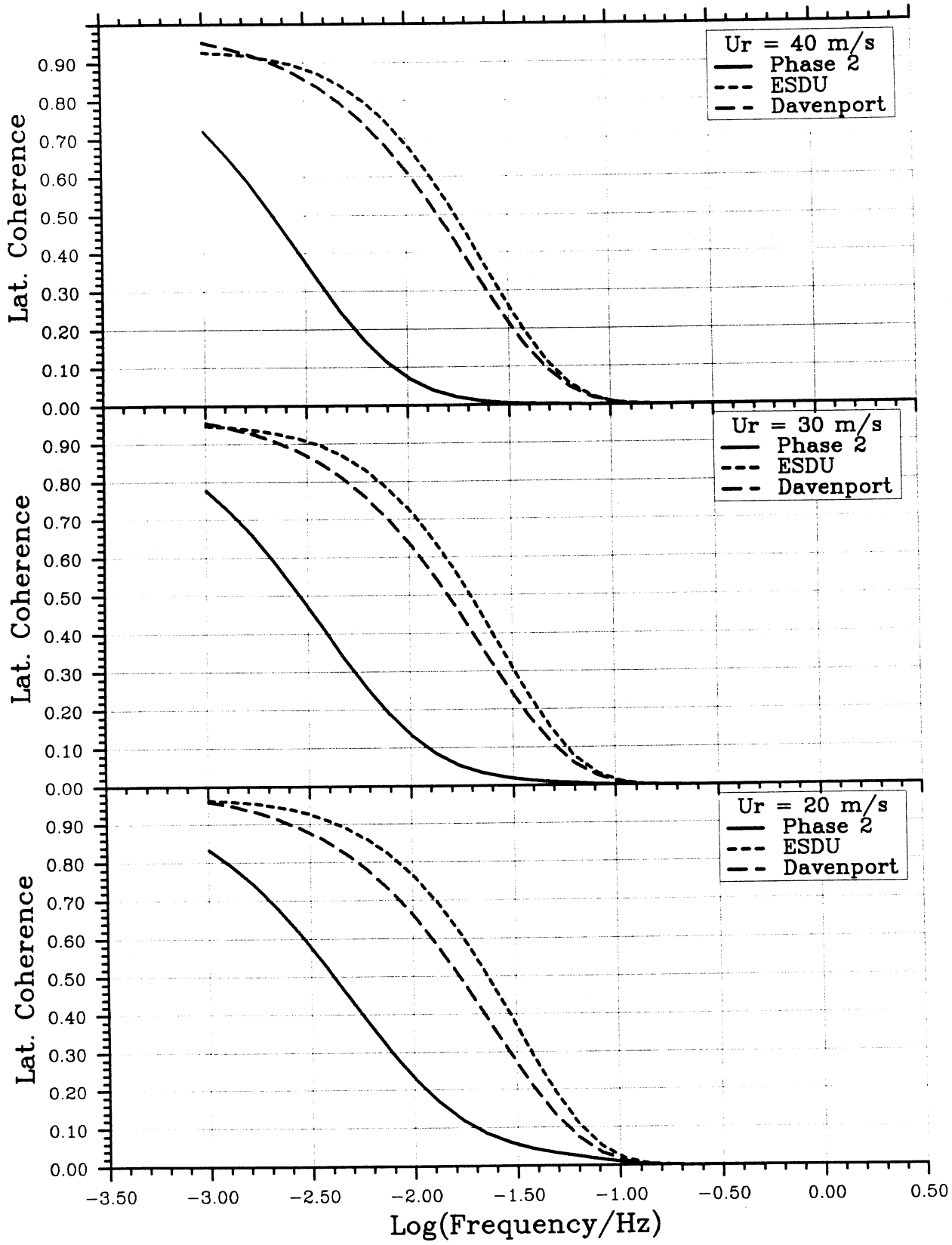

Fig. 8.3.1 Coherence calculated from Phase 2, Bowen and ESDU models versus frequency for a lateral separation of 50 m, a height of 46 m and for reference wind speeds of 20, 30 and 40 m/s.